ANALYSIS AND SYNTHESIS OF FIXTURING DYNAMIC STABILITY IN MACHINING ACCOUNTING FOR MATERIAL REMOVAL EFFECT

A Dissertation
Presented to
The Academic Faculty

by

Haiyan Deng

In Partial Fulfillment
of the Requirements for the Degree
Doctor of Philosophy in the
School of Mechanical Engineering

Georgia Institute of Technology
Atlanta, Georgia

December 2006

ANALYSIS AND SYNTHESIS OF FIXTURING DYNAMIC STABILITY IN MACHINING ACCOUNTING FOR MATERIAL REMOVAL EFFECT

Approved by:

Dr. Shreyes N. Melkote, Advisor
School of Mechanical Engineering
Georgia Institute of Technology

Dr. Thomas R. Kurfess
Department of Mechanical Engineering
College of Engineering and Science
Clemson University

Dr. Kok-Meng Lee
School of Mechanical Engineering
Georgia Institute of Technology

Dr. Chen Zhou
School of Industrial and Systems Engineering
Georgia Institute of Technology

Dr. Roshan J. Vengazhiyil
School of Industrial and Systems Engineering
Georgia Institute of Technology

Date Approved: September 25, 2006

To

My mother, Yuxiang Wang,

My father, Guowen Deng,

for their love and support.

ACKNOWLEDGEMENTS

I would like to express my deepest gratitude to my advisor Dr. Shreyes N. Melkote for his guidance and support during the course of this thesis research. Without his trust, encouragement, and patience, I would be unable to finish this thesis. I extend my deep appreciation to Dr. Thomas R. Kurfess, Dr. Kok-Meng Lee, Dr. Chen Zhou, and Dr. Roshan J. Vengazhiyil for serving on my Ph.D. reading committee. I would also like to thank the National Science Foundation for providing a grant (DMI-0218113) to support this research.

I give my special thanks to Dr. Farrokh Mistree for his encouragement and help during my Ph.D. study. I also want to thank Dr. Aldo A. Ferri for teaching me the advanced knowledge of dynamics and vibrations, which was very helpful to this thesis.

I would like to thank Dr. Hasan U. Akay, Dr. Jie Chen, and Dr. Hazim El-Mounayri from my MS school, Purdue School of Engineering and Technology, for their continuous care and encouragement even after I graduated.

I want to thank my fellow students Sathyan Subbiah, Ramesh Singh, Adam Cardi, Xavier Brun, and Thomas Newton in the Precision Machining Research Consortium (PMRC) for their friendship and useful discussions on various research topics. I give my special thanks to David M. Breland for his assistance in the experimental work reported in this thesis. I extend my appreciation to Steven Sheffield, John Morehouse, and other staff members in the PMRC for their support in my thesis research and Ph.D. study.

Finally, I give my deep gratefulness to my parents, sisters, relatives, and friends for their love and support throughout my graduate studies.

TABLE OF CONTENTS

LIST OF TABLES

LIST OF FIGURES

NOMENCLATURE

Abbreviations

Al	Aluminum.
C	Clamp.
CAFD	Computer-Aided Fixture Design.
CE	Complex Exponential.
C.G.	Center of gravity.
CMIF	Complex Mode Indicator Function.
DOF	Degree of freedom.
FE	Finite element.
FRF	Frequency response function.
GA	Genetic algorithm.
HSS	High speed steel.
L	Locator.
LP	Linear programming.
M	Machining point.
MRE	Material removal effect.
MRR	Material removal rate.
PSO	Particle swarm optimization.
RMS	Root mean square.
SQP	Sequential Quadratic Programming.

Symbols (English)

A_{if}	Cross-sectional area of the ith fixture element.
$\overline{a}_A$	Translational acceleration vector of workpiece at the point where accelerometer is mounted.
$\overline{a}_G$	Translational acceleration vector of workpiece at C.G.
a_i	Radius of the ith fixture-workpiece contact region due to clamping.
a_x	Workpiece acceleration in the x direction during machining.
a_y	Workpiece acceleration in the y direction during machining.
a_z	Workpiece acceleration in the z direction during machining.
C	Number of clamps in a fixture-workpiece system.
c	Contact.
c_1, c_2	Constants balancing local and global search (in PSO search).
$\overline{d}$	Workpiece contact dynamic displacement vector.
$\overline{d}_i$	Workpiece dynamic displacement vector at the ith contact during machining.
d_{if}	Diameter of the ith fixture element.
$d_{ij}(t)$	Workpiece dynamic displacement at the ith contact in the j direction due to machining.
E	Young's modulus.
E_{if}	Young's modulus of the ith fixture element.
$\overline{F}$	Resultant force of a fixture-workpiece system under clamping.
$\overline{F}(t)$	Cutting force vector.
$\overline{F}_c$	Clamping force vector.
${}^1\overline{F}_c^{opt}$, ${}^2\overline{F}_c^{opt}$	Optimal clamping force vectors during the first and last tool passes.
$\left\lVert \overline{F}_c \right\rVert_2$	2-norm of clamping force vector.

F_{cj}	The jth clamping force ($j = L+1, \ldots, L+C$).
f	Fixture.
f_t	Tooth passing frequency in milling.
G	Shear modulus.
G_{if}	Shear modulus of the ith fixture element.
gbest	Index of the particle that has the best performance in the group (in PSO search).
$[I]$	Centroidal inertia matrix of workpiece.
I_{if}	Polar moment of inertia of the ith fixture element.
i	The ith fixture element or fixture-workpiece contact (i = 1 to $L+C$).
j	Axis index of a contact coordinate system ($j = x, y$, or z).
$[K]$	Intrinsic stiffness matrix of a fixture-workpiece system.
$[K_c]$	Local stiffness matrix of a fixture-workpiece system.
$[K_i]$	Local stiffness matrix at the ith fixture-workpiece contact.
k	Index of iteration in PSO search.
k_{ijc}	Contact stiffness at the ith fixture-workpiece contact in the j direction.
k_{ijf}	Structural stiffness of the ith fixture element in the j direction.
k_{ijw}	Structural stiffness of workpiece reflected at the ith contact in the j direction.
L	Number of locators in a fixture-workpiece system.
$\overline{L}_b$	Upper bound of clamping force vector.
l_{if}	Length of the ith fixture element.
$\overline{M}$	Resultant moment of a fixture-workpiece system under clamping.
$[M]$	Inertia matrix of a fixture-workpiece system.

$[\dot{M}]$	Rate of change of system inertia matrix ($[\dot{M}] = d[M]/dt$).
m	Mass of workpiece.
N	Number of flutes in a cutting tool.
$\bar{p}_i$	Position vector of the ith fixture-workpiece contact in the workpiece frame.
pbest	Objective function value corresponding to *pbestx* (in PSO search).
pbestx	Best solution that a particle has achieved so far (in PSO search).
Q_{ix}, Q_{iy}	Tangential reaction forces at the ith contact due to clamping.
$\bar{q}$	Workpiece dynamic displacement vector during machining.
$\dot{\bar{q}}$	Workpiece velocity vector during machining.
$\ddot{\bar{q}}$	Workpiece acceleration vector during machining.
R	Relative curvature at a fixture-workpiece contact.
$\bar{R}$	Resultant reaction force at a fixture-workpiece contact.
Rand, rand	Generators of random numbers between 0 and 1.
R_f	Tip radius of a fixture element.
R_w	Local radius of workpiece surface at a fixture-workpiece contact.
$\bar{r}_{A/G}$	Displacement vector from C.G. of workpiece to position of accelerometer.
$\bar{r}_m(t)$	Position vector from C.G. of workpiece to machining point *M*.
$[S]$	Configuration matrix of a fixture-workpiece system.
SS	Spindle speed.
$[S_i]$	Configuration matrix of the ith fixture-workpiece contact.
S_y	Yield strength of workpiece material.
$\bar{s}_{ij}$	Direction vector of the *j* axis of the ith contact frame in the workpiece frame.

T	Kinetic energy of a fixture-workpiece system in machining.
t	Machining time.
U_3	3×3 identity matrix.
$\overline{U}_b$	Lower bound of clamping force vector.
V	Potential energy of a fixture-workpiece system.
$\overline{v}_i$	Velocity of the ith particle (in PSO search).
w	Workpiece.
w_i	Inertia weight of the ith particle (in PSO search).
$\overline{x}_i$	Position of the ith particle (in PSO search).

Symbols (Greek)

$\overline{\alpha}$	Workpiece angular velocity vector during machining.
$\overline{\Gamma}(t)$	Cutting torque vector.
$\Delta\overline{r}$	Workpiece translational displacement vector during machining.
Δt	Time increment of sampling in data collection.
Δx	Workpiece translational displacement in the x direction during machining.
Δy	Workpiece translational displacement in the y direction during machining.
Δz	Workpiece translational displacement in the z direction during machining.
$\Delta\alpha$	Workpiece rotational displacement about the x axis during machining.
$\Delta\beta$	Workpiece rotational displacement about the y axis during machining.
$\Delta\gamma$	Workpiece rotational displacement about the z axis during machining.

$\Delta_{ij}(t)$	Total displacement of a fixture-workpiece system at the ith contact in the j direction due to combined effect of clamping and machining.
δ_{ij}	Total elastic deformation of the fixture-workpiece system at the ith contact in the j direction due to clamping.
δ_{ijc}	Elastic deformation of workpiece at the ith contact in the j direction due to clamping.
δ_{ijf}	Elastic deformation of the ith fixture element in the j direction due to clamping.
Θ	Half angle of virtual friction cone at a fixture-workpiece contact.
μ_S^i	Static coefficient of friction at the ith fixture-workpiece contact.
ξ_r	Damping ratio corresponding to the rth mode of a fixture-workpiece system.
Π_c	Complementary energy from fixture-workpiece contacts under clamping.
Π_f	Complementary energy from fixture elements under clamping.
Π_t	Total complementary energy of a fixture-workpiece system under clamping.
υ	Poisson's ratio.
$\overline{\omega}$	Workpiece angular acceleration vector during machining.
ω_r	Natural frequency corresponding to the rth mode of a fixture-workpiece system.

SUMMARY

A machining fixture is a critical link in a machining system as it directly affects the operational safety and part quality. The design of a machining fixture must enable the workpiece to remain stable throughout the machining process. Numerous efforts have been made in the past in modeling, analysis, and synthesis of machining fixture-workpiece systems. The majority of prior work treats the fixture-workpiece system as quasi-static and ignores the system dynamics. In addition, the material removal effect on fixture-workpiece system properties and behavior is generally ignored.

The primary goal of this thesis is to develop a model-based framework for analysis and synthesis of the dynamic performance, emphasizing fixturing dynamic stability, of a machining fixture-workpiece system accounting for the material removal effect. The five major accomplishments of this thesis are as follows.

First, a systematic procedure for analysis of fixturing dynamic stability of an arbitrarily configured machining fixture-workpiece system is developed with consideration of the effect of material removal on fixture-workpiece dynamics.

Second, models and approaches for simulation of fixture-workpiece dynamics and analysis of fixturing dynamic stability are experimentally validated. Good agreement between model outputs and measurements is found. It is concluded that consideration of dynamics and characterization of system dynamic properties are crucial for an accurate analysis of the machining fixture-workpiece system.

Third, an in-depth theoretical and experimental investigation of the material removal effect on fixture-workpiece dynamics is performed. The results show that the

dynamic behavior and properties of the fixture-workpiece system change substantially when a significant portion of material is removed. Approaches developed in this thesis are shown to be capable of capturing the effect of material removal.

Fourth, the roles of important fixture design and machining process parameters in affecting the fixturing dynamic stability are studied and understood via a parameter effect analysis. Certain parameters are found to have a more pronounced impact on fixture-workpiece dynamics than others. Additionally, the fixturing dynamic stability is found to be sensitive to the parameter imprecision.

Finally, a generic approach for the determination of the minimum clamping forces that ensure fixturing dynamic stability in machining is developed. Because of the material removal effect, dynamic clamping is found to be an option to achieve the best possible performance of the system.

Models and approaches developed in this thesis are generic and can be used as simulation tools in fixture design. Insights obtained from this research will advance the fixturing knowledge base and provide general fixture design guidelines.

CHAPTER 1

INTRODUCTION

1.1 Background

Fixtures are widely used as workholding devices in virtually all manufacturing processes such as machining, assembly, and inspection. This thesis focuses on machining fixtures. A machining fixture is used to establish and maintain the required position and orientation of a workpiece in a machine tool so that cutting operations can be performed on the workpiece. It is a critical link in the machining system as it directly affects operational safety and part quality. A typical machining fixture consists of a base plate and a number of locators and clamps. Locators are passive fixture elements used to position the workpiece while clamps are active fixture elements that can be actuated mechanically, pneumatically, or hydraulically to apply clamping forces onto the workpiece so that it can resist external forces generated by the machining operation.

There are a variety of fixture designs. The geometry of the contact region between a fixture element and the workpiece can be a point, line, or plane. In addition, several configuration schemes are available to restrain the workpiece. For example, shown in Figure 1.1 is a 3-2-1 machining fixture that is suitable for a prismatic workpiece in a milling operation. The fixture includes a base plate used to support the fixture bodies (blocks on which the fixture elements are mounted), six locators with three in the primary, two in the secondary, and one in the tertiary datum planes, and two hydraulic clamps.

This thesis concentrates on a machining fixture-workpiece system in which the workpiece has an arbitrary shape and is surrounded by an arbitrary number of fixture elements that make small-area (compared to the surface area of the workpiece) frictional contact with the workpiece.

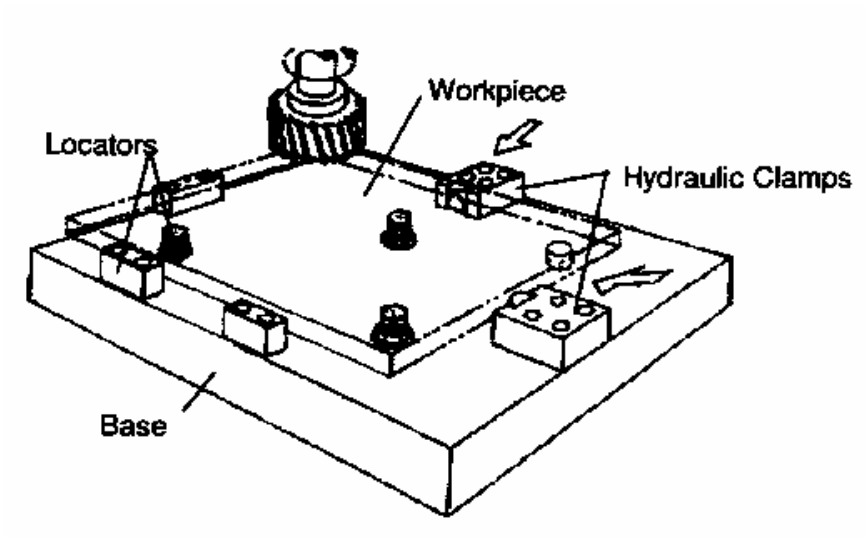

Figure 1.1 A typical 3-2-1 milling fixture [1]

A machining fixture design, in general, should satisfy the following four major requirements:

1) Locating accuracy – the fixture must accurately and uniquely position the workpiece relative to the machine coordinate system;
2) Total restraint – the fixture must securely hold the workpiece and effectively resist external forces from the machining operation;
3) Sufficient rigidity – the fixture must limit any elastic and/or plastic deformation of the workpiece due to external forces; and

4) No interference – the fixture must not interfere with the cutting tool path.

Other desirable characteristics of a fixture include quick loading and unloading, portability, low cost, etc.

An extension of the second requirement is that a fixture must be designed such that the workpiece remains stable throughout the machining process. In other words, a fixture must be able to fully restrain a workpiece during machining. Therefore, detachment (or lift-off) of the workpiece from the fixture and gross sliding (or macro-slip) of the workpiece against a fixture element at any instant of the machining process are considered to be indicators of fixturing instability. These instabilities should be eliminated through proper fixture design. Fixturing dynamic stability is the primary focus of this thesis work.

Fixture planning and design is a highly complicated, multi-disciplinary task because of the contradictory nature of some of the design requirements and desired characteristics as well as the complexity of part geometry and manufacturing constraints. In industrial practice, workpieces (or other structures/objects) are often inappropriately clamped due to the lack of reliable scientific tools, resulting in unsafe operations or excessive part distortion.

Significant research efforts have been made in past decades to improve the fundamental understanding of fixturing principles and to provide fixture designers with scientific tools. These efforts can be classified into three categories: i) machining set-up planning and fixture planning, ii) fixture element design, and iii) fixture analysis and synthesis. The first two categories focus on conceptual (or high-level) design of fixtures

while the third category concentrates on detailed (or low-level) fixture design. This thesis work falls into the third category.

Literature on machining fixture analysis and synthesis is large. The majority of prior work treats the fixture-workpiece system as quasi-static and ignores the system dynamics. In reality, machining processes such as milling are characterized by periodic forces. When the excitation frequency is in the vicinity of a natural frequency of the fixture-workpiece system, consideration of system dynamics becomes crucial.

A few researchers have considered fixture-workpiece dynamics in their research. However, the material removal effect is generally ignored. Continuous material loss and the resulting change in fixture-workpiece system dynamics are characteristic of a machining process. As shown later in this thesis, ignoring the material removal effect can lead to erroneous analysis of system performance, especially under aggressive machining conditions or when a large percentage of material is removed in an operation.

In summary, models for fixture analysis and synthesis accounting for the fixture-workpiece system dynamics and material removal effect are limited in the open literature.

1.2 Research Goal

The overall goal of this thesis research is to advance the knowledge base of machining fixture design by overcoming the limitations of existing efforts and to develop a series of simulation tools that can eventually be integrated into a Computer-Aided Fixture Design (CAFD) system.

Specifically, a systematic, model-based framework for analysis and synthesis of the dynamic behavior (emphasizing the fixturing dynamic stability) of an arbitrarily configured fixture-workpiece system in machining accounting for the material removal effect is to be established and experimentally validated. Insights into the role of the fixture and the effect of material removal on the dynamic properties and performance of the machining fixture-workpiece system are to be obtained via theoretical and experimental investigations.

1.3 Thesis Outline

This thesis is organized as follows. Prior work on modeling and analysis of the machining fixture-workpiece system dynamics and fixturing stability is reviewed in Chapter 2. Chapter 2 also surveys the literature on sensitivity analysis of the performance of a fixture-workpiece (or hand-object) system and fixture design optimization.

Chapter 3 establishes a mathematical, systematic procedure for modeling and analysis of the fixturing dynamic stability of a machining fixture-workpiece system accounting for the material removal effect. Development of models that simulate the vibratory behavior of the fixture-workpiece system during machining and the system behavior change due to material removal are discussed in detail. Chapter 3 also gives an example that demonstrates the fixturing stability analysis procedure.

Experimental validation of the theoretical models and procedure using machining and modal impact tests is described in Chapter 4. Measured and predicted dynamic

responses, modal properties, and the fixturing stability of a machining fixture-workpiece system under various conditions are compared and discussed.

Chapter 5 presents a systematic study of the material removal effect on the fixture-workpiece system dynamics in machining. Models are developed to capture a variety of material removal induced phenomena such as changes in system inertia, changes in geometry and stiffness, and rate of change of system inertia. Experimental data collected in a pocketing process including modal impact tests are used to validate the models. Insight into the material removal effect on fixture-workpiece system dynamics and global properties is provided.

Chapter 6 investigates the roles of important fixture design and machining process parameters in affecting the dynamic performance of a machining fixture-workpiece system and the sensitivity of the fixturing dynamic stability to the imprecision in fixture design.

Chapter 7 addresses the issue of clamping force optimization and develops an approach for determination of the minimum required clamping forces that ensure the fixturing dynamic stability of a machining fixture-workpiece system. The effect of material removal on clamping force optimization is investigated via an application example.

The major conclusions drawn from this thesis research and recommendations for future work are summarized in Chapter 8.

CHAPTER 2

LITERATURE REVIEW

This chapter reviews the current state of knowledge in the area of machining fixtures including some robotic grasping work relevant to this thesis. The first section introduces prior work on modeling and analysis of machining fixture-workpiece systems concentrating on fixture-workpiece dynamics and material removal effect. The second section reviews previous works that deal with analysis and verification of fixturing stability in machining. Prior efforts on sensitivity analysis of the performance of a fixture-workpiece (or hand-object) system are discussed in the third section. The fourth section surveys the literature in the area of fixture synthesis. The last section summarizes the issues that require further investigation and form the central topics of this thesis.

2.1 Modeling and Analysis of Machining Fixture-Workpiece Systems

Numerous research efforts have been reported in the past decades for modeling and analysis of machining fixture-workpiece systems. The majority of prior work treats the fixture-workpiece system as quasi-static and ignores the system dynamics (e.g., [2]-[8]). In reality, machining processes such as milling are characterized by periodic forces. When the excitation frequency is in the vicinity of a natural frequency of the fixture-workpiece system, consideration of system dynamics is crucial.

Prior to 1990, research on the fixture-workpiece system dynamics was limited and largely experimental in nature. For example, Shawki and Abdel-Aal [9]-[12] experimentally studied the rigidity of fixture-workpiece systems with linear and nonlinear contact elastic deformations under static and dynamic conditions. Daimon et al. [13] described a method for selecting additional supports to improve the workpiece dynamic rigidity based on a finite element (FE) model. Other early works on analysis of fixture-workpiece system dynamics include [14]-[16], which experimentally examined the effect of a fixture on machining system outputs. While these empirical studies reported insightful results and interpretations, they are limited to specific machining environments and hence are difficult to generalize.

In 1991, Mittal et al. [17] modeled a fixture-workpiece system using the Dynamic Analysis and Design System (DADS) software with the fixture-workpiece contact modeled as a lumped spring-damper-actuator element. Liao and Hu [18] extended Mittal et al.'s work by considering the workpiece structural compliance and contact friction through the combined use of DADS and the finite element (FE) method. In both studies, lift-off of the workpiece from the fixture elements during machining was analyzed, but macro-slip was not considered. Liao and Hu [19] also presented an integrated FE model of a fixture-workpiece-machine tool system and investigated the effect of system vibrations on the surface error of the machined workpiece. Their approach partially relied on experimental data and the issue of fixturing stability was not addressed. More recently, Deiab et al. [20] modeled the fixture-workpiece dynamics using an FE-based method and investigated its effect on the chip load and the resulting machining process dynamics.

Having observed the difficulty and sensitivity of the FE method to the boundary condition representation of a fixture-workpiece system, Hockenberger and DeMeter [21] developed meta-contact mechanics functions and applied them to simulate the nonlinear conditions of stick, slip, and lift-off at a fixture-workpiece interface. Tao et al. [22] presented a sensor-integrated fixture system, in which real-time reaction forces of locators during machining were measured in order to estimate the dynamic behavior of the fixture-workpiece system. In general, sensor-based approaches are accurate but they greatly increase the production cost.

A couple of researchers have investigated the effect of friction induced damping on the fixture-workpiece dynamics. Fang et al. [23]-[24] developed a dynamic model, which considers the vibrations of both the workpiece and fixture elements, to predict the friction damping under different clamping forces. Friction damping was found to increase and then decrease as the clamping force increases due to the phenomenon of interface locking. Similar findings were reported by Motlagh et al. [25] who employed a combination of the bristles concept and a modified version of the Armstrong friction model to study the dynamic interactions of the fixture and the workpiece.

Despite the aforementioned works that address the fixture-workpiece system dynamics, none considers the material removal effect in machining. Continuous material loss and the resulting change in fixture-workpiece system dynamics are characteristic of a machining process. As shown later in this thesis, ignoring the material removal effect can lead to erroneous analysis of system performance especially under aggressive machining conditions or when a large percentage of material is removed in an operation, e.g., machining of monolithic aerospace parts. Liu and Strong [26] modeled the change in

workpiece weight during machining, but the fixture-workpiece system was treated as quasi-static. Kaya and Öztürk [27] applied an element death technique to simulate the chip removal process for fixture layout verification. In their study, the machining process was discretized into a number of steps and at each step a static analysis was performed.

It should be mentioned that work has been reported on modeling and analysis of the dynamics of a multi-fingered hand-object system. Such a system is employed in robotic grasping applications. However, there are three major differences between machining fixtures and robotic grasps:

1) all contacts in robotic grasping are active while in fixturing only clamps are active (locators are not);
2) an object grasped by a multi-fingered robotic hand generally experiences free vibrations resulting from external perturbations while forced vibrations occur to a fixtured workpiece in a machining operation; and
3) a grasped object usually needs to move along a designed trajectory to perform a task while a fixtured workpiece in machining must stay stable in the machine tool.

Therefore, work done in the area of robotic grasping is not included in this review unless it is directly relevant to this thesis.

2.2 Fixturing Stability Analysis

Fixturing stability is an important concern in machining fixture design and refers to the ability of a fixture to fully restrain a workpiece that is subjected to external forces generated by the machining operation. An unstable workpiece in machining will result in poor part quality or even operational accidents.

The majority of prior work on fixturing stability analysis is static or quasi-static. Early efforts in this area focused on the study of form closure and force closure. Form closure is defined as the ability of a fixture to prevent the workpiece from moving in any direction. Lakshminarayana [28] reported a mathematical proof that a minimum of seven contact points are needed to form close an object. Xiong et al. [29] proposed two quantitative indices, sum of all normal contact forces and the maximum normal contact force, to assess form-closure fixtures. A force closure is a fixture/grasp configuration in which the contact forces and torques can be adjusted to balance any applied external load. Unlike form closure, force closure is achieved with the aid of contact friction. Markenscoff et al. [30] proved that at least four frictional point contacts are needed to force close an object.

The concept of friction cone has been widely used in quasi-static verification of fixturing stability (e.g., [3], [6]-[8], and [31]). A virtual friction cone, shown in Figure 2.1, is defined for each fixture-workpiece contact. The tip of the cone coincides with the contact point and the half angle of the cone, θ, equals ($\tan^{-1}\mu$), where μ is the static coefficient of friction at the contact. To achieve stable fixturing, the resultant contact

force, $\overline{R}$, must lie inside the cone at all times to prevent slip and loss of contact between the fixture and the workpiece.

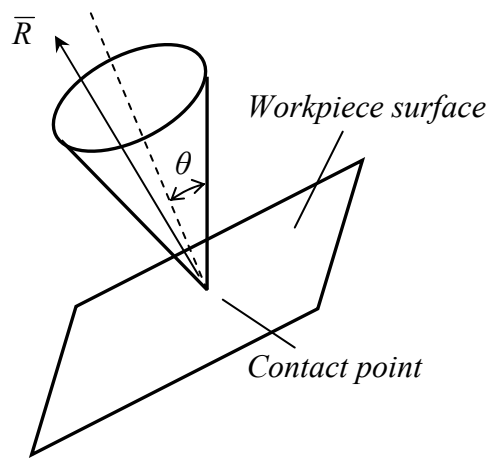

Figure 2.1 Virtual friction cone at a fixture-workpiece contact

Roy and Liao [32] presented a methodology for analysis of the stability of a fixtured workpiece, and the workpiece stability was defined as its capability of resisting disturbance and remaining in static equilibrium. Hurtado and Melkote [33] reported a model to analyze the effect of fixture conformability on the static stability of a fixture-workpiece system. In their work, the smallest eigenvalue of the stiffness matrix of the fixture-workpiece system was used as a measure of fixturing stability based on the fact that all eigenvalues of the stiffness matrix must be nonnegative for the fixtured workpiece to be stable. This type of stability measure has been widely used in the area of robotic grasping (e.g., [34]-[36]). Other grasping stability measures have been reported but are beyond the scope of this review.

Limited work has been done on analysis of fixturing stability in machining considering the fixture-workpiece dynamics. Mittal et al. [17] presented a dynamic model of the fixture-workpiece system to analyze the fixturing stability of the system. In their work, the fixturing instability is defined as loss of contact between the workpiece and locators but slip at the fixture-workpiece contact is not considered. In addition, they used the trial and error method to find appropriate clamping forces with all clamps assumed to apply the same amount of force. Similar limitations can be found in the work of Liao and Hu [18], which reported a dynamic analysis of the machining fixture-workpiece system using an FE-based approach and verified the system contact stability by obtaining the time history of the workpiece motion at the fixture-workpiece contact. In general, FE-based methods suffer from high computational cost and high sensitivity of model outputs to inaccuracies in representing the boundary condition. In addition, both prior efforts discussed above ignored the material removal effect in machining.

It should be mentioned that works have been reported on fixturing and machining of aerospace monolithic parts that involve large volume of material removal and thin features. Tlusty et al. [37] developed a thin web machining technique that uses the stiff, uncut portion of the workpiece to support the flexible section being cut. Smith and Dvorak [38] reported strategies to achieve chatter-free machining of thin web parts. The tool path is chosen strategically so that the tool always cuts the floor near the support of the uncut workpiece. However, neither of these works considered fixture-workpiece dynamics and material removal effect because they do not use unilateral frictional contacts to fixture the part. However, for parts that require unilateral contacts, these effects are important to consider.

2.3 Sensitivity Analysis of Fixture Performance

The performance of a machining fixture, measured by the fixturing stability and part quality, is affected by the precision of fixture design parameters (e.g., fixture layout and clamping forces). In reality, all fixture design parameters have some degree of imprecision. Therefore, it is important to investigate the sensitivity of fixture performance measures to fixture imprecision in order to design robust fixtures. In addition, sensitivity analysis can be used to assess and compare the roles of individual fixture parameters.

The open literature has no information on sensitivity analysis of the dynamic performance of machining fixtures. However, substantial work has been done on modeling and analysis of variation (or uncertainty) propagation (or accumulation) in fixturing, machining, and assembly processes based on kinematic or quasi-static models. Some of these works are reviewed here because they are relevant to the sensitivity analysis of fixture performance. Cai et al. [39] presented a geometrical method to minimize the resultant workpiece quality error due to the workpiece surface errors and fixture set-up errors. Estrems et al. [40] modeled the machining inaccuracies in the presence of dimensional errors of the workpiece and fixture elements. Liu and Hu [41] developed models to predict the mechanistic variation of the assembly of sheet metal parts with the combined use of FE and statistical methods. Camelio et al. [42] evaluated the propagation of dimensional variations of various components including the fixture in a multi-station system for assembly of flexible parts. Zhong [43] reported a model based on the combined use of Monte Carlo simulation and the homogeneous transformation

matrix method for calculation of the variation propagation in integrated machining-assembly systems. Shen and Duffie [44] analyzed the uncertainty in coordinate transformation in manufacturing systems due to a variety of error sources including the geometric variation of the workpiece and locators and the inaccuracies in coordinate measurements.

A couple of works that are more relevant to this thesis are found in the literature on robotic grasping. Shimoga and Goldenberg [45] analyzed the sensitivity of the three features (stability, decoupled force/motion relation, and decoupled time response) achieved by a grasp with an admittance center [46] to the imprecision on the grasp configuration and finger tip impedance parameters. Based on an optimization model that calculates the contact forces in a multi-fingered grasp, Hershkovitz and Teboulle [47] studied the effect of perturbing model parameters on the grasping quality measures. In this work, the sensitivity analysis was performed by transforming the primal, constrained optimization problem into a dual, unconstrained formulation. Analytical methods, however, are difficult to apply on a grasp or fixture whose quality measures are highly nonlinear functions of the design parameters.

2.4 Fixture Synthesis

Fixture design is essentially an optimization problem. Major concerns in fixture synthesis include the determination of minimum required clamping forces and optimization of fixture design parameters to achieve objectives such as stability of the

fixtured part, specified part tolerances, etc. Many researchers have investigated the issue of machining fixture synthesis, resulting in a large number of papers. However, none has simultaneously considered the fixture-workpiece system dynamics and its continuous change during machining due to the material removal effect.

The problem of clamping force optimization has been investigated extensively. The majority of previous work treats the fixture-workpiece system as quasi-static and ignores the system dynamics. It is quite common in prior work to use fixturing stability as the objective in clamping force optimization. DeMeter et al. [48] developed a linear programming (LP) model to estimate the minimum required clamping loads that prevent slip at the fixture-workpiece contacts during machining. The fixture-workpiece system deformations due to clamping and machining are considered to be static. Kang et al. [8] calculated the minimum clamping forces with the help of a contact stability index sensitivity matrix, which is a variation of the friction cone concept. Meyer and Liou [49] also presented an LP model in which the time-varying machining loads were discretized to fit the quasi-static analysis. Xiong et al. [50] formulated the clamping optimization problem as a constrained nonlinear programming problem based on the concept of passive force closure. Li et al. [51] reported a model that calculates the reaction forces and moments at the fixture-workpiece contacts for machining fixtures with large contact areas and then the model was used to determine the minimum clamping force that enables the workpiece to remain in static equilibrium during machining. Several researchers such as Wang et al. [52], Tao et al. [53], and Liu and Strong ([26] and [54]) proposed the idea of dynamic clamping to take into consideration the time-varying nature of the machining loads. In their works, the tool path was discretized and the points where the peak

machining force was assumed to appear were selected and used in the quasi-static analysis.

Another common objective in clamping force optimization is part quality error. Gui et al. [55] examined the impact of clamping forces on the workpiece location accuracy based on a static model. Huang and Wang [56] minimized the static elastic deformation of the workpiece by varying the clamping force. Nee et al. [57] reported a sensor-assisted fixture that was capable of delivering varying clamping loads, calculated from a quasi-static model, to minimize the workpiece distortion.

Other objectives can also be achieved via clamping force optimization. For example, Hurtado and Melkote [58] presented a multi-objective nonlinear optimization model that can be used to find the minimum clamping loads for achieving workpiece shape conformability and fixture stiffness goals.

In addition to lack of consideration of the fixture-workpiece system dynamics, the previous work (e.g., [48], [55], and [59]) on clamping force optimization generally assumes that the fixture-workpiece contact stiffness is independent of the clamping force, which, for non-planar contact geometries, is not true as shown later in this thesis.

A number of researchers have developed models to solve the fixture layout optimization problem for achieving the specified tolerances of the workpiece features. Wang [60] used a configuration matrix to describe the relationship between the workpiece localization error and the positioning deviations of the fixture elements. Then, the critical properties of the matrix were used as objectives to find the optimal locator layout that reduces the geometric variations at critical points on the machined features. Li and Melkote [61] presented a contact mechanics-based model to improve the workpiece

location accuracy through optimal placement of locators and clamps around the workpiece. Huang and Hoshi [62] optimized the fixturing support layout to reduce the surface flatness error due to the cutting heat.

The genetic algorithm (GA) technique has been widely used to solve the fixture optimization problem. Kulankara et al. [63] applied the GA in fixture layout and clamping force optimization for minimization of the workpiece static deformation. Liao [64] also used the GA to find the optimal numbers of locators and clamps as well as their optimal positions in sheet metal assembly such that the workpiece deformation and variation are minimized. In these models, the locations of the fixture elements are often represented by nodes in the FE model to facilitate the application of the GA. Vallapuzha et al. [65] investigated the use of spatial coordinates to represent the locations of the fixture elements in their fixture layout optimization model solved using the GA. Vallapuzha et al. [66] also compared the effectiveness of four fixture layout optimization methods – continuous GA, discrete GA, continuous SQP (Sequential Quadratic Programming), and discrete SQP. The continuous GA method was found to have the best overall performance.

Many models reported in the literature for fixture performance evaluation are FE-based. When these models are used for fixture synthesis, the FE model needs to be solved many times and consequently the computational cost is extremely high. To overcome this drawback, DeMeter [67] developed a fast support layout optimization model to minimize the maximum displacement-to-tolerance ratio of a set of workpiece features by recognizing the unique properties of the support layout problem and eliminating the degrees of freedom of irrelevant nodes from the full stiffness model. Based on the same

approach, Sayeed and DeMeter [68] presented a linear, mixed-integer programming model for determination of the optimal fixture layout to reduce the effect of the workpiece static deformation on the geometric error of the machined features.

A few researchers have examined the effect of clamping sequence on part quality based on quasi-static models. Cogun [69] found that the effect of clamping forces on the workpiece deformation could be controlled by creating adequate contact frictional forces through choice of a rational clamping sequence. Raghu and Melkote [70] modeled the effect of clamping sequence on the workpiece location error.

In the fixture synthesis literature, the only work that considers the fixture-workpiece system dynamics was reported by Li and Melkote [59] who presented an approach for simultaneous optimization of the fixture layout and clamping force to improve the workpiece location accuracy. In their work, the equations of motion governing the fixture-workpiece system dynamics in machining were derived using the Newton-Euler method. However, the material removal effect was ignored and the fixturing stability issue was not addressed.

2.5 Summary

An extensive review of previous work in the area of modeling, analysis, and synthesis of machining fixture-workpiece systems has been conducted in this chapter. Major conclusions of this review are summarized as follows:

- The volume of literature in research on machining fixtures is large. However, the majority of prior work has treated the fixture-workpiece system as quasi-static and ignored the system dynamics.
- Dynamics has been considered by a few researchers in modeling and analysis of machining fixture-workpiece systems and fixturing stability verification. However, none has taken into account the effect of material removal on the system characteristics and dynamic behavior during machining.
- A couple of efforts in the literature addressed the issue of material removal in machining but both treat the fixture-workpiece system as quasi-static.
- Despite numerous models and approaches reported in the area of fixture synthesis, only one [59] simulated the fixture-workpiece dynamics during machining but again ignored the material removal effect.
- Experimental investigation of the dynamic performance of a fixture-workpiece system in machining and the effect of material removal on the dynamic behavior and properties of the system is absent in the open literature.

To overcome limitations of the existing works and advance the knowledge base of machining fixtures, this thesis work is aimed at establishing a model-based framework for analysis and synthesis of the dynamic behavior with an emphasis on fixturing dynamic stability of a machining fixture-workpiece system considering the material removal effect. At the same time, machining experiments and modal impact tests are to be designed and performed to validate the theoretical models and procedures and to

investigate the role of the fixture and the effect of material removal on the dynamic properties and performance of the machining fixture-workpiece system.

CHAPTER 3

MODELING AND ANALYSIS OF FIXTURING DYNAMIC STABILITY IN MACHINING

A fixture-workpiece system subjected to machining operations shows significant dynamics that directly affects operational safety and part quality. This chapter presents a systematic mathematical procedure for modeling and analysis of the fixturing dynamic stability of an arbitrarily configured fixture-workpiece system in machining. The procedure consists of a static model to calculate the workpiece contact deformation due to clamping, a dynamic model to predict the workpiece motion due to machining, a geometric model to capture the continuous change of system geometry and inertia due to the material removal effect, and a module to simulate the overall behavior of the fixtured workpiece and detect instabilities at fixture-workpiece interfaces.

This chapter is organized as follows. First, the problem of modeling and analysis of fixturing dynamic stability in machining is formulated and the overall approach is introduced. Then, the criteria for fixturing dynamic stability are defined, followed by the development of theoretical models that form the procedure for analysis of fixturing dynamic stability. Next, a simulation example is given to illustrate the models and procedure and the results discussed. Finally, the current chapter is summarized and major conclusions are drawn.

3.1 Problem Formulation and Approach

This chapter focuses on a structurally rigid workpiece (e.g., a solid block) surrounded by L locators and C clamps and subjected to a machining operation as shown schematically in Figure 3.1. The workpiece can be of arbitrary shape but needs to be convex at the fixture-workpiece contacts since only non-conformable contacts are considered in this thesis. The structural compliance of the workpiece is assumed to be negligible compared to the fixture-workpiece contact compliance and the structural compliance of the fixture elements. The validity of this assumption is analyzed later in this chapter in the simulation example. This work also assumes that the machine tool and the fixture bodies (e.g., steel blocks used to mount fixture tips) are rigid. In addition, the fixture-workpiece contact stiffness is considered to be clamping force dependent but independent of workpiece vibration.

Three coordinate systems are used to describe the position and orientation of the workpiece (see Figure 3.1): 1) global coordinate system (XYZ), 2) workpiece coordinate system (xyz), which is fixed to the center of gravity of the workpiece with its coordinate axes aligned with the principal inertia axes of the workpiece, and 3) local coordinate system ($x_iy_iz_i$), which is fixed at the ith fixture-workpiece contact such that the z_i axis coincides with the inward pointing normal to the workpiece and the x_i and y_i axes lie in the tangent plane of the workpiece.

Unless noted otherwise, matrices given in this thesis to describe the system properties are represented in the (xyz) frame.

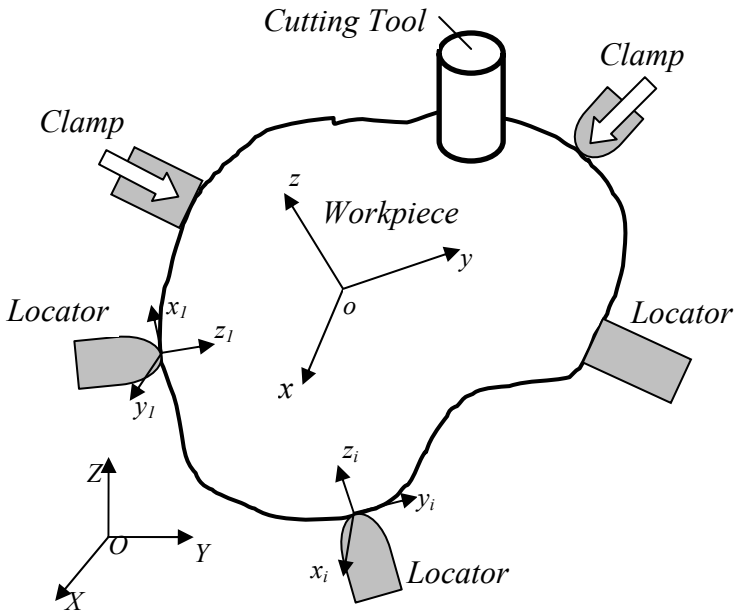

Figure 3.1 An arbitrarily configured machining fixture-workpiece system

The workpiece undergoes rigid body motion during clamping and machining due to elastic deformation, slip, and/or lift-off at the fixture-workpiece contacts. From the standpoint of operational safety and machining accuracy, lift-off and macro-slip at the fixture-workpiece contacts are undesirable because they result in loss of total restraint of the workpiece in the fixture. Hence, the dynamic status of each fixture-workpiece contact during machining needs to be modeled and evaluated to detect lift-off and macro-slip.

Two models are developed to calculate the contact elastic deformation of the workpiece due to clamping and its dynamic motion due to machining, respectively. The static and dynamic displacements of the workpiece at each fixture-workpiece contact are then superposed and the stability criteria, described in Section 3.2, are applied to detect the onset of fixturing instabilities. To capture the material removal effect in machining, a

geometric model is developed to extract the time-varying information of the system geometry and inertia and this information is fed to the dynamic model. The procedure for analysis of fixturing dynamic stability in machining is summarized in the block diagram shown in Figure 3.2. Note that the static model is also used to generate the stiffness matrix of the fixture-workpiece system in addition to the workpiece elastic deformation.

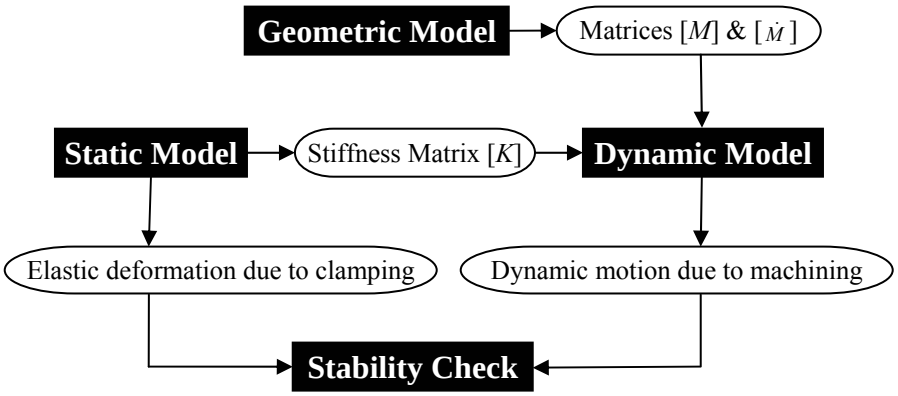

Figure 3.2 Procedure for analysis of fixturing dynamic stability in machining

3.2 Criteria for Fixturing Dynamic Stability

As illustrated in Figure 3.3, the status of a fixture-workpiece contact during machining falls into one of the following three types – full stick, macro-slip, and lift-off. Macro-slip and lift-off have been identified as two types of fixturing instabilities. Physically, lift-off occurs when the localized elastic deformation (compression) of the workpiece at a fixture-workpiece contact due to clamping is smaller than the maximum

workpiece displacement away from the fixture element due to machining loads; macro-slip occurs when the Coulomb friction law (assumed to apply at each contact) is violated under the combined effects of clamping and machining.

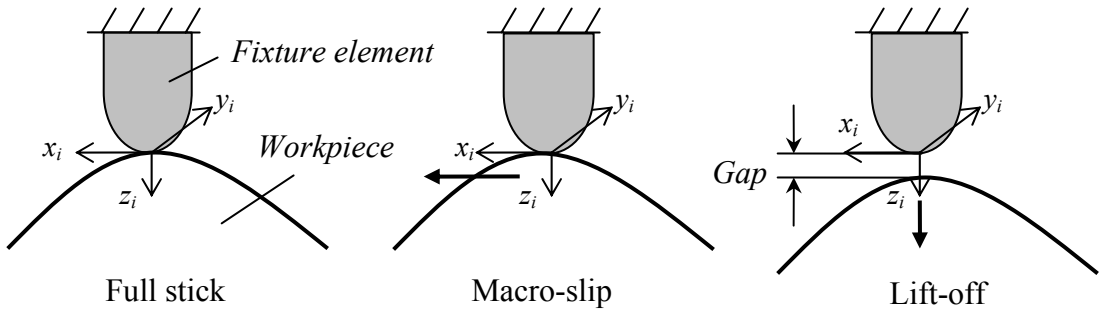

Figure 3.3 Dynamic status at a fixture-workpiece contact

In the contact coordinate system ($x_iy_iz_i$ in Figures 3.1 and 3.3), lift-off is equivalent to a positive displacement of the workpiece in the z_i direction, and macro-slip occurs when the resultant friction force in the x_iy_i plane exceeds a limit determined by the normal force in the z_i direction and the static coefficient of friction at the contact. Therefore, the criteria for fixturing dynamic stability can be written as follows:

$$\max_t \{\Delta_{iz}(t)\} \le 0 \tag{3.1}$$

$$\max_t \{\sqrt{[k_{ix}\,\Delta_{ix}(t)]^2 + [k_{iy}\,\Delta_{iy}(t)]^2} - \mu_S^i [k_{iz}|\Delta_{iz}(t)|]\} \le 0$$

where, t is the machining time; $\Delta_{ix}(t)$, $\Delta_{iy}(t)$, and $\Delta_{iz}(t)$ are the superposed displacements of the workpiece at the ith fixture-workpiece contact in the x_i, y_i, and z_i directions, respectively; i = 1 to (L+C); μ_S^i is the static coefficient of friction at the ith contact; k_{ix}, k_{iy}, and k_{iz} are the local composite stiffnesses in the x_i, y_i, and z_i directions, respectively.

The total displacement of workpiece at the ith fixture-workpiece contact due to the combined effects of clamping and machining is given by:

$$\Delta_{ij}(t) = d_{ij}(t) - \delta_{ij} \qquad for\ \ j = x,\ y,\ z \tag{3.2}$$

where symbols d and δ represent the dynamic and static displacements, respectively.

Models needed to compute the two types of displacements in Equation (3.2) are developed next.

3.3 The Dynamic Model

The workpiece is modeled as a rigid body (as analyzed in Section 3.2) with its motion descried by a vector $\overline{q}$ and $\overline{q} = \{\Delta\overline{r} \quad \Delta\overline{\theta}\}^T \in R^6$, where $\Delta\overline{r} = \{\Delta x \quad \Delta y \quad \Delta z\}^T$ represents the three translations and $\Delta\overline{\theta} = \{\Delta\alpha \quad \Delta\beta \quad \Delta\gamma\}^T$ the three rotations. Note that the rigid body assumption is relaxed in Chapter 5 to account for the influence of the workpiece structural compliance.

Assuming the mass of the fixture elements (locators and clamps) to be negligible compared to the mass of the workpiece, the kinetic energy of the fixture-workpiece system can be written as,

$$T = \frac{1}{2}\dot{\overline{q}}^T[M]\dot{\overline{q}} \tag{3.3}$$

where, $[M] = \begin{bmatrix} mU_3 & 0 \\ 0 & I \end{bmatrix} \in R^{6\times 6}$ is the inertia matrix and m is the mass of the workpiece; U_3 is a 3×3 identity matrix; and $[I] \in R^{3\times 3}$ is the workpiece centroidal inertia matrix.

The small motion assumption allows Taylor's expansion of the potential energy function $V = V(\overline{q})$ of the system about its equilibrium position. By ignoring the higher order terms and noting that the gradient of the potential energy is zero at the equilibrium position, V can be approximated by,

$$V \approx V(0) + \frac{1}{2}\overline{q}^T [K]\overline{q} \tag{3.4}$$

where $[K]$ is the intrinsic stiffness matrix of the fixture-workpiece system.

Damping, experimentally shown later (Chapters 4 and 5) to be rather light for the cases and workpiece materials analyzed in this thesis, is not considered here.

The Lagrange's Energy Method [71], given in Equation (3.5), is applied to derive the governing equations of motion of the fixture-workpiece system.

$$\frac{d}{dt}\left(\frac{\partial T}{\partial \dot{\overline{q}}}\right) - \frac{\partial T}{\partial \overline{q}} + \frac{\partial V}{\partial \overline{q}} = \overline{Q} \tag{3.5}$$

Assuming $[M]$ is independent of $\dot{\overline{q}}$, which is valid for Newtonian motion, the first term in Equation (3.5) is obtained by differentiating Equation (3.3),

$$\frac{d}{dt}\left(\frac{\partial T}{\partial \dot{\overline{q}}}\right) = \frac{d}{dt}([M]\dot{\overline{q}}) = [\dot{M}]\dot{\overline{q}} + [M]\ddot{\overline{q}} \tag{3.6}$$

where $[\dot{M}] = \begin{bmatrix} \left(\frac{dm}{dt}\right)U_3 & 0 \\ 0 & \frac{d[I]}{dt} \end{bmatrix} \in R^{6\times 6}$ is the rate of change of system inertia. Note that, for a machining fixture-workpiece system, this term exists because the workpiece continuously loses material during machining and hence the system inertia changes instantaneously.

The second term in Equation (3.5) vanishes and the third term is obtained as follows,

$$\frac{\partial V}{\partial \overline{q}} = [K]\overline{q} \tag{3.7}$$

Therefore, a second-order differential equation that governs the vibratory motion of the fixtured workpiece during machining is obtained as follows,

$$[M]\ddot{\overline{q}} + [\dot{M}]\dot{\overline{q}} + [K]\overline{q} = \overline{Q}(t) \tag{3.8}$$

The right hand side of Equation (3.8), $\overline{Q}(t)$, represents the external loads applied to the system. For a typical fixtured prismatic workpiece subjected to end milling for instance (see Figure 3.4), $\overline{Q}(t)$ is given by,

$$\overline{Q}(t) = \begin{Bmatrix} \overline{F}(t) \\ \overline{\Gamma}(t) + \overline{r}_m(t) \times \overline{F}(t) \end{Bmatrix} \in R^6 \tag{3.9}$$

where, $\overline{F}(t)$ and $\overline{\Gamma}(t)$ represent the machining force and torque vectors, respectively, and $\overline{r}_m(t)$ is the position vector from the center of gravity (C.G.) of the workpiece to the machining point *M*.

The machining point *M*, as shown in Figure 3.5, is defined simply as the center of a curved region that represents the instantaneous area of contact between the tool and the workpiece. The real tool/workpiece in-cut geometry is quite complicated for a multi-tooth machining process. However, a more precise analysis is unnecessary since it is computationally expensive and, as will be seen later in this thesis, unwarranted. Note that the workpiece weight is not present in Equation (3.8) because it is considered in the static model that calculates the contact stiffness of the fixture-workpiece system and is described in the next section.

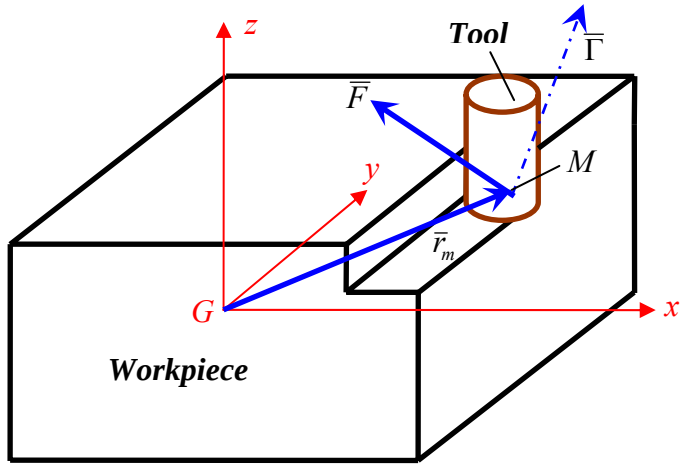

Figure 3.4 Cutting load vectors imposed on a prismatic workpiece during end milling

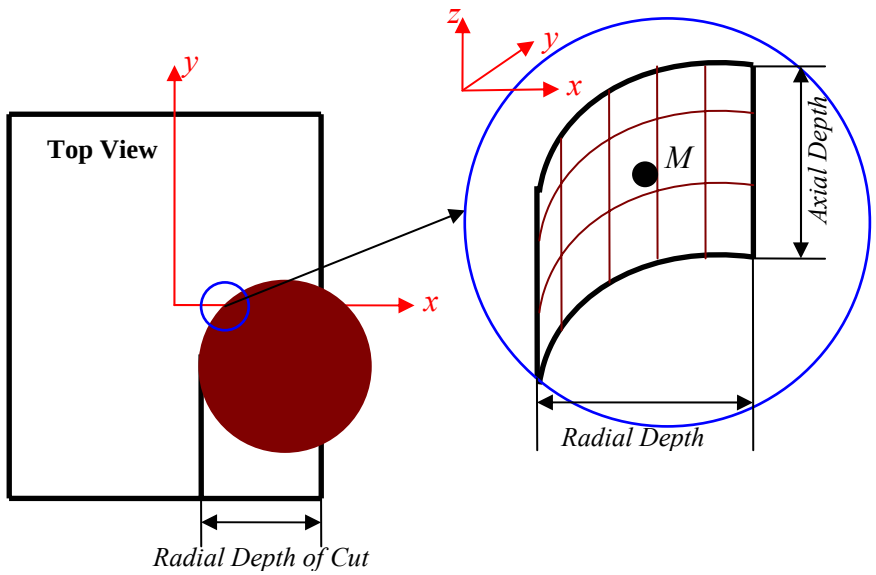

Figure 3.5 Approximation of the point of machining force application

3.4 The Static Model and Fixture-Workpiece System Stiffness

In this section, the static model mentioned in Figure 3.2 is developed to calculate the contact elastic deformation of the workpiece due to clamping loads and to derive the fixture-workpiece contact stiffness, which is considered to vary with the clamping loads. Then the intrinsic stiffness matrix of the fixture-workpiece system is derived from the local stiffness at the fixture-workpiece contacts. The local stiffness of the system includes the contact stiffness and the structural stiffness of the fixture elements. Each fixture element is modeled as a cantilever and its stiffness is calculated accordingly.

3.4.1 The Static Model

Upon clamping, the workpiece is in static equilibrium under the action of clamping loads and its weight. To calculate the elastic deformation of the workpiece at a fixture-workpiece contact due to clamping, the contact reaction force must be known. The principle of minimum total complementary energy [72] is applied here to develop a model that yields the reaction force at each fixture-workpiece contact.

Because the structural compliance of the workpiece is not considered, the total complementary energy of the fixture-workpiece system is composed of two parts: energy from the fixture-workpiece contacts and energy from the fixture elements.

The complementary energy of fixture-workpiece contacts can be computed from the contact force-displacement relationships, reported in the contact mechanics literature. For a spherical-tipped fixture element pressed against a curved workpiece surface, the relationship is given by [73],

$$\delta_z = \left[\frac{9P^2}{16R(E^*)^2} \right]^{1/3} \tag{3.10}$$

$$\delta_j = \frac{Q_j}{8a} \left(\frac{2-\upsilon_w}{G_w} + \frac{2-\upsilon_f}{G_f} \right) \qquad \text{for } j = x \text{ or } y$$

where, δ_z and P represent the contact deformation and reaction force in the normal (z) direction, respectively, while δ_j and Q_j ($j = x$ or y) represent the contact deformation and reaction force in the tangential (x or y) direction, respectively; $R = (1/R_w + 1/R_f)^{-1}$ is the relative curvature at the contact with R_w being the local radius of the workpiece surface and R_f being the tip radius of the fixture element; $1/E^* = (1-\upsilon_w^2)/E_w + (1-\upsilon_f^2)/E_f$; υ, E, and G represent the Poisson's ratio, Young's modulus, and shear modulus of the material, respectively; the subscripts w and f refer to the workpiece and fixture elements, respectively; $a = (3PR/4E^*)^{1/3}$ is the radius of the contact region. Force-displacement relationships for other contact geometries are also available [73].

It is clear from Equation (3.10) that the relationship between the contact force and the resulting deformation for a spherical-tipped fixture element is nonlinear. Therefore, the complementary energy from all (L+C) fixture-workpiece contacts is written as,

$$\Pi_c = \sum_{i=1}^{(L+C)} \left(\int_0^{P_i} \delta_{izc}\, dP_i + \int_0^{Q_{ix}} \delta_{ixc}\, dQ_{ix} + \int_0^{Q_{iy}} \delta_{iyc}\, dQ_{iy} \right) \tag{3.11}$$

where the subscript c refers to contact while $i = 1, \ldots, (L+C)$.

The fixture elements are modeled as linear springs and the complementary energy of the (L+C) fixture elements is as follows,

$$\Pi_f = \frac{1}{2} \left(\frac{P_i^2}{k_{izf}} + \frac{Q_{ix}^2}{k_{ixf}} + \frac{Q_{iy}^2}{k_{iyf}} \right) \tag{3.12}$$

where k_{ixf}, k_{iyf}, and k_{izf} are the structural stiffnesses of the ith fixture element in the x_i, y_i, and z_i directions, respectively.

The total complementary energy of the fixture-workpiece system is then given by,

$$\Pi_t = \Pi_c + \Pi_f \tag{3.13}$$

The contact reaction forces can be found by minimizing Equation (3.13) subject to a set of constraints. The first constraint comes from the static equilibrium condition of the system and is given as follows,

$$\sum \overline{F} = \overline{0} \tag{3.14}$$

$$\sum \overline{M} = \overline{0}$$

where $\overline{F}$ and $\overline{M}$ represent the resultant force and moment vectors at the center of gravity of the workpiece in the (xyz) frame, respectively.

The second constraint results from the assumption that constant clamping forces are used and is written as,

$$P_j = F_{cj} \qquad \text{for} \quad j = (L+1), \ldots, (L+C) \tag{3.15}$$

Assuming the Coulomb friction law applies at each fixture-workpiece contact, the third constraint is obtained as follows,

$$\sqrt{(Q_{ix})^2 + (Q_{iy})^2} - \mu_S^i P_i \leq 0 \tag{3.16}$$

The unilateral nature of a fixture-workpiece contact gives the fourth constraint as,

$$P_i \geq 0 \tag{3.17}$$

The last one is the non-yielding constraint on the contact stress and is given by,

$$P_i - S_y(\pi a_i^2) \leq 0 \tag{3.18}$$

where S_y is the yield strength of the workpiece material and a_i is the radius of the ith

contact region as noted earlier.

Therefore, the static model is obtained by combining Equations (3.11) through (3.18) and is summarized as follows,

$$\underset{P_i,\, Q_{ix},\, Q_{iy}}{Minimize}\ \Pi_t \tag{3.19}$$

$$\begin{aligned}
&Subject\ to: \\
&\quad \sum \overline{F} = \overline{0},\ \sum \overline{M} = \overline{0} \\
&\quad P_j = F_{cj} && \text{for } j = (L+1),...,(L+C) \\
&\quad \sqrt{(Q_{ix})^2 + (Q_{iy})^2} - \mu^i_S P_i \le 0 && \text{for } i = 1, \ldots, (L+C) \\
&\quad P_i \ge 0 && \text{for } i = 1,\ldots,(L+C) \\
&\quad P_i - S_y(\pi a_i^2) \le 0 && \text{for } i = 1,\ldots,(L+C)
\end{aligned}$$

Solving Equation (3.19) yields the contact reaction forces, P_i, Q_{ix}, and Q_{iy} with $i = 1$ to $(L+C)$, which are then substituted into Equation (3.10) to obtain the clamping force induced elastic deformation of the workpiece at each contact, δ_{ixc}, δ_{iyc}, and δ_{izc}.

3.4.2 Derivation of System Stiffness Matrix

The system stiffness matrix $[K]$ is derived from the stiffness of the fixture-workpiece system evaluated at the $(L+C)$ contacts as follows.

The workpiece motion, given by $\overline{q}$, results from the localized deformation of the workpiece at the $(L+C)$ fixture-workpiece contacts. Let $\overline{d}_i = \{d_{ix} \quad d_{iy} \quad d_{iz}\}^T \in R^3$ be the displacement vector of the workpiece at the ith contact in the local frame $(x_i y_i z_i)$ and $\overline{s}_{ix}, \overline{s}_{iy}$, and $\overline{s}_{iz}$ be the direction vectors of the x_i, y_i, and z_i axes in the (xyz) frame, respectively. From kinematics, it can be shown that,

$$\overline{d}_i = [S_i]^T \overline{q} \tag{3.20}$$

where, $[S_i] = \begin{bmatrix} \bar{s}_{ix} & \bar{s}_{iy} & \bar{s}_{iz} \\ \bar{p}_i \times \bar{s}_{ix} & \bar{p}_i \times \bar{s}_{iy} & \bar{p}_i \times \bar{s}_{iz} \end{bmatrix} \in R^{6\times 3}$ is the configuration matrix of the ith contact in the (xyz) frame, and $\bar{p}_i$ is the position vector of the ith contact in (xyz).

By writing $\bar{d} = [\bar{d}_1^T, \ldots, \bar{d}_i^T, \ldots, \bar{d}_{L+C}^T]^T \in R^{3(L+C)}$, the relationship between the local displacements of the workpiece and its motion at the center of gravity is given by,

$$\bar{d} = [S]^T \bar{q} \tag{3.21}$$

where, $[S] = [[S_1], \ldots, [S_i], \ldots, [S_{(L+C)}]] \in R^{6\times 3(L+C)}$ is the configuration matrix of the system and depends only on the fixture layout and the workpiece geometry. The derivations of matrices $[S_i]$ and $[S]$ are given in Appendix A.1.

The local stiffness matrix at the ith contact can be written as follows,

$$[K_i] = \mathrm{Diag}[k_{ix} \quad k_{iy} \quad k_{iz}] \in R^{3\times 3} \tag{3.22}$$

For a given fixture layout, arranging the (L+C) such matrices diagonally yields the contact stiffness matrix of the system, $[K_C]$,

$$[K_C] = \mathrm{BlockDiag}[[\mathrm{K}_1], \ldots, [K_i], \ldots, [K_{L+C}]] \in R^{3(L+C)\times 3(L+C)} \tag{3.23}$$

The potential energy of the fixture-workpiece system can then be written as,

$$V \approx V(0) + \frac{1}{2}\bar{d}^T [K_C]\bar{d} \tag{3.24}$$

Substitution of Equation (3.21) into Equation (3.24) yields,

$$V \approx V(0) + \frac{1}{2}\bar{q}^T [S][K_C][S]^T \bar{q} \tag{3.25}$$

Comparing Equations (3.4) and (3.25) gives,

$$[K] = [S][K_C][S]^T \tag{3.26}$$

3.4.3 Local Stiffness

At each fixture-workpiece interface, the overall compliance comes from three sources – fixture element, contact, and workpiece. Assuming that the contact deformation and stress are highly localized (valid when the workpiece is not very compliant and the contact area is small compared to the surface area of the workpiece), each source of compliance can be modeled as three linear springs in the x_i, y_i, and z_i directions of the local frame, respectively. The torsional compliance from all sources is considered to be negligible.

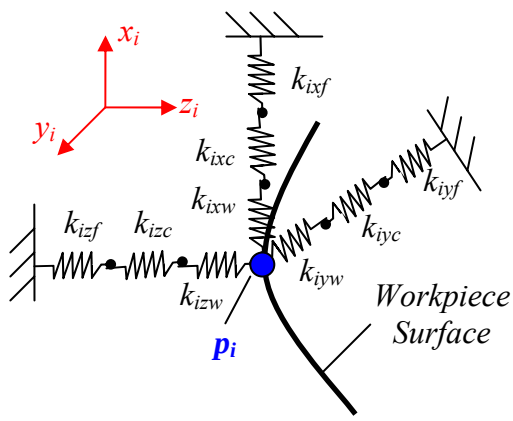

Figure 3.6 Composite stiffness at the ith fixture-workpiece contact

Therefore, as shown in Figure 3.6, the composite stiffness at the ith fixture-workpiece contact, p_i, is the summation in series of three stiffness components, k_{ijf}, k_{ijc}, and k_{ijw} ($j = x$, y, and z), representing the stiffness of the fixture element, contact, and workpiece, respectively. Equation (3.27) summarizes the calculation of the local stiffness of the fixture-workpiece system.

$$k_{ij} = [(k_{ijf})^{-1} + (k_{ijc})^{-1} + (k_{ijw})^{-1}]^{-1} \tag{3.27}$$

As mentioned earlier, this chapter focuses on structurally rigid workpieces whose structural compliance is considered to be negligible compared to other sources of compliance of the system and therefore k_{ijw} in Figure 3.6 and Equation (3.27) is equal to infinity here. Chapter 5, which discusses the material removal effect in machining, presents an FE-based approach to calculate k_{ijw} for relatively compliant parts.

The local stiffness quantities obtained from Equation (3.27) are used by Equations (3.22), (3.23), and (3.26) to derive the intrinsic stiffness matrix, [*K*], of the fixture-workpiece system.

3.4.4 Fixture-Workpiece Contact Stiffness

The fixture-workpiece contact stiffness, k_{ijc} in Equation (3.27), can be obtained by differentiating Equation (3.10) and is given by,

$$k_{zc} = \frac{\partial P}{\partial \delta_z} = \left(\frac{3}{2}\right)\left(\frac{16R(E^*)^2}{9}\right)^{1/3} P^{1/3} \tag{3.28}$$

$$k_{jc} = \frac{\partial Q_j}{\partial \delta_j} = 8a\left(\frac{2-\upsilon_w}{G_w} + \frac{2-\upsilon_f}{G_f}\right)^{-1} \qquad \text{for } j = x \text{ or } y$$

The static model, given by Equation (3.19), can be solved using standard nonlinear program solvers. Its solution, the reaction forces at the fixture-workpiece contacts due to clamping, is then substituted into Equation (3.28), in order to compute the contact stiffness.

3.4.5 Structural Stiffness of Fixture Element

A fixture element (locator or clamp) is modeled as a short or long cylindrical cantilever, depending on its length-to-diameter ratio. The following formulae derived from [74] are used to calculate the structural stiffness of a fixture element,

$$\begin{aligned} &\text{Bending Stiffness}: \; k_{ixf} = k_{iyf} = \begin{cases} (3E_{if}I_{if})/l_{if}^3, & (l_{if}/d_{if}) \geq 3 \\ (3G_{if}A_{if})/4l_{if}, & (l_{if}/d_{if}) < 3 \end{cases} \\ &\text{Axial Stiffness}: \; k_{izf} = \frac{E_{if}A_{if}}{l_{if}} \end{aligned} \tag{3.29}$$

where, E_{if}, G_{if}, l_{if}, A_{if}, d_{if}, and I_{if} are the Young's modulus, shear modulus, length, cross-sectional area, diameter, and polar moment of inertia of the ith fixture element, respectively.

3.5 The Geometric Model

The material removal process is simulated via a geometric model developed in ACIS®, a geometric modeling kernel. The approach involves discretizing the tool path into a series of increments whose size depends on the desired accuracy. At each increment, information such as the volume, center of gravity, and orientation of principal inertia axes of the machined workpiece is extracted. The information is then used to derive two time-varying matrices, inertia matrix $[M]$ and rate of change of inertia matrix $[\dot{M}]$, which are required by the dynamic model given in Equation (3.8).

Figure 3.7 illustrates the geometric simulation of material removal using ball-end milling as an example. A detailed, systematic investigation of the material removal effect on the fixture-workpiece system dynamics is presented in Chapter 5.

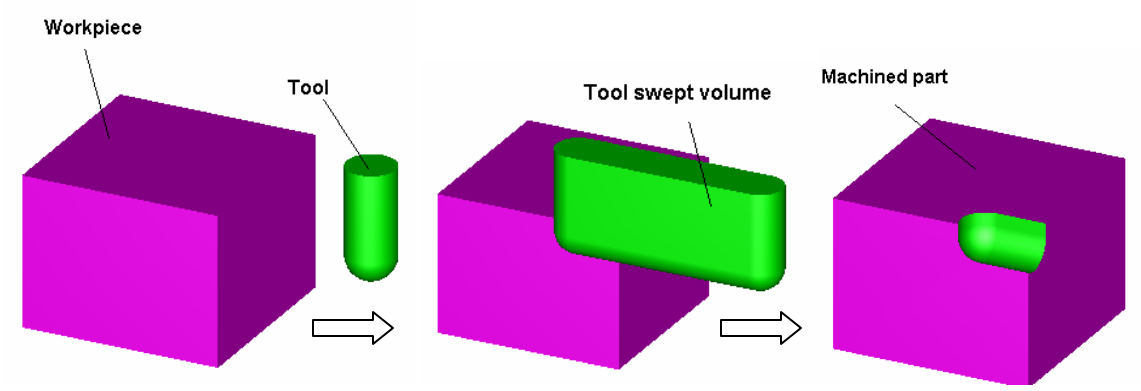

Figure 3.7 Geometric simulation of material removal

3.6 Simulation Example

This section gives a simulation example to demonstrate the developed models and procedure for analysis of fixturing dynamic stability in machining. Experimental validation of the models and procedure is presented in the next chapter.

3.6.1 Problem Data

This example considers an end milling operation. As illustrated in Figure 3.8, the original workpiece is a solid block of aluminum 7075 and the operation involves milling a step cut on the top surface of the workpiece. The operation consists of 30 depth levels along the *Z* axis, with 20 tool passes along the *Y* axis at each level. Therefore, there are a total of 600 passes with the first pass at the right end of the workpiece. The removed volume is about 43% of the total volume of the original workpiece. Cutting conditions

used in this example and the resulting machining forces are given and discussed in Section 3.6.3.

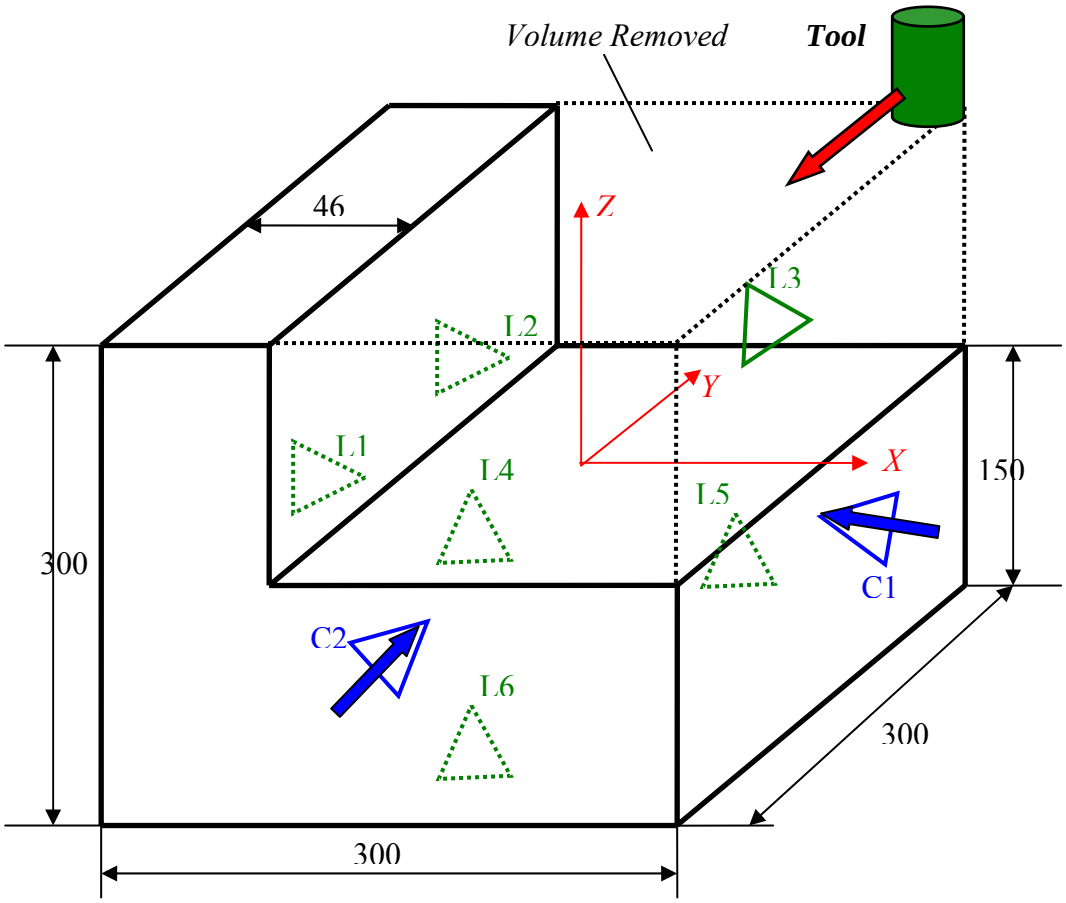

Figure 3.8 Final part and fixture layout (L1-L6: locators; C1-C2: clamps)
(Note: all dimensions are in mm.)

As seen in Figure 3.8, the workpiece is constrained by a 3-2-1 locator layout (L1-L6) and two side clamps (C1-C2) in this example. The two clamps are allowed to apply different forces but each force needs to remain constant during a single tool pass, which is achieved via hydraulic or pneumatic devices. The clamping forces used in this

operation vary with tool pass and are determined such that fixturing dynamic stability is achieved in each pass (see details in Section 3.6.5). The spatial coordinates of the fixture-workpiece contacts in the (*xyz*) frame are listed in Table 3.1. All fixture elements are identical with a cylindrical body (radius=20 mm and length=30 mm) and a spherical tip (radius=19.8 mm). The material properties of the workpiece and the fixture elements are given in Table 3.2.

Table 3.1 Coordinates of fixture-workpiece contacts

Locator	Coordinate (x, y, z) (mm)	Clamp	Coordinate (x, y, z) (mm)
L1	(-150, -50, -50)	C1	(150, 0, -50)
L2	(-150, 50, -50)	C2	(0, -150, -50)
L3	(0, 150, -50)		
L4	(-75, 75, -150)		
L5	(75, 75, -150)		
L6	(0, -75, -150)		

Table 3.2 Material properties

Parameter	Workpiece	Fixture Elements
Material	Aluminum 7075-T6	Hardened Steel
Density (kg/m^3)	2700	-
Young's modulus (GPa)	70.3	201
Poisson's ratio	0.354	0.296
Yield strength (MPa)	500	-
Static coefficient of friction	0.35	

3.6.2 Evaluation of Workpiece Rigid Body Assumption

As stated earlier, this chapter focuses on structurally rigid workpieces such as the solid block used in this example and hence the structural compliance of the workpiece is assumed to be negligible compared to other compliance sources of the fixture-workpiece system (e.g., fixture-workpiece contacts and fixture elements). To investigate the validity of this assumption, modal analyses were performed in ANSYS® 10.0, a commercial finite element (FE) software package, on the original and final fixture-workpiece systems used in this example. The two meshed models are shown in Figure 3.9. The element type used is SOLID45, which has eight nodes with three translational DOFs at each node. The fixture-workpiece contacts are modeled as linear springs whose constants are given by Equation (3.28).

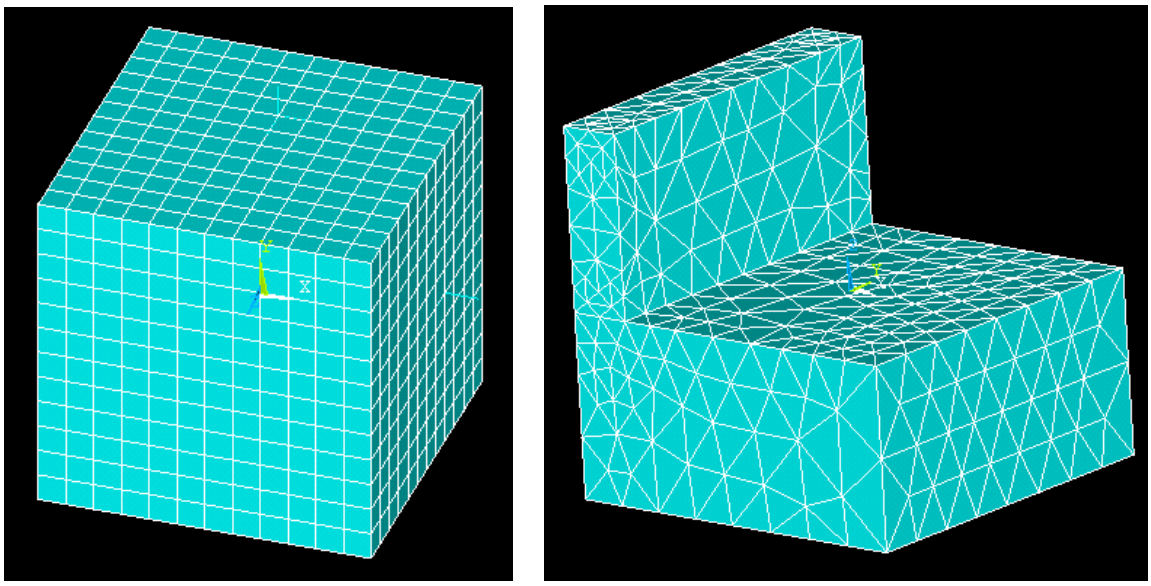

(a) Original workpiece (b) Final part

Figure 3.9 Meshed models

The first four natural frequencies of the fixture-workpiece system predicted by the dynamic model (*without* considering the workpiece structural compliance) and by the FE analysis (*with* consideration of the workpiece structural compliance) in the beginning (during the first tool pass) and at the end (during the last tool pass) of the example milling operation are listed in Table 3.3.

As expected, the natural frequencies predicted by the FE analysis are generally lower because the system is more compliant when the workpiece structural compliance is considered. However, the discrepancies are small (see Table 3.3) especially in the beginning of the operation (less than 3%). At the end of machining, the workpiece is less rigid and hence the difference between the two predictions becomes larger but still relatively small (11.5% in maximum). According to these results, the rigid body assumption of the workpiece is reasonable at least for parts of the type used in this example. Another observation is that the listed natural frequencies increase as the workpiece loses material. This is because the system inertia decreases faster than the system stiffness does during machining.

Table 3.3 Comparison of natural frequencies

Machining		Natural Frequency (Hz)			
		1	2	3	4
Beginning	(a)*	246.7	260.5	406.1	421.1
	(b)†	240.1	253.4	395.4	410.2
End	(a)*	342.5	323.4	422.5	551.5
	(b)†	303.1	321.4	423.2	494.3

(*: Predicted by the dynamic model given in Equation (3.8))
(†: Predicted by the FE analysis)

3.6.3 Amplitude of Workpiece Vibration vs. Spindle Speed

It is desirable to examine the significance of the fixture-workpiece system dynamics during machining. This is achieved through a harmonic analysis, which compares the amplitudes of the workpiece vibrations at different excitation frequencies. It is known that the dominant harmonic of the excitation in the milling process is given by the tooth passing frequency, which is determined by the spindle speed and the number of cutter teeth used in the process. Results of the harmonic analysis of the fixture-workpiece system in the beginning and at the end of the milling operation are shown in Figure 3.10 as plots of the vibration amplitude vs. spindle speed. The three resonance regions in either plot in Figure 3.10 correspond to the three groups of natural frequencies of the fixture-workpiece system. It is seen that the resonance regions shift to the right as the workpiece loses material because the system natural frequencies become higher (see Table 3.3).

A spindle speed of 2,500 rpm, which is in the curved region of the plots in Figure 3.10, is selected in this example so as to disqualify a quasi-static analysis but not in the immediate vicinity of the peak areas to avoid resonance. Other machining conditions are listed in Table 3.4. The instantaneous machining forces, shown in Figure 3.11 (during two tool revolutions), are obtained from an ideal milling force model derived from [75]. Note that the effect of the helix angle on the cutting forces is neglected in the force model, resulting in a zero force in the Z direction. In general, the cutting force in the Z (axial) direction in milling is small especially for the small axial depth of cut (5 mm) and relatively small helix angle (30º) employed in the current example.

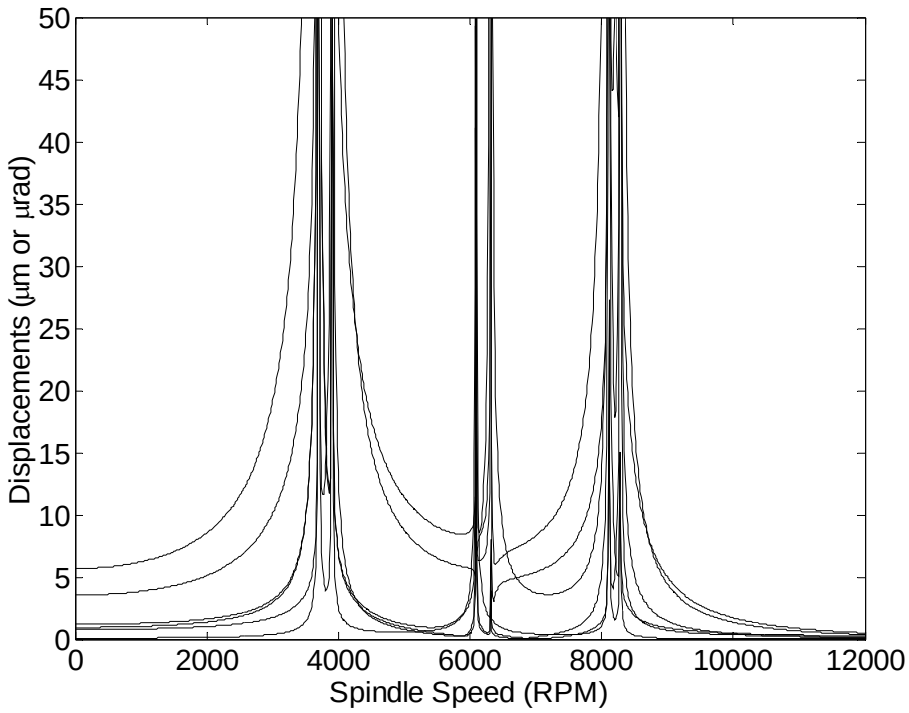

(a) At the start of machining

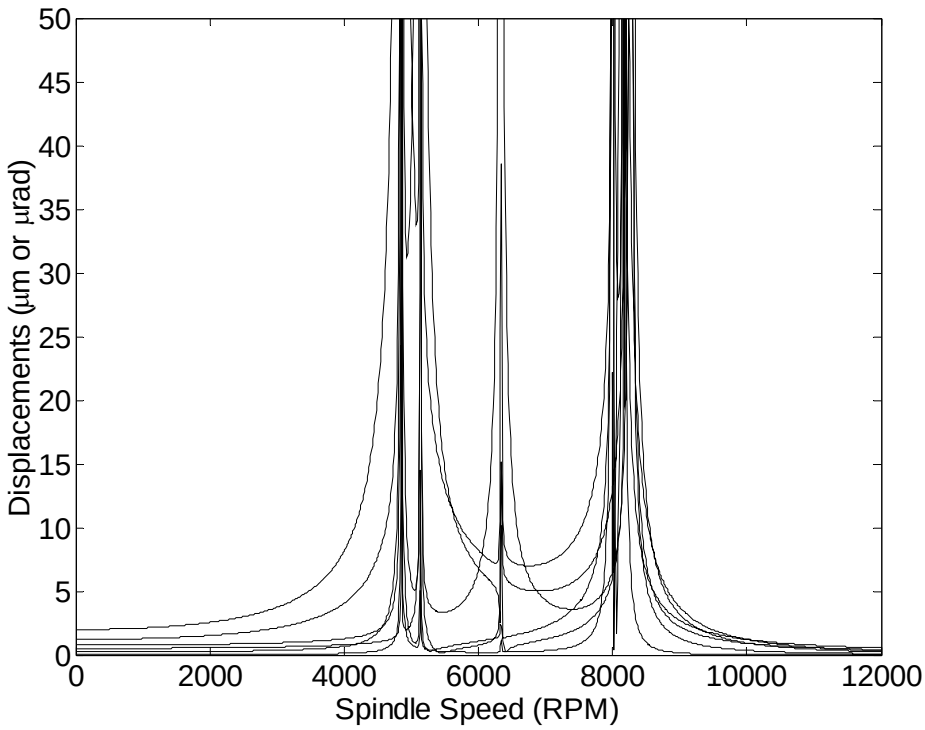

(b) At the end of machining

Figure 3.10 Amplitude of workpiece vibration vs. spindle speed

Table 3.4 Machining conditions used in the simulation example

Feed Rate (mm/sec)	Axial Depth (mm)	Radial Depth (mm)	Spindle Speed (rpm)
100	5	12.7	2500

(Tool: end mill, HSS, 25.4 mm, 4-flute, and 30º helix)

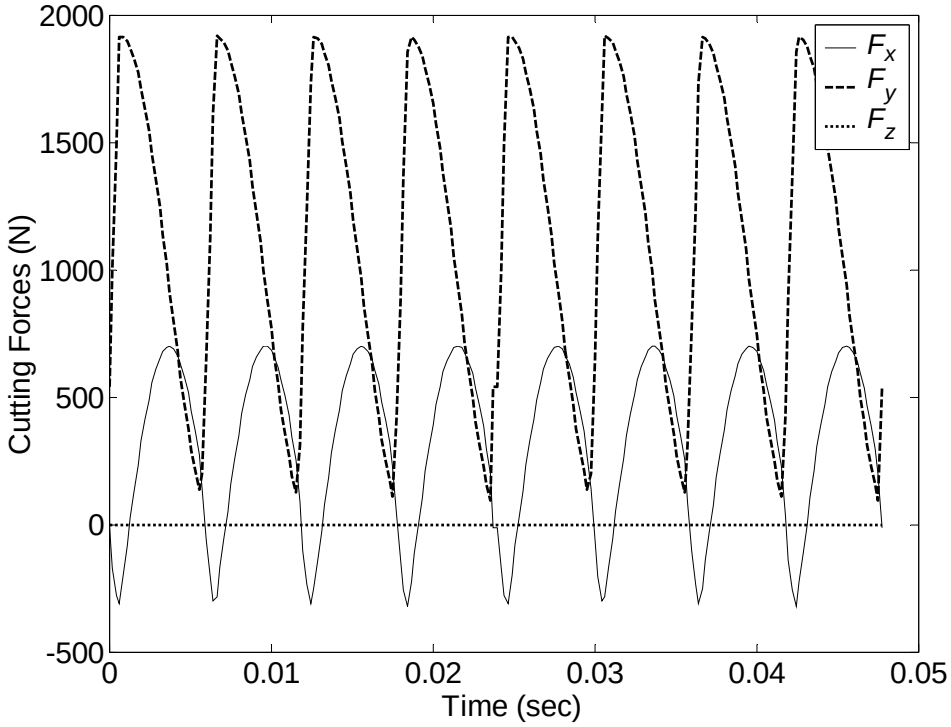

Figure 3.11 Simulated milling forces

3.6.4 Solution Techniques

The geometric model was developed in ACIS® R10. All other models were coded in Matlab® 7.0. The static model given in Equation (3.19) was solved using the Matlab® subroutine *fmincon* and the dynamic model given in Equation (3.8) was solved using the Runge-Kutta technique.

3.6.5 Results

Figures 3.12 and 3.13 compare the dynamic motions of the workpiece during the first and last tool passes. Note that workpiece motions during only two tool revolutions (0.048 sec) are shown in each plot. As seen from these plots, the workpiece vibrations (including three translations and three rotations) change significantly during the last pass in which 43% material has been removed.

The material removal affects the workpiece vibrations because of the following reasons whose relative significances are case specific:

1) change of workpiece volume and geometry (and hence inertia),
2) rate of change of system inertia (represented by $[\dot{M}]$ in the dynamic model given in Equation (3.8)), and
3) change of system natural frequencies (and hence the dynamic amplification of system motion).

Note that the workpiece structural compliance also changes during machining but is not considered here because in this chapter the workpiece is treated as a rigid body except at the contact regions. The workpiece structural compliance is considered in Chapter 5.

The fixturing dynamic stability during the first and last tool passes are analyzed using the previously established procedure (see Figure 3.2). The clamping forces used during the first and last passes are determined by a random search procedure in the range of 1,000 N to 10,000 N such that enough static elastic pre-deformations of the system at the fixture-workpiece contacts are generated to offset the workpiece vibrations during machining and thereby avoid contact instabilities.

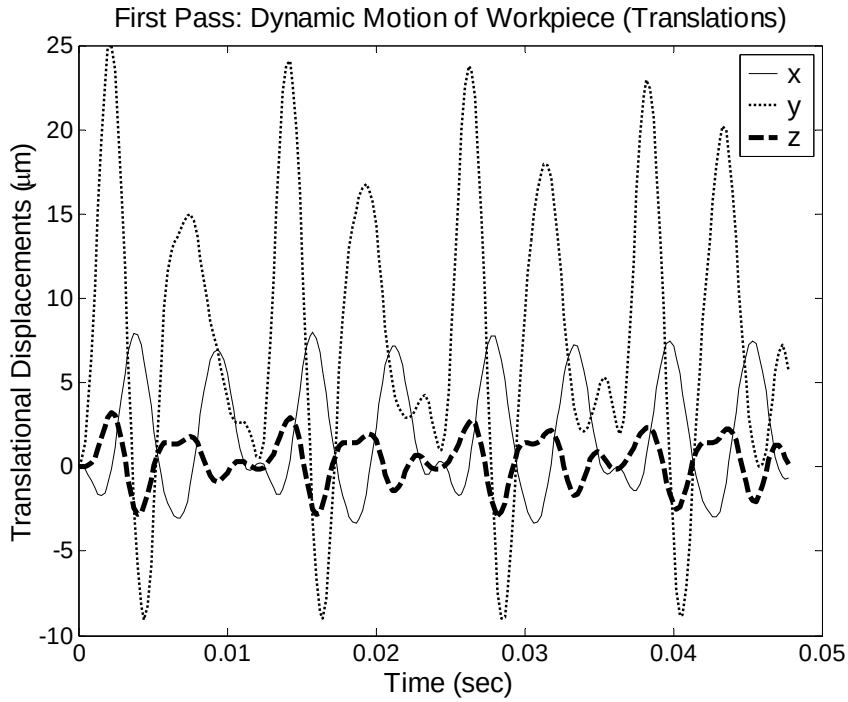

(a) Workpiece translations

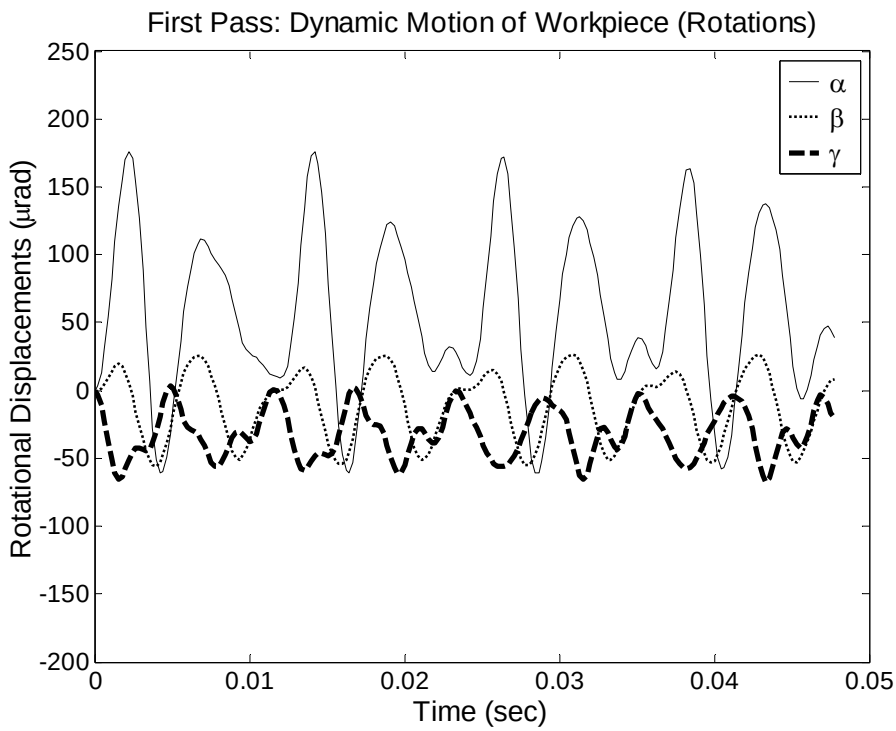

(b) Workpiece rotations

Figure 3.12 Dynamic motion of workpiece during the first pass

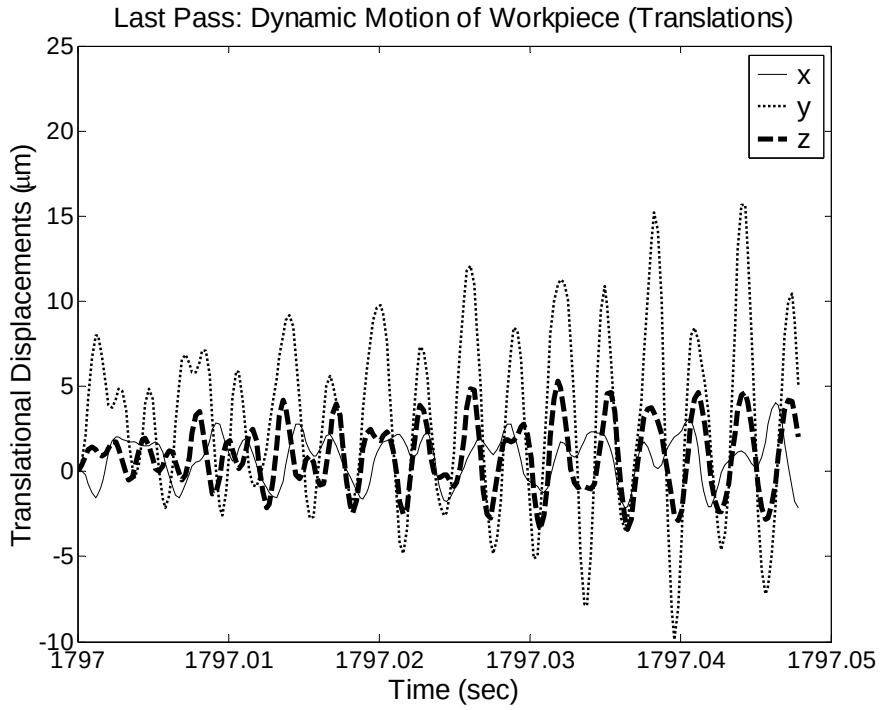

(a) Workpiece translations

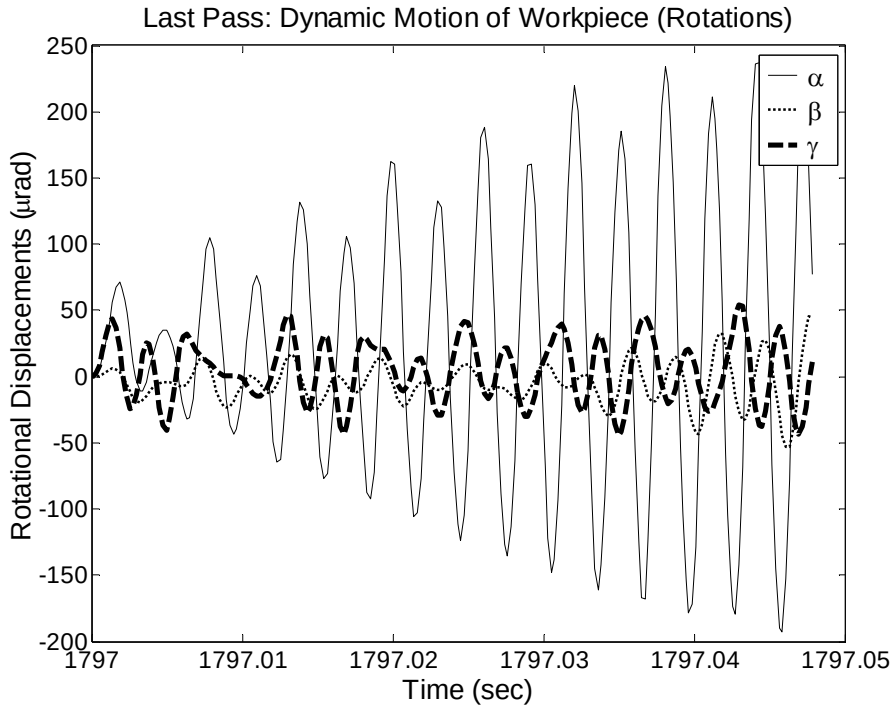

(b) Workpiece rotations

Figure 3.13 Dynamic motion of workpiece during the last pass

As an example, the fixturing dynamic stability of the system operating under clamping forces of 1,646 N (applied by C1) and 6,082 N (applied by C2) during the first pass is shown in Figure 3.14. The horizontal axis of both plots in Figure 3.14 represents the fixture-workpiece contact indices, which range from 1 to 8 corresponding to L1, L2, L3, L4, L5, L6, C1, and C2 (see Figure 3.8), respectively. The vertical axes of plots (a) and (b) in Figure 3.14 stand for the left hand sides of the two fixturing dynamic stability criteria (given in Equation (3.1)), respectively. Therefore, a stem above the zero horizontal line in Figure 3.14 (a) or (b) is an indicator of lift-off or macro-slip at the corresponding fixture-workpiece contact. The height of a stem represents the degree of fixturing dynamic stability (if below zero) or instability (if above zero) of the contact.

It is seen from Figure 3.14 that the two clamping forces are unable to stabilize the workpiece during machining. Specifically, the workpiece lifts off at L6 and macro-slip occurs at L1, L2, and C1. With the help of Figures 3.8 and 3.11, it can be concluded that the fixturing instabilities are due to the inappropriate combination of the two clamping forces. The clamping force applied by C2 (6,082 N), pointing in the $+Y$ direction, is much higher than that applied by C1 ((1,646 N) while the cutting force in the $+Y$ direction is significantly higher than the cutting forces in the other two directions. Therefore, the workpiece is pushed hard against L3, resulting in the previously identified fixturing instabilities.

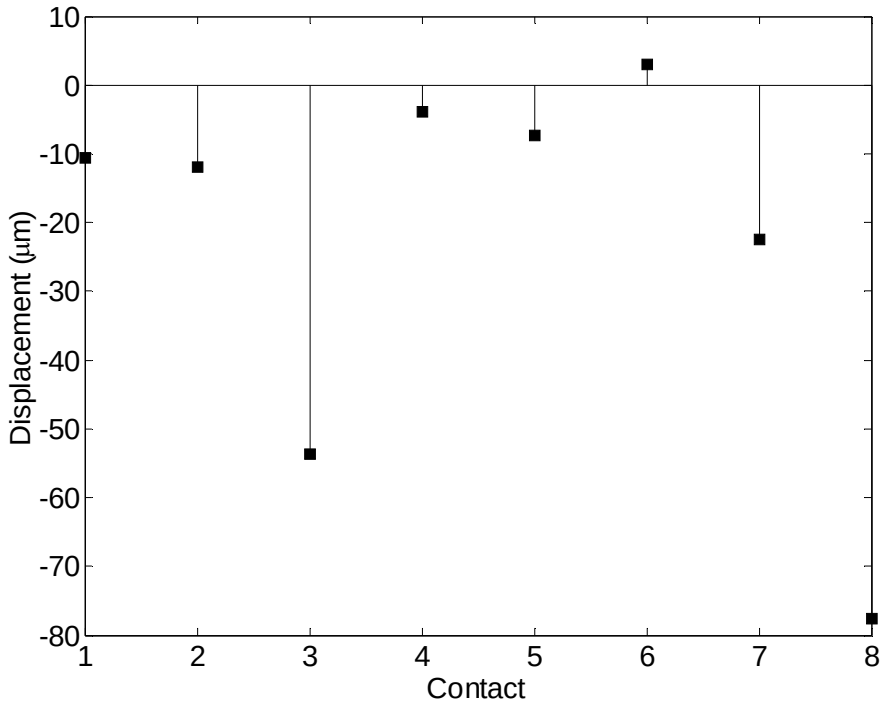

(a) Lift-off check

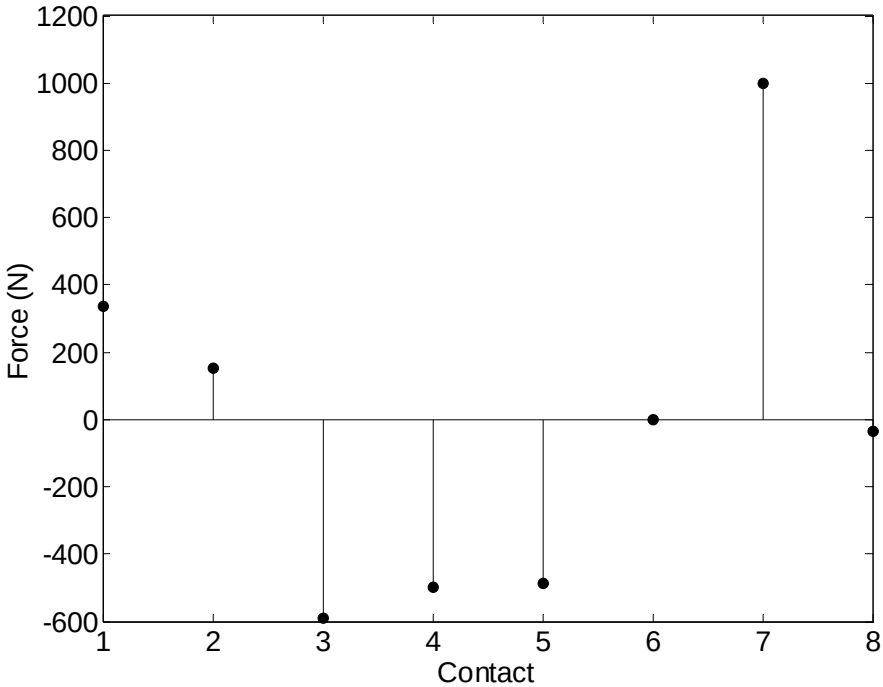

(b) Macro-slip check

Figure 3.14 Fixturing dynamic stability in the first pass under clamping forces of 1,646 N and 6,082 N

The two clamping forces are then adjusted and it is found that clamping forces of 7,861 N and 5,527 N are able to achieve fixturing dynamic stability in the first pass. For the last pass, a lower set of clamping forces, 5,546 N and 5,055 N, is found to be adequate to stabilize the workpiece. This can be explained by looking back at Figures 3.12 and 3.13, which show that the amplitudes of workpiece vibrations during the first pass are generally higher than those during the last pass due to the material removal effect and thus higher clamping forces are required to stabilize the workpiece. Note that the workpiece vibration results shown earlier were generated from stable fixturing scenarios, that is, clamping forces of 7,861 N and 5,527 N were used in the first pass while 5,546 N and 5,055 N were used in the last pass.

3.7 Summary

A systematic procedure for analysis of the fixturing dynamic stability of a fixture-workpiece system in machining has been established in this chapter. The criteria for fixturing dynamic stability were defined first with lift-off and macro-slip identified as the two types of fixturing instabilities that should be eliminated via proper fixture design. Models that form the fixturing stability analysis procedure were then developed. A dynamic model was developed to simulate the vibratory motion of the workpiece within the fixture during machining and to calculate the resulting dynamic displacements of the workpiece at the fixture-workpiece contacts. A static model was developed to find the contact elastic deformations of the workpiece due to clamping as well as the fixture-

workpiece contact stiffness, which is considered to be dependent on the clamping forces. The overall stiffness property of the fixture-workpiece system was then characterized. The contact deformations caused by clamping were superposed with the contact dynamic displacements obtained from the dynamic model to compute the total contact displacements under the combined effect of clamping and machining. The fixturing dynamic stability criteria were then applied to detect fixturing instabilities (lift-off and macro-slip) during machining. The effect of material removal on the fixture-workpiece system dynamics was considered and captured by a geometric model, which extracts the instantaneous system inertia and geometry information as material is removed from the workpiece.

A simulation example involving an end milling operation was given to illustrate the theoretical models and stability check procedure. From the results of the example, the key findings are as follows:

- The fixture-workpiece system during the end milling operation presents significant dynamics when certain spindle speeds are used such that the excitation frequency is in the vicinity of a natural frequency of the system. In this scenario, consideration of the fixture-workpiece system dynamics is critical for an accurate analysis of the system.
- Material removal in machining continuously changes the properties of the fixture-workpiece system, e.g., inertia and geometry. When a large portion of material is removed from the workpiece (43% in the simulation example), the fixture-workpiece system behaves quite differently (in the example, the amplitudes of workpiece vibrations were found to be higher during the first

tool pass than during the last pass). As a result, higher clamping forces are required to stabilize the workpiece during the first pass than during the last pass.

- Because of the material removal effect, dynamic clamping is an option to achieve the best possible performance of a machining fixture-workpiece system. In addition, allowing different forces at different clamps with a good combination of the clamping forces can improve the overall fixture performance.
- For structurally rigid workpieces (e.g., solid blocks), the structural compliance of the workpiece can be considered to be negligible compared to other sources of compliance in the system such as fixture-workpiece contacts and fixture elements, especially when spherical-tipped contacts and long, slim fixture elements are used in the system.

CHAPTER 4

EXPERIMENTAL VALIDATION

The open literature has very little information on experimental investigation of the dynamics of a machining fixture-workpiece system. This thesis is aimed at overcoming this limitation and the efforts made are presented in this and the next chapter. This chapter focuses on experimental validation of the theoretical models and procedure established in Chapter 3 for simulation of the vibratory motion and fixturing dynamic stability of a fixture-workpiece system in machining.

The dynamic model given in Equation (3.8) is validated first using machining and modal impact tests. Then, the procedure for analysis of fixturing dynamic stability is validated with machining experiments in which the instantaneous status of the fixture-workpiece contacts is monitored and fixturing instabilities are detected. Next, the effect of clamping forces on fixture-workpiece system properties is reported. Finally, the major conclusions of this chapter are given.

4.1 Validation of the Dynamic Model

Two methods are used to validate the dynamic model: machining tests and modal impact tests. In the machining tests, cutting forces are measured and used to feed the dynamic model to obtain the simulated dynamic response of the workpiece, which is then

compared with the measured response. The modal impact tests are used to extract the modal frequencies and damping ratios of the fixture-workpiece system. The measured and predicted modal frequencies are then compared.

4.1.1 Machining Tests

The experimental setup used to validate the dynamic model is shown schematically in Figure 4.1, where an end milling operation is being performed on a solid block of aluminum in a CNC milling machine. The workpiece was constrained by a 3-2-1 locator layout and two side clamps, which were actuated by a hydraulic hand pump. In some of the tests, an additional mechanically actuated clamp was used as shown in Figure 4.2. The three locators on the primary datum (*XY* plane) were mounted on a steel base plate while the other locators and the two side clamps were mounted on steel blocks (fixture bodies) assembled on the base plate. A Kistler® 9257B dynamometer and a Kistler® 8762A10 tri-axial accelerometer (frequency response 0-6 KHz) were used to measure the dynamic cutting forces and accelerations of the workpiece, respectively. The dynamometer was placed under the base plate and the accelerometer was mounted on the workpiece (see Figure 4.1). Data were collected using an NI® PCI-4472 dynamic signal acquisition board and the LabVIEW® 7.1 software.

A total of ten machining tests were performed. The experimental conditions used in these tests are summarized in Table 4.1. Each test had at least one variable that was different from all others. Other conditions such as the spindle speed (5,000 rpm), data sampling rate (12,000 Hz), locator layout, and cutting tool (HSS end mill, 25.4 mm, 4-flute, and 30° helix) were fixed for all the tests. No cutting fluid was used in any test.

Figure 4.2 shows pictures of two representative test cases, one of which used two side clamps while the other used three with the third clamp applied to the top face of the workpiece. The hand pump was calibrated, as shown in Appendix A.2, to convert the clamping pressure (psi) to force (N). The clamping force applied by the top clamp was measured by the dynamometer before cutting was initiated.

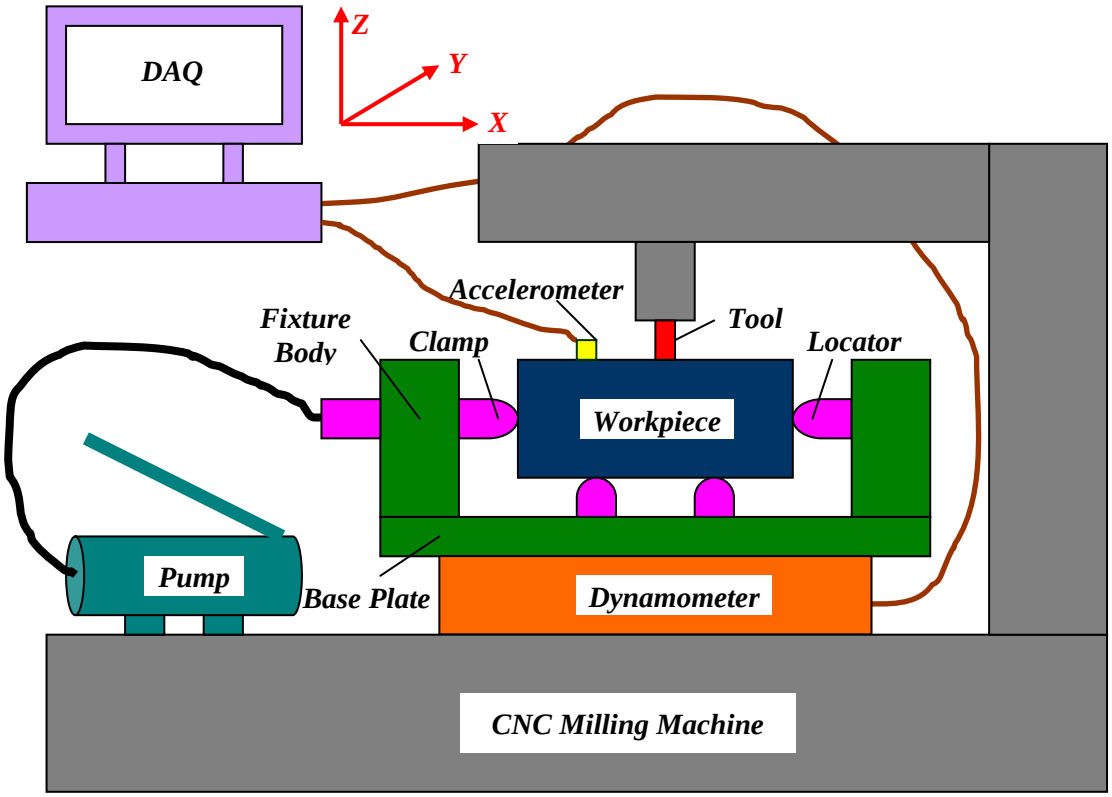

Figure 4.1 Schematic of experimental setup used in the machining tests

Table 4.1 Summary of machining tests for validation of dynamic model

Case	Workpiece		Cutting Conditions				Fixture Design	
	Material	Dimension* (mm)	Axial (mm)	Radial (mm)	Feed (m/min)	Cutting Dir.†	Clamping (psi)	Top clamp and force
1	Al-6061	127×152.4×76.2	4.06	19.05	2.032	L→R	1500	No
2	Al-7075	127×152.4×85.7	2.54	6.35	0.254	R→L	3000	No
3	Al-7075	127×152.4×85.7	2.54	6.35	0.254	B→F	3000	No
4	Al-7075	127×152.4×85.7	2.54	12.7	0.508	L→R	3000	Yes, 697.8 N
5	Al-7075	127×152.4×85.7	2.54	12.7	0.508	F→B	3000	Yes, 697.8 N
6	Al-7075	127×152.4×85.7	2.54	12.7	0.508	F→B	2000	Yes, 151.2 N
7	Al-7075	127×152.4×85.7	2.54	12.7	0.508	L→R	2000	Yes, 151.2 N
8	Al-7075	127×152.4×85.7	5.08	12.7	1.016	L→R	2000	Yes, 151.2 N
9	Al-7075	127×152.4×83.2	2.54	12.7	0.762	L→R	2000	No
10	Al-7075	127×152.4×83.2	5.08	12.7	0.508	L→R	2000	No

(*: length×width×height)

(†: L – left, R – right, F – front, B – back, when facing the machine tool)

The material properties of the workpiece and the fixture elements are given in Table 4.2. Table 4.3 shows the layout and spatial coordinates of all the fixture elements around the 127mm×152.4mm×76.2mm workpiece in the (*xyz*) frame. All fixture elements are hexagonal (inscribed radius = 6.35 mm or 7.11 mm) cylinders (height = 10.31 mm or 9.53 mm) with a spherical tip (radius = 19.81 mm or 34.93 mm). Note that the values shown in Table 4.3 change as the geometry of the workpiece and hence the (*xyz*) frame changes continuously during machining. This phenomenon is captured by the geometric model mentioned in Chapter 3 and detailed in Chapter 5. When the volume removed in the operation is small, the change in workpiece geometry may be ignored to reduce the computational cost without loss of accuracy (<5%).

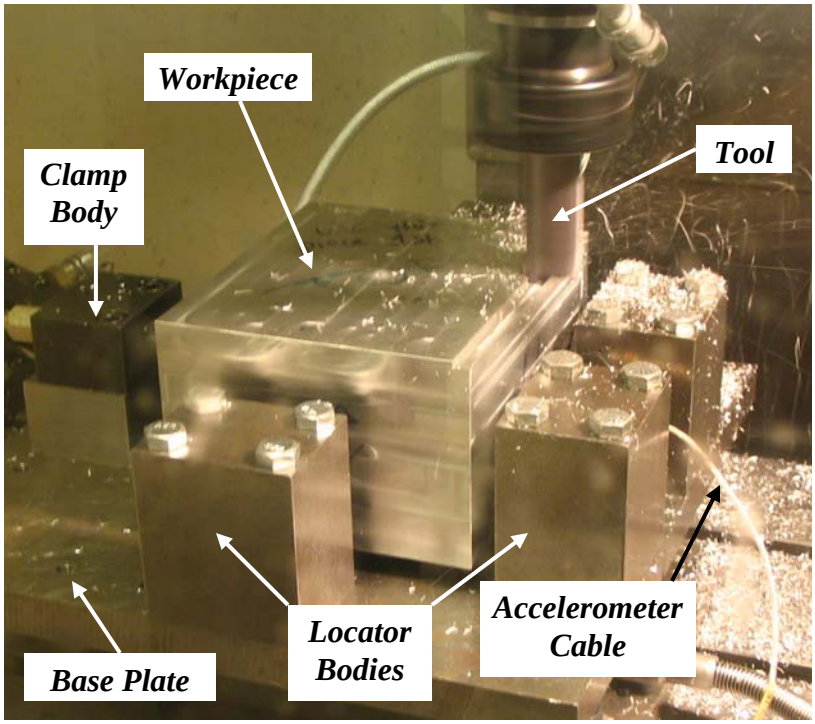

(a) Two clamps

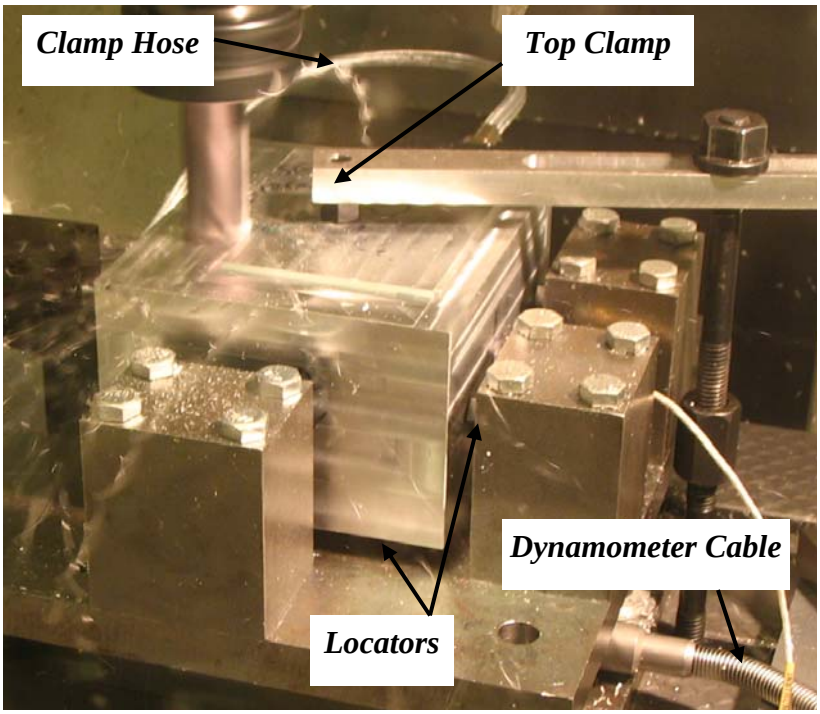

(b) Three clamps

Figure 4.2 View of experimental setup

Table 4.2 Material properties

	Workpiece		Fixture Element
Material	Al-6061	Al-7075	Hardened Steel
Density (kg/m^3)	2700	2800	-
Young's modulus (GPa)	70	72	200
Poisson's ratio	0.33	0.33	0.285
Yield strength (MPa)	270	480	-
Static coefficient of friction	0.375 (measured)		

Table 4.3 Fixture layout (locators L1-L6 and clamps C1-C3)

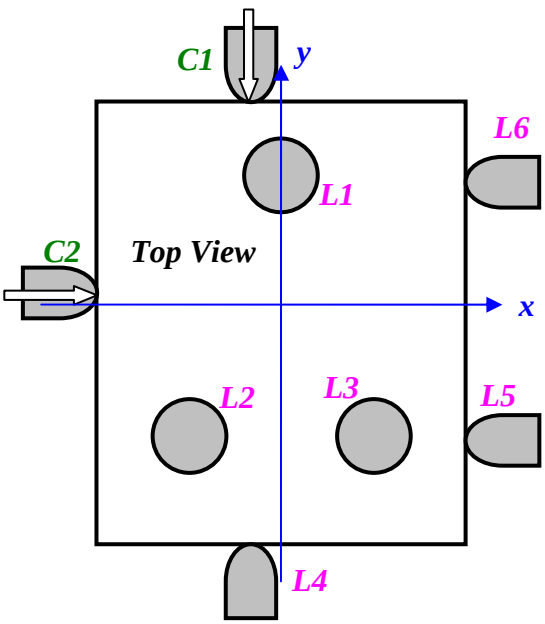

Fixture Element	Coordinate (x, y, z) (mm)
L1	(0.97, 54.1, -38.1)
L2	(-44.75, -64.26, -38.1)
L3	(45.09, -64.26, -38.1)
L4	(-16.51, -76.2, -0.51)
L5	(63.5, -46.23, -0.38)
L6	(63.5, 55.63, 0)
C1	(-1.52, 76.2, 0.51)
C2	(-63.5, 5.08, 1.02)
C3	(0, 0, 38.1)

To reduce the error sources, the measured cutting forces were used in the dynamic model to simulate workpiece motion. The geometric model was coded in ACIS® R10 while all other models were implemented in Matlab® 7.0. The static model was solved using the Matlab® subroutine *fmincon* while the dynamic model was solved using the Newmark-beta numerical integration method.

The measured and simulated acceleration signals are compared in three ways. First, their steady state root mean square (RMS) values are compared. The steady state signals, which do not contain the transient impact dynamics caused by initial plunging of the tool into the workpiece, are used because the dynamic model developed here is for the simulation of steady state dynamics. Nevertheless, as shown later in this chapter, the model is able to capture the major variations in the workpiece motion even during initial tool impact. The RMS is chosen as a metric for comparison for two reasons: i) it is a measure of signal energy and degree of workpiece vibration, which is of most interest to this study; ii) it contains information from all individual data points and hence is less sensitive to outliers.

A comparison of the RMS values is shown in Figure 4.3. Good agreement between the measured and predicted values is found in all three directions. The average prediction error for all ten cases is 15.58%. Some of the observed discrepancies may result from: i) inexact modeling of system properties such as neglecting the structural compliance and damping of the workpiece and other components; ii) unstable fixturing scenarios, e.g., intermittent contacts were not considered in the simulation; and iii) errors in data collection due to various noise sources. It can be seen that, as expected, heavier cuts and lower clamping forces generally result in higher workpiece vibration. Also, the additional top clamp helps stabilize the workpiece. However, the model prediction accuracy seems to be insensitive to the cutting conditions (including cutting direction) and the fixturing scenarios.

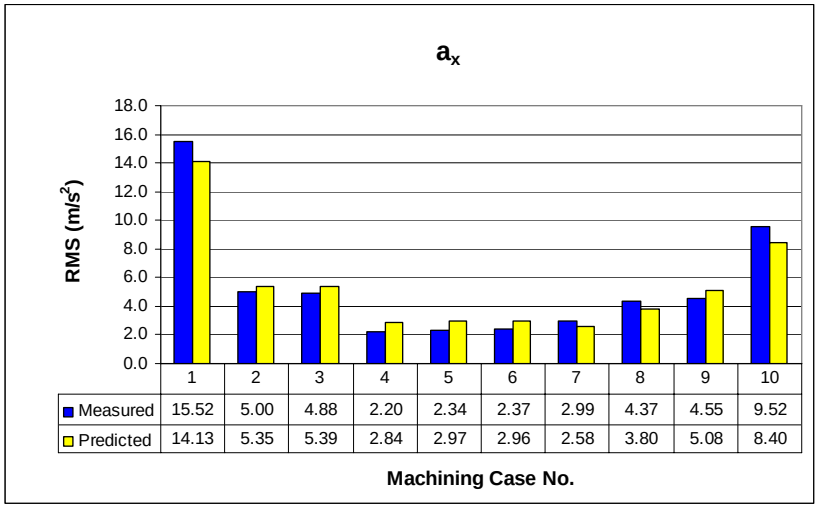

	1	2	3	4	5	6	7	8	9	10
Measured	15.52	5.00	4.88	2.20	2.34	2.37	2.99	4.37	4.55	9.52
Predicted	14.13	5.35	5.39	2.84	2.97	2.96	2.58	3.80	5.08	8.40

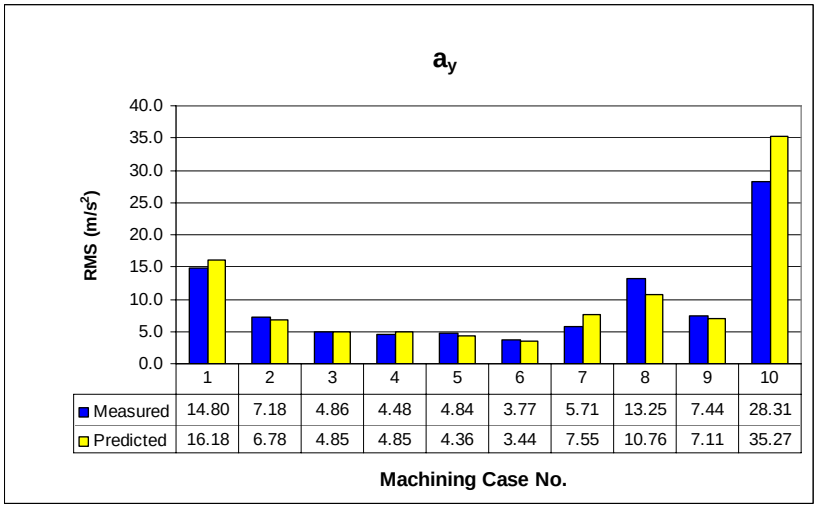

	1	2	3	4	5	6	7	8	9	10
Measured	14.80	7.18	4.86	4.48	4.84	3.77	5.71	13.25	7.44	28.31
Predicted	16.18	6.78	4.85	4.85	4.36	3.44	7.55	10.76	7.11	35.27

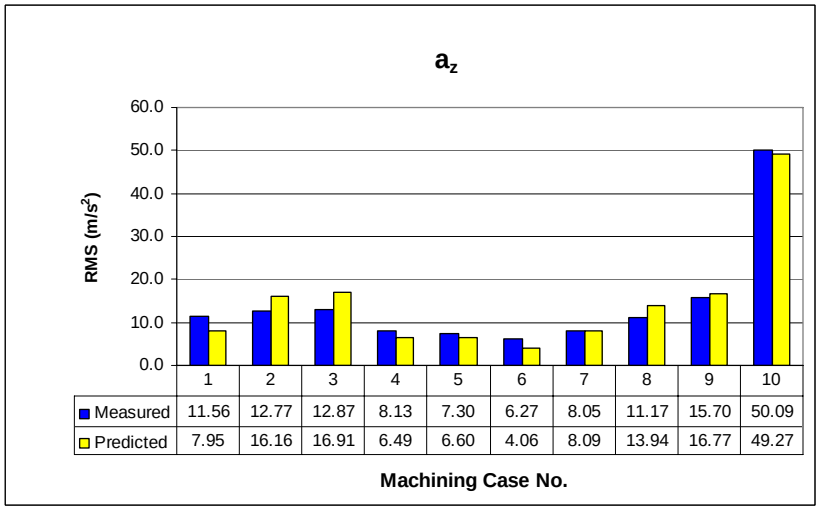

	1	2	3	4	5	6	7	8	9	10
Measured	11.56	12.77	12.87	8.13	7.30	6.27	8.05	11.17	15.70	50.09
Predicted	7.95	16.16	16.91	6.49	6.60	4.06	8.09	13.94	16.77	49.27

Figure 4.3 Predicted vs. measured RMS accelerations

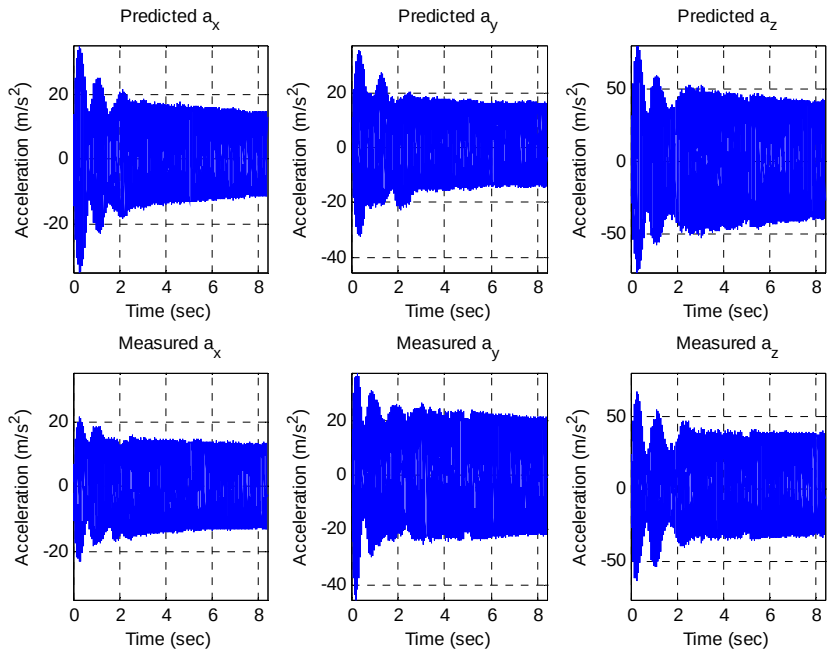

(a) Case #2

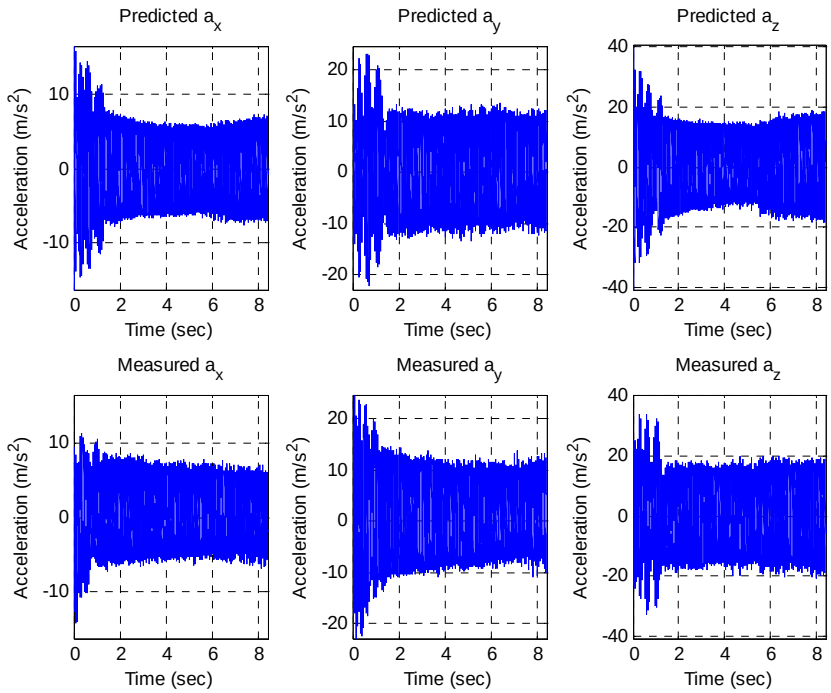

(b) Case #4

Figure 4.4 Predicted vs. measured accelerations in time domain

A comparison of the raw acceleration data in time domain including both tool impact and steady-state dynamics for two representative cases (#2 and #4) is shown in Figure 4.4. Predictions are seen to agree reasonably well with the measured counterparts in both amplitudes and major variations of the signals. The complete results for all ten cases are given in Appendix A.3.

The third comparison, shown in Figure 4.5 for a representative case (#2), is of the frequency content of the measured and predicted acceleration signals including both tool impact and steady-state dynamics. Note that the vertical axes in Figure 4.5 and all other frequency-domain graphs in this chapter are plotted in logarithmic ($\log_{10}$) scale. It is seen that all frequencies in the measured signal are also present in the predicted response.

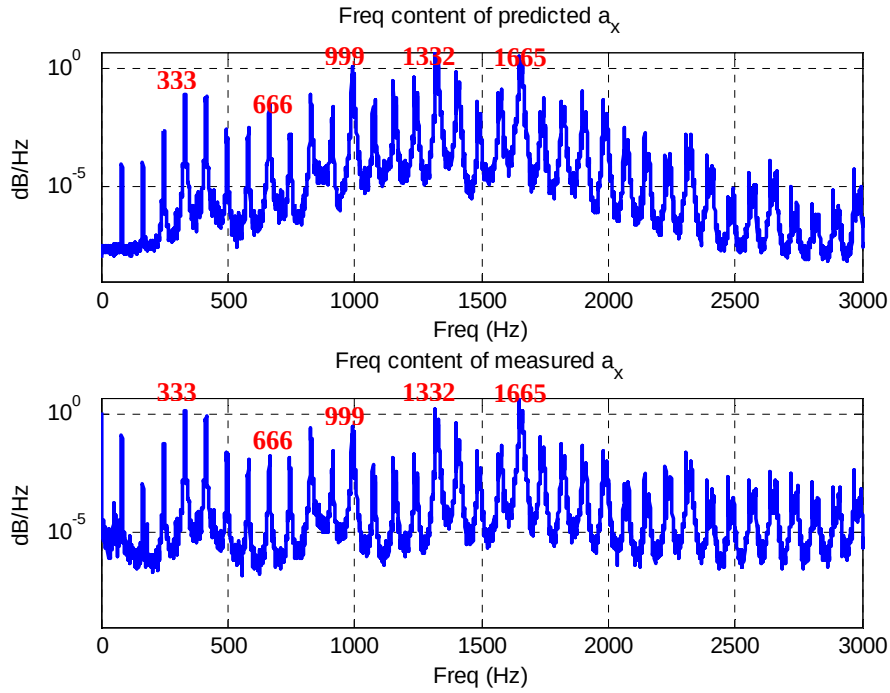

(a) a_x

Figure 4.5 Predicted vs. measured accelerations in the frequency domain for case #2 (Note: numbers used to label selected peaks are in Hz.)

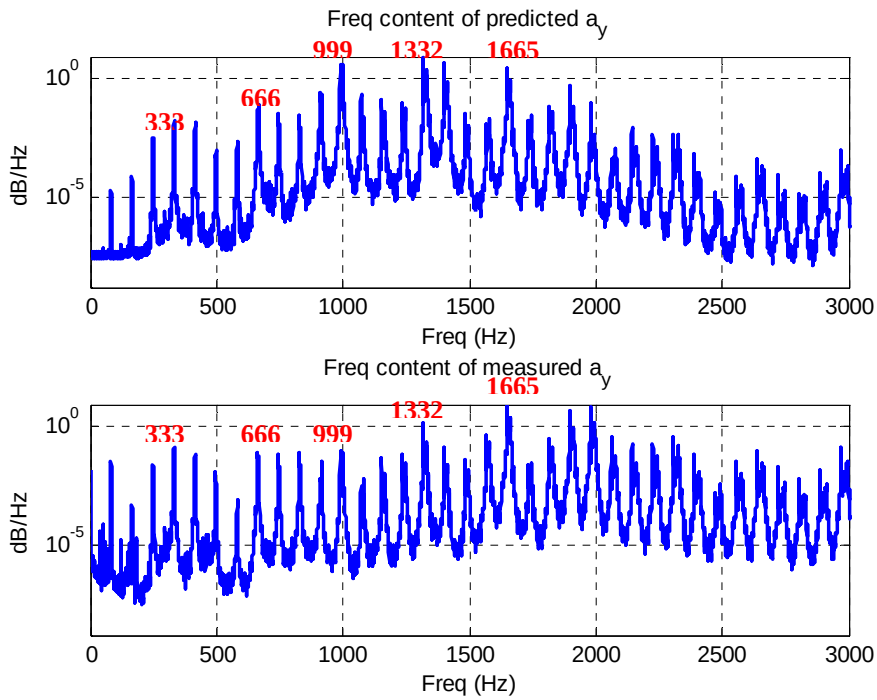

(b) a_y

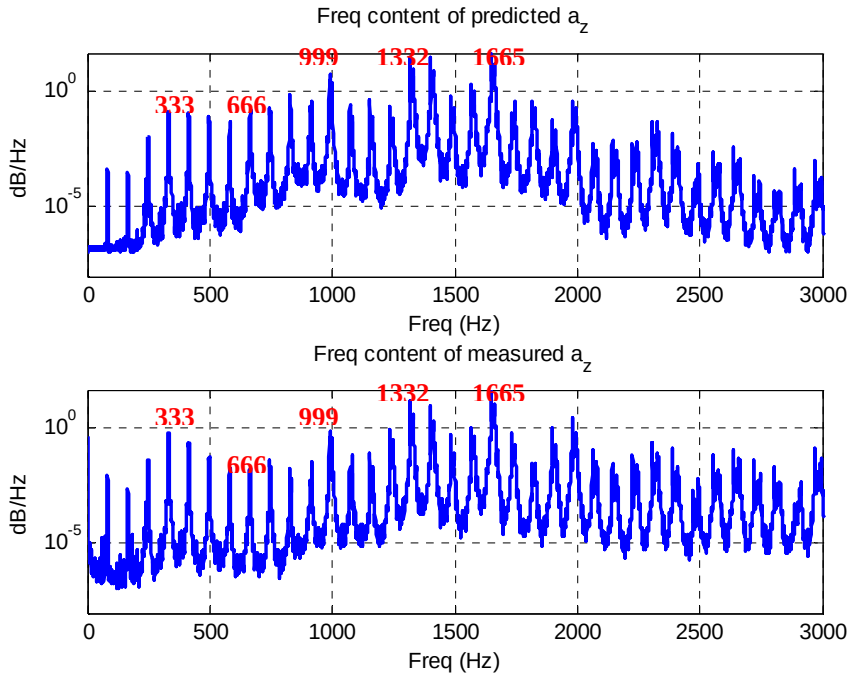

(c) a_z

Figure 4.5 Continued

4.1.2 Modal Impact Tests

It is also desirable to obtain the global modal properties (e.g., natural frequencies) of the fixture-workpiece system and compare them with their simulated counterparts. Consequently, modal impact tests were conducted for cases #2 and #9 given in Table 4.1. A picture of the setup used in the impact tests is shown in Figure 4.6, where a Kistler® 9722A2000 impulse hammer with a medium-hard rubber tip was used to impact the fixtured workpiece and the accelerations were measured in three orthogonal directions.

The Complex Exponential (CE) Algorithm [76] was used to estimate the modal parameters of the system from the raw data. Shown in Figure 4.7 are the frequency response function (FRF) and the corresponding coherence for an input/output (or impact/acceleration) pair of the system for case #2. Note that the coherence at frequencies with low FRF amplitude is generally low as well because the small response of the system at those frequencies results in low signal-to-noise ratio.

The experimental and simulated modal frequencies are compared in Table 4.4 for cases #2 and #9 and good agreement is found. As listed in Table 4.1, the clamping pressure used in case #2 is 3000 psi while it is 2000 psi in case #9. Therefore, the fixture-workpiece system in case #2 is expected to be stiffer than in case #9. However, the workpiece in case #2 is a little heavier than in case #9. As a result, the natural frequencies (both measured and predicted) of the system in case #2 are generally higher than in case #9. Also listed in Table 4.4 are the corresponding modal damping ratios. It is seen that damping of the system is rather light thus justifying the assumption made earlier (see Chapter 3).

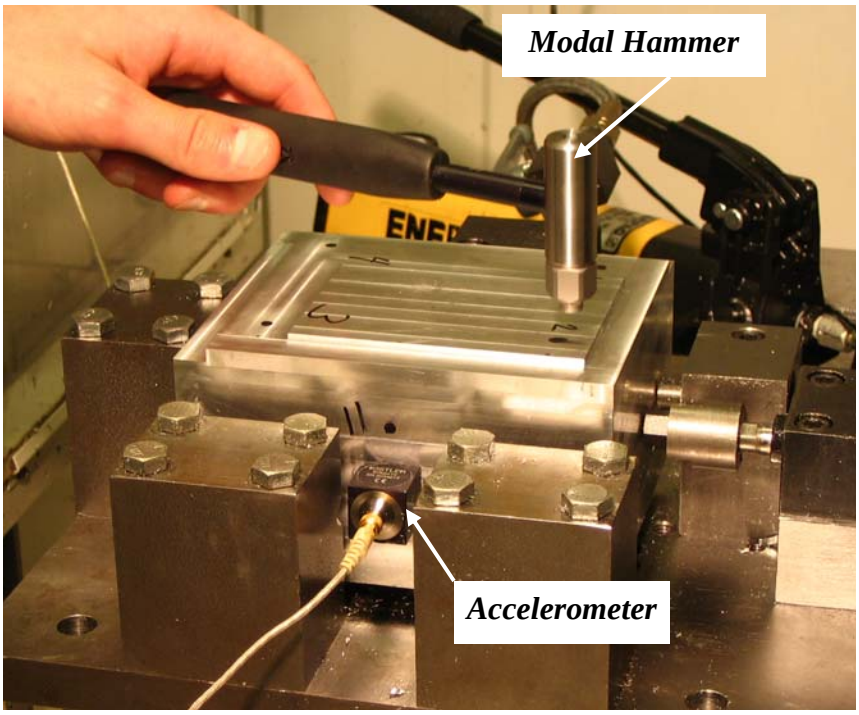

Figure 4.6 Setup for modal impact test

Table 4.4 Experimental vs. simulated modal properties

Mode	Natural Frequency ω_r (Hz) Measured		Predicted		Diff (%)		Damping ratio ξ_r (%)	
	Case 2	Case 9	Case 2	Case 9	Case 2	Case 9	Case 2	Case 9
1	1315	1345	1317	1292	0.15	-3.94	8.85	8.18
2	1690	1424	1622	1427	-4.02	0.21	4.85	7.31
3	1922	1630	2066	1553	7.49	-4.72	3.29	7.09
4	2153	1890	2217	2016	2.97	6.67	2.74	5.68

Figure 4.5 reveals something interesting: the two dominant harmonics of the acceleration signal are 1,332 Hz and 1,665 Hz, which are four and five times the tooth passing frequency (333 Hz), respectively. Note that the harmonic of 333 Hz is dominant in the excitation (cutting force) signal. This shift in dominant harmonics is because 1,332

Hz and 1,665 Hz are near two of the natural frequencies (1,315 Hz and 1,690 Hz) of the fixture-workpiece system (see Figure 4.7) and therefore their corresponding modes are greatly amplified. A static analysis would be unable to reveal this.

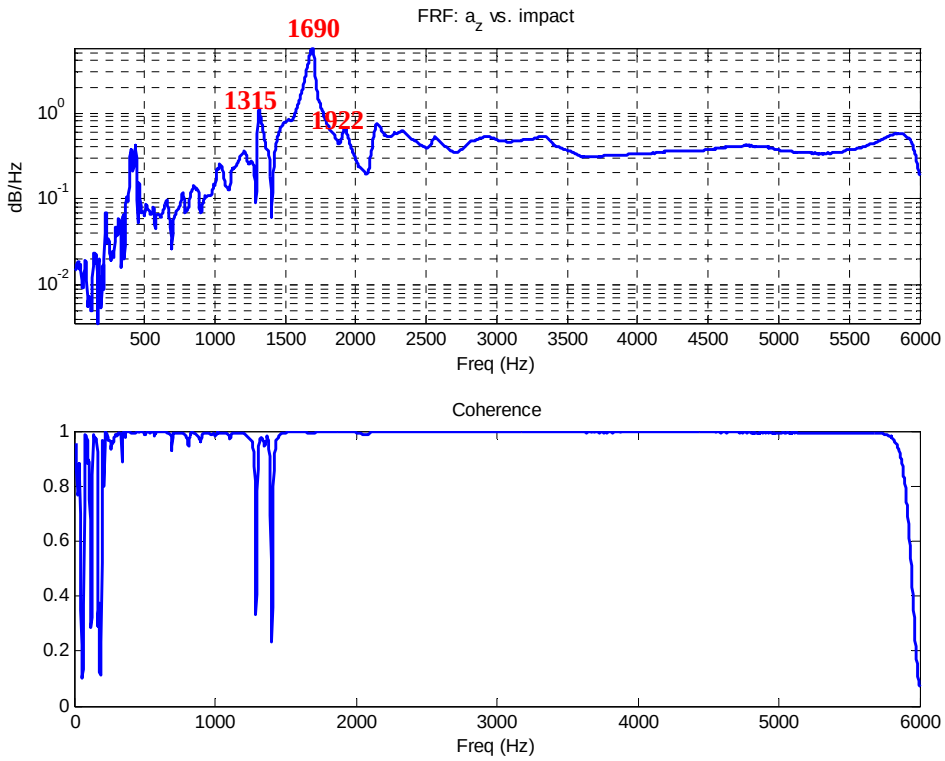

Figure 4.7 FRF and coherence for machining case #2
(Note: numbers used to label peaks are in Hz.)

4.2 Validation of Fixturing Stability Analysis Procedure

The procedure for analysis of the fixturing dynamic stability in machining summarized in Figure 3.2 was validated via machining tests in which three thin piezoresistive ink based FlexiForce® force sensors (A201-100) were placed on the three

locators (L1-L3) in the primary datum (the *XY* plane) to detect lift-off during machining, as shown in Figure 4.8. The thin film sensors were zeroed before use. The dynamometer was used to collect the cutting force data required by the dynamic model. The fixture layout was the same as that listed in Table 4.3 except that the top clamp C3 was not used. This left the workpiece loosely restrained in the +*Z* direction giving rise to the possibility of lift-off at locators L1-L3.

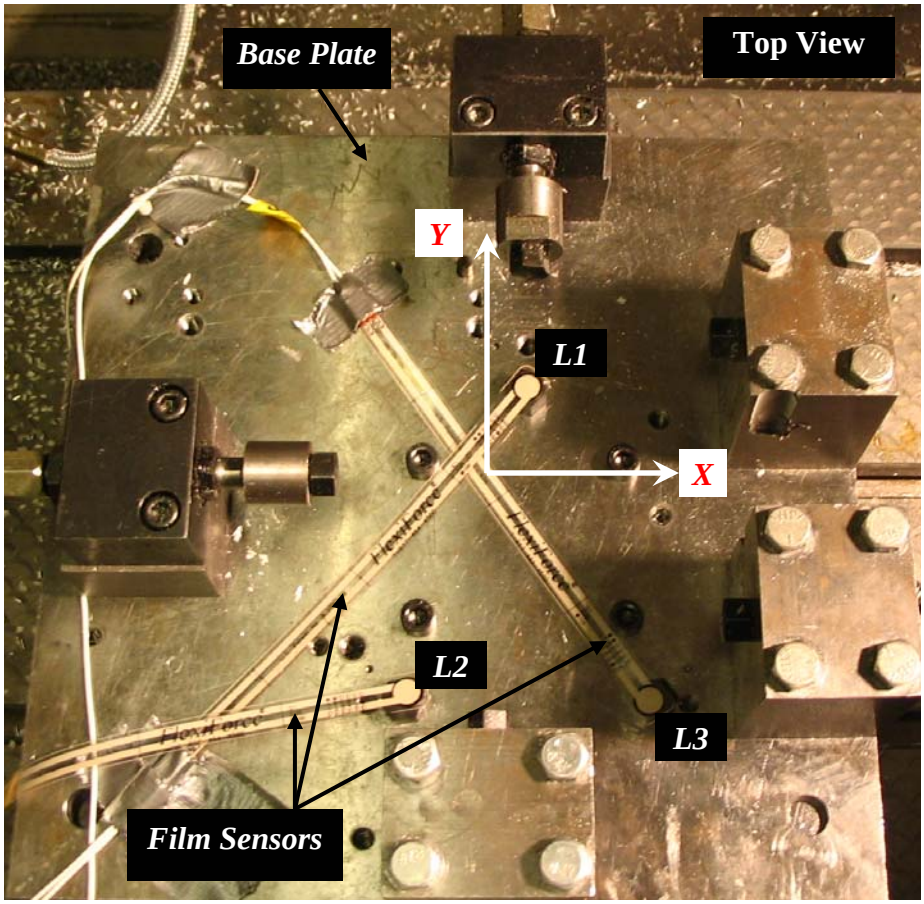

Figure 4.8 Experimental setup used to detect lift-off in machining

A total of five machining tests were conducted. Experimental conditions used in the tests and the stability verification results are summarized in Table 4.5. Conditions that were fixed for all tests include the workpiece material (Al-7075) and dimensions (127mm×152.4mm×76.2mm), spindle speed (5,000 rpm), axial depth of cut (2.54 mm), radial depth of cut (12.7 mm), cutting direction (in the $-Y$ direction), and sampling rate (10,000 Hz).

Table 4.5 Experimental conditions and stability verification results

Case	Feed (m/min)	Clamping (psi)	Experiment/Simulation Results (Lift-off?) L1	L2	L3
1	0.254	1200	N/N	B/B	N/N
2	0.457	1200	N/N	B/B	N/N
3	0.635	1200	N/B	B/B	N/N
4	0.457	1000	N/B	B/Y	N/N
5	0.635	1000	B/B	B/Y	N/N

(Note: N – no, Y – yes, and B – on the borderline)

Figure 4.9 gives a detailed comparison of the measured vs. predicted degree of contact (in)stability indicated by the height of the bar, which, for the experiment, represents the mean value of the film sensor signal (in Volts) and for the simulation represents the degree to which the lift-off constraint (in N) is violated. All bars in the plots are normalized by the tallest bar of the same group (measurement or prediction). A band formed by the two dashed lines is used to divide each plot into three areas: stable (below the band), unstable (above the band), and on the borderline (within the band). The band was established from the film sensor response at zero force (i.e., when it is exposed to air). The half width of the band is equal to 3σ, where σ is the standard deviation of the zero force signal caused by noise. It is seen from Table 4.5 and Figure 4.9 that the

fixturing dynamic stability analysis procedure developed in Chapter 3 is able to predict the onset and the degree of contact (in)stability quite well. Even though the prediction for L1 in cases #3 and #4 and L2 in cases #4 and #5 do not exactly match the experimental results (see Table 4.5), the predicted (in)stability is very weak and near the borderline as seen in Figure 4.9. On the other hand, as expected, the fixturing dynamic stability is found to degrade at lower clamping pressures (cases #4 and #5) and heavier cutting conditions (cases #3 and #5).

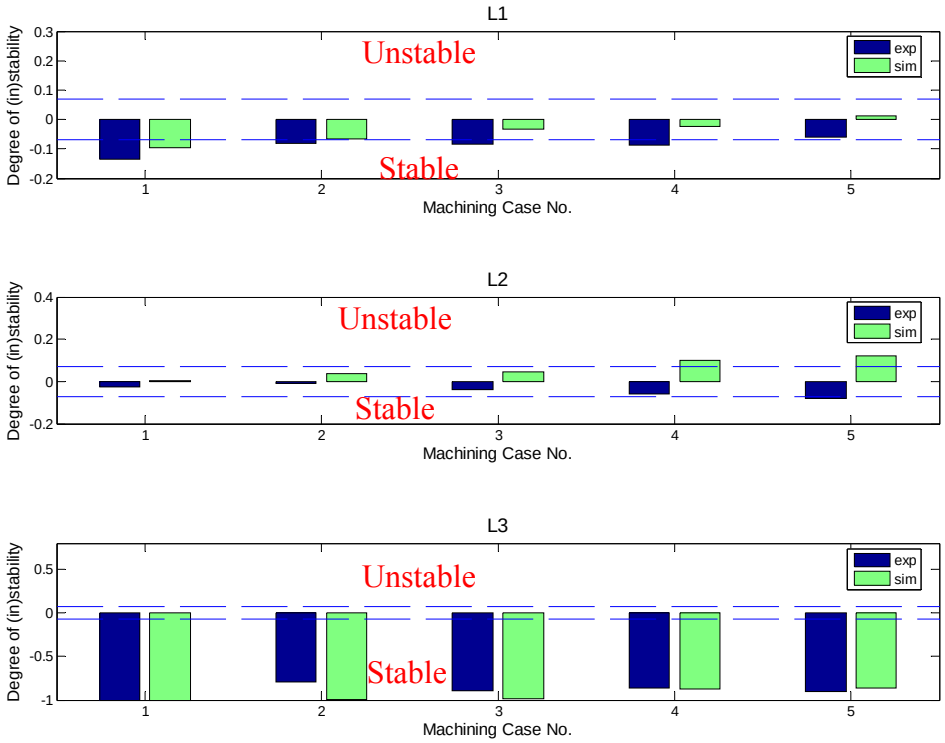

Figure 4.9 Verification of fixturing stability: simulation vs. experiment

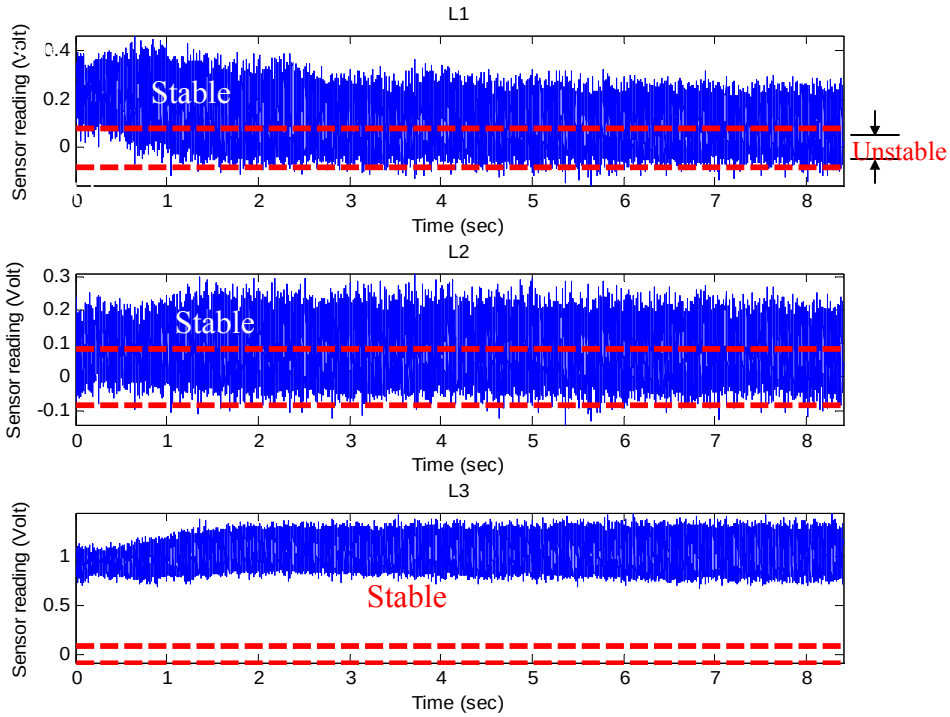

(a) Lift-off check by experiment

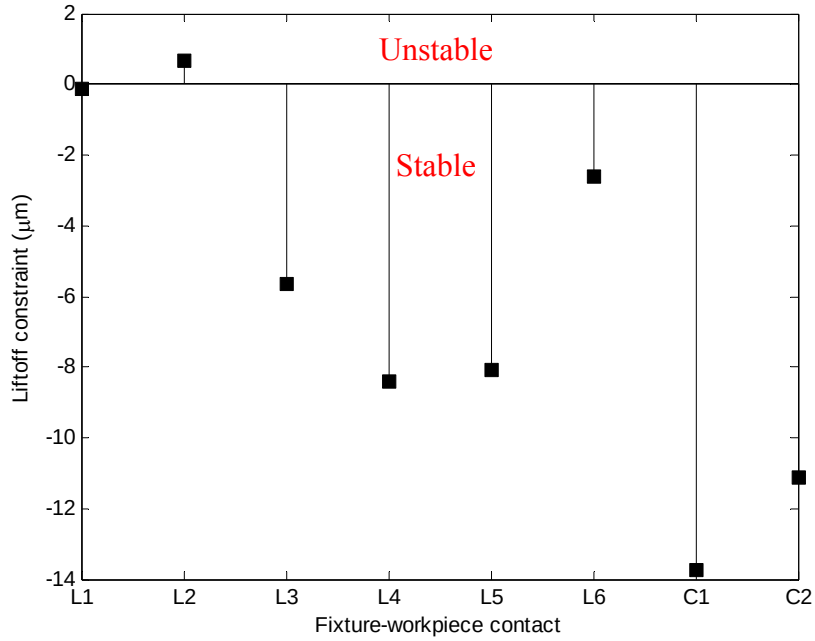

(b) Lift-off check by simulation

Figure 4.10 Film sensor data and simulation results for case #5

Representative film sensor data and simulation results are shown for case #5 in Figure 4.10. In both prediction and measurement, it is seen that L1 is marginally stable (on the borderline), L2 lifts off, and L3 is in contact with the workpiece during machining. Complete results for all five cases are shown in Appendix A.4. Note that simulation results are not shown as a function of time because any loss of contact results in a new fixturing configuration. Therefore, accurate dynamic analysis of workpiece motion after lift-off occurs requires the reconfiguration and re-solution of the dynamic model, which is computationally expensive and unnecessary since the main objective here is to establish the capability of the fixture to maintain contact with the workpiece rather than simulation of workpiece motion once contact has been lost.

4.3 Effect of Clamping Forces on System Modal Properties

As noted earlier in the description of the static model (see Section 3.4.1), this thesis work explicitly considers the effect of clamping pressure on the stiffness of the fixture-workpiece system, which is often treated as being independent of the clamping forces. To investigate this effect, modal impact tests were performed for different clamping pressures applied to the fixture-workpiece system presented in the previous section. Table 4.6 compares the measured and predicted modal frequencies of the system at different clamping pressures. It is clear from the table that increase in the clamping pressure results in an increase in the system stiffness. Consequently, this effect must be considered in modeling the fixture-workpiece system.

Table 4.6 Effect of clamping pressure on system natural frequencies (Hz)

	Clamping Pressure (psi)						
Mode	1000	1500	2000	2500	3000	3500	4000
	Experiment						
1	1266	1280	1272	1298	1315	1324	1387
2	1400	1490	1517	1650	1690	1714	1731
3	1580	1580	1610	1907	1922	1933	1947
4	2050	2075	2105	2132	2153	2174	2187
	Simulation						
1	1274	1359	1421	1471	1513	1549	1580
2	1535	1639	1715	1776	1827	1870	1908
3	1734	1848	1932	2000	2057	2106	2149
4	1808	1928	2019	2091	2151	2204	2250

4.4 Summary

The model-based framework developed in Chapter 3 for analysis of the dynamic performance (emphasizing the fixturing dynamic stability) of a fixture-workpiece system in machining was experimentally validated in this chapter.

Machining tests differing in cutting and fixturing conditions were designed and conducted and the system excitation (cutting force) and response (acceleration) data were collected. Measured dynamic response of the fixture-workpiece system was compared with the output of the dynamic model and the results were discussed. Impact tests were performed to extract the modal properties of the fixture-workpiece system. The system natural frequencies estimated from the impact test data were compared with the predicted results from the dynamic model.

The procedure for fixturing dynamic stability analysis was validated using machining tests in which thin film force sensors were placed at the fixture-workpiece contacts to monitor the instantaneous status of the contacts during machining and the measurements were compared with the simulation results.

The effect of clamping forces on the system modal frequencies was also examined via modal impact tests.

The following key conclusions can be drawn from the work described in this chapter:

- The workpiece vibratory behavior simulated by the dynamic model agrees reasonably with the experimental results in a variety of fixturing and machining scenarios. The average prediction error of the RMS acceleration for the ten machining cases examined is 15.58%. This indicates that the simulation is able to capture the majority of the workpiece motion, although whether a model is accurate enough depends on the requirements of a specific application.
- The procedure for fixturing stability verification is able to predict well both the onset of lift-off and the degree of fixturing (in)stability, which can serve as a guideline for improving an existing fixture design for a given machining application.
- Consideration and modeling of workpiece dynamics is crucial for an accurate analysis of the fixture-workpiece system subjected to machining forces. For the example system analyzed in this chapter, the dominant frequencies (1,332 Hz and 1,655 Hz) of the workpiece response (acceleration) signal were found to be four and five times the dominant frequency (333 Hz = tooth passing frequency) of the

excitation (cutting force), respectively, because 1,332 Hz and 1,665 Hz are near two natural frequencies (1,315 Hz and 1,690 Hz) of the system and the corresponding harmonics are greatly magnified. This dynamic magnification feature cannot be revealed by a static or quasi-static analysis.

- Higher clamping forces result in a stiffer fixture-workpiece system and therefore the system stiffness should be modeled as being clamping force dependent. For the example system studied in this chapter, its modal frequencies were found to be higher when the clamping pressure was increased.

CHAPTER 5

INVESTIGATION OF MATERIAL REMOVAL EFFECT

Machining is characterized by continuous loss of material from the workpiece resulting in time-varying properties of the fixture-workpiece system. This material removal effect (MRE) is either often ignored or modeled in a quasi-static way. This chapter presents a systematic study of MRE on the dynamic behavior of a fixture-workpiece system during machining based on models and approaches developed in Chapter 3 and the current chapter. A variety of material removal induced phenomena such as change of system inertia, geometry, and stiffness and the rate of change of system inertia are modeled and studied in detail. Experimental data collected in a pocket milling process including modal impact tests at different points of the process are used to validate the theoretical models and approaches and to obtain insight into the MRE on fixture-workpiece dynamics.

This chapter is organized as follows: first, the problem is formulated and the overall approach is introduced; next, models that capture the MRE on different system properties are presented and the results of model validation and experimental investigation of MRE are reported and discussed; finally, main accomplishments and conclusions from the study in this chapter are summarized.

5.1 Problem Formulation and Approach

The objective of this chapter is to investigate the material removal effect (MRE) on the dynamic behavior of an arbitrarily configured machining fixture-workpiece system shown schematically in Figure 3.1. All assumptions and coordinate systems defined in Chapter 3 remain the same for the study in this chapter. In addition, the workpiece material is considered to be linearly elastic and isotropic.

The workpiece undergoes dynamic motion during machining. This motion, assumed to be small, is dependent on the dynamic characteristics of the fixture-workpiece system such as inertia, damping, and stiffness. Due to the MRE, the system characteristics are subject to continuous change during machining. Therefore, simulation of the dynamic behavior of the workpiece in machining requires characterization of the instantaneous dynamic properties of the fixture-workpiece system.

The overall approach used in this chapter to study MRE is described by the block diagram in Figure 5.1, which is slightly different from Figure 3.2. The dynamic motion (i.e., displacements, velocities, and accelerations) of the fixtured workpiece during machining is simulated by the dynamic model given in Equation (3.8), whose coefficient matrices are time-varying due to the MRE and are supplied by the geometric model (mentioned in Chapter 3 and detailed in the current chapter) that gives the system inertia properties, a finite element (FE) model (developed in this chapter) that captures the changes in workpiece structural compliance, and the static model given in Equation (3.19) that computes the system stiffness properties. Note that the fixturing dynamic stability, which has been extensively studied in Chapters 3 and 4, is not addressed here to avoid

repetition. Instead, the focus of this chapter is given to the dynamic motion of the fixtured workpiece.

All models except the FE model in Figure 5.1 have been established in Chapter 3. This chapter, based on a pocketing operation and modal impact tests at different points of the pocketing process, presents an in-depth study of MRE on fixture-workpiece dynamics, featuring both theoretical and experimental investigations.

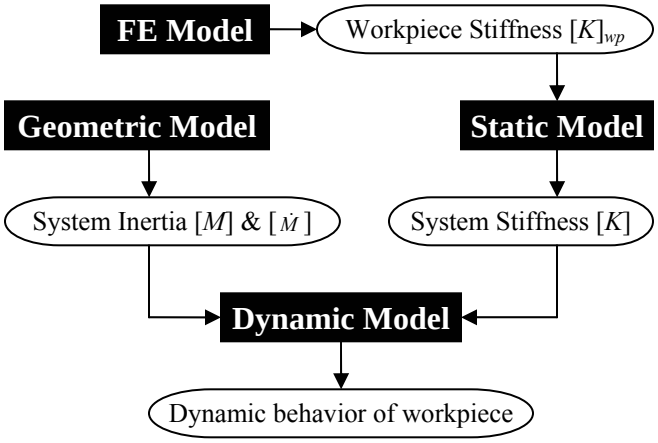

Figure 5.1 Overview of fixture-workpiece dynamics simulation

5.2 Experimental Setup and Problem Data

A pocketing (end milling) operation is performed in this chapter to study the material removal effect. A schematic of the experimental setup is shown in Figure 5.2, where a pocket is being made in the center of the top face of a solid block of aluminum in a CNC milling machine. Pictures of the actual setup are shown Figure 5.3. The workpiece is constrained by a 3-2-1 locator layout and two side clamps that are actuated by a

hydraulic hand pump. The three locators on the primary datum (*XY* plane) are mounted on a steel base plate while the remaining locators and the two side clamps are mounted on steel blocks (fixture bodies) assembled on the base plate. A Kistler® 9257B dynamometer and a Kistler® 8762A10T tri-axial accelerometer (frequency response 0-6 KHz) are used to measure the instantaneous cutting forces and the accelerations of the workpiece, respectively. The dynamometer is placed under the base plate and the accelerometer is mounted on a side face of the workpiece (see Figures 5.2 and 5.3). Data collection was performed using an NI® PCI-4472 dynamic signal acquisition board and the LabVIEW® 7.1 software.

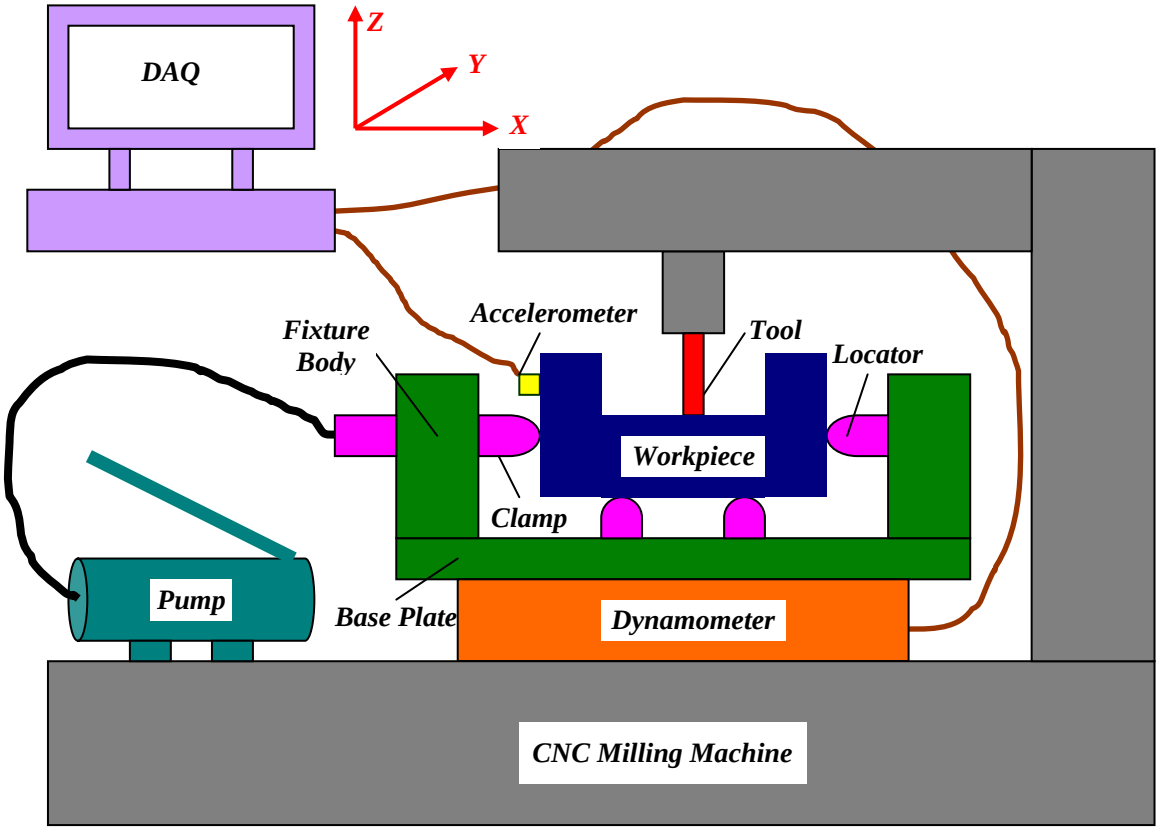

Figure 5.2 Schematic of the pocketing experimental setup

The experimental conditions used in the pocketing process are summarized in Table 5.1. The pocket was formed by moving the tool in the -*Z* (downward) direction with the depth of each level equal to the axial depth of cut (2.54 mm). At each level, a contour cut was first made, leaving some material at the center. This material was then removed in six straight tool passes. The radial depth of cut was 6.35 mm for the first and last passes and 12.7 mm for the rest of the passes. Dry cutting was performed. The sampling rate used for data collection was 12,000 Hz.

The material properties of the workpiece and the fixture elements are given in Table 4.2. Table 4.3 shows the layout and spatial coordinates of all fixture elements in the (*xyz*) frame. The fixture elements are hexagonal (inscribed radius = 6.35 mm or 7.11 mm) cylinders (height = 10.31 mm or 9.53 mm) with a spherical tip (radius = 19.81 mm or 34.93 mm). Note that the values shown in Table 5.3 change as the geometry of the workpiece and hence the location and orientation of the (*xyz*) frame change continuously during machining. This phenomenon is captured by the geometric model.

Table 5.1 Experimental conditions used in pocketing

Workpiece Material	Dimension* (mm)		Pocket Dimension* (mm)	
Al-6061	127×152.4×76.2		88.9×114.3×63.5	
Cutting Conditions				Fixture Design
Axial (mm)	Radial (mm)	Feed (m/min)	Spindle Speed (rpm)	Clamping (psi)
2.54	6.35	0.508	5000	1200
	12.7			

(*: length×width×height)
(Cutting tool: HSS end mill, 25.4 mm, 4-flute, and 30° helix)

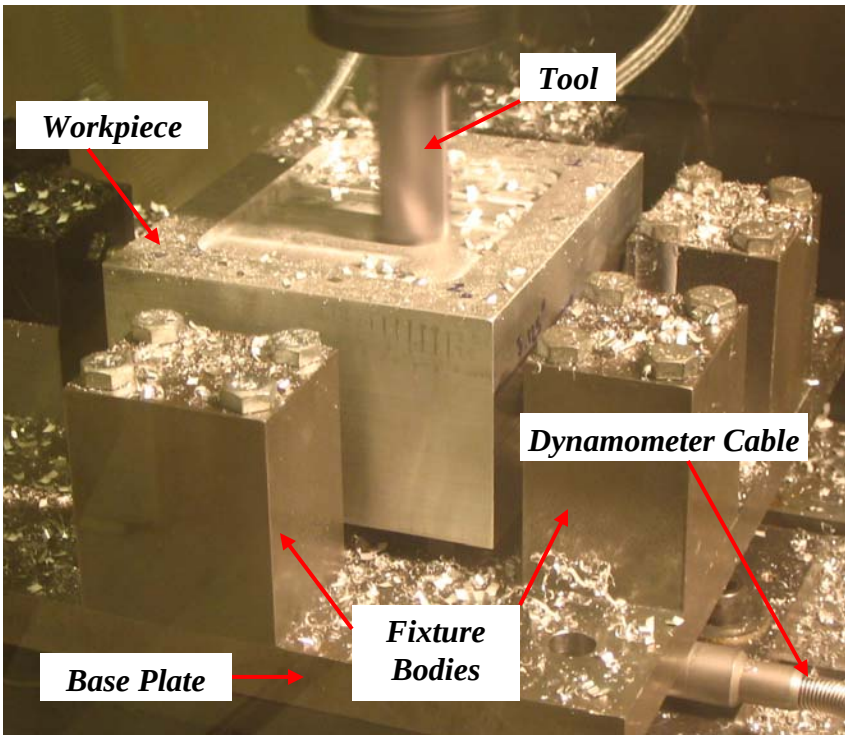

(a)

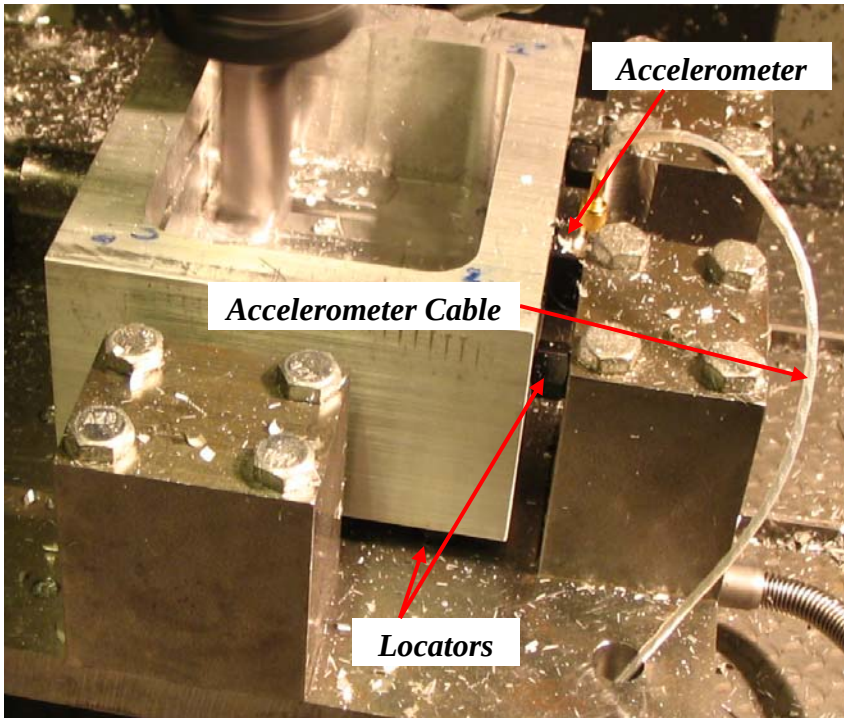

(b)

Figure 5.3 Snapshots of the pocketing experiment

Table 5.2 Material properties

	Workpiece	Fixture Element
Material	Al-6061	Hardened Steel
Density (kg/m^3)	2700	-
Young's modulus (GPa)	70	200
Poisson's ratio	0.33	0.285
Yield strength (MPa)	270	-
Static coefficient of friction	0.375 (measured)	

Table 5.3 Fixture layout (locators L1-L6 and clamps C1-C2)

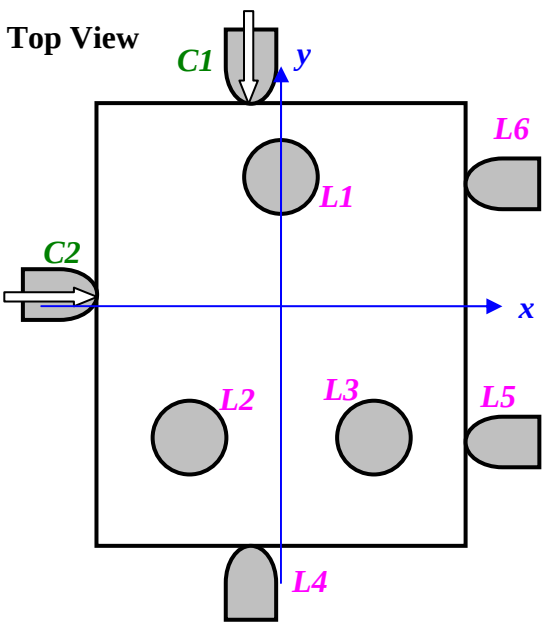

Fixture Element	Coordinate (x, y, z) (mm)
L1	(0.97, 54.1, -38.1)
L2	(-44.75, -64.26, -38.1)
L3	(45.09, -64.26, -38.1)
L4	(-16.51, -76.2, -0.51)
L5	(63.5, -46.23, -0.38)
L6	(63.5, 55.63, 0)
C1	(-1.52, 76.2, 0.51)
C2	(-63.5, 5.08, 1.02)

5.3 Effect of Material Removal on System Inertia

The inertia of the fixture-workpiece system changes instantaneously during machining due to continuous loss of material from the workpiece. Specifically, the mass, moments of inertia, the center of gravity (C.G.), and the orientation of the principal inertia axes of the workpiece vary with time. As described in Chapter 3, these changes are captured by a geometric model developed in ACIS®. The approach involves discretizing a tool path into a number of increments. At each increment, the following steps are taken: i) sweep the cutting tool along the increment; ii) subtract the swept volume from the workpiece via a Boolean operation; and iii) perform a geometric analysis on the remaining workpiece to obtain its volume, location of C.G., and orientation of the principal inertia axes with respect to the global frame (*XYZ*). Typical geometric simulations for the pocketing operation are shown by Figure 5.4.

From the geometric model output, the inertia matrix [*M*] is evaluated at each machining instant (approximated by the increments mentioned earlier). The rate of change of inertia $[\dot{M}]$ is calculated using the forward finite difference method. The machining loads, measured by the dynamometer with respect to the (*XYZ*) frame, are transformed to the instantaneous (*xyz*) frame. Matrices [*M*] and $[\dot{M}]$ and the transformed loads are then input to the dynamic model.

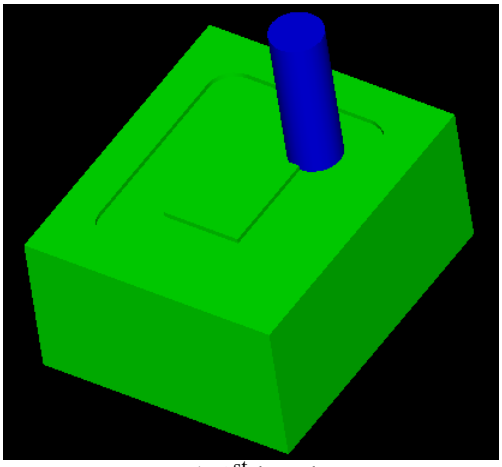

a) 1st level

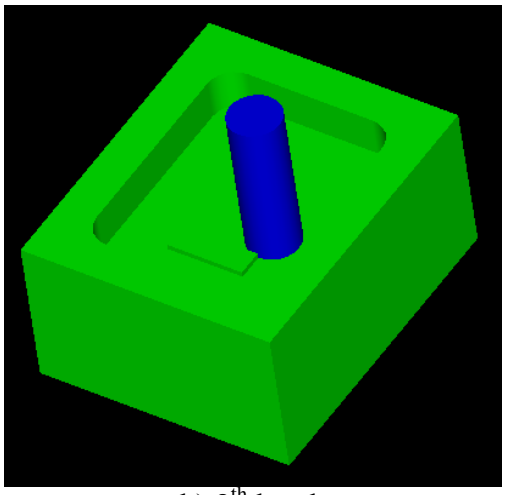

b) 8th level

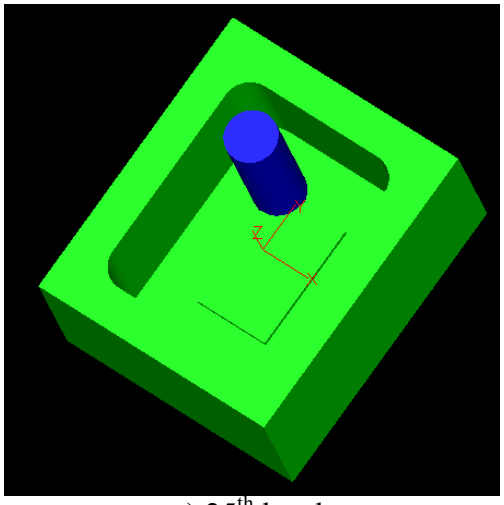

c) 25th level

Figure 5.4 Geometric modeling of the pocketing process

5.4 Effect of Material Removal on System Stiffness

Significant material removal affects the fixture-workpiece system stiffness via the following changes: i) change in the fixture-workpiece contact stiffness due to change in workpiece weight and the (*xyz*) frame; and ii) change in workpiece structural compliance evaluated at the fixture-workpiece contacts.

The fixture-workpiece contact stiffness, as seen in Section 3.4.1, is obtained from the solution of Equation (3.19). The first constraint in Equation (3.19) results from the equilibrium condition of the fixture-workpiece system under clamping loads. This constraint needs to be updated and Equation (3.19) needs to be solved again as the workpiece weight and the geometric configuration of the system change.

As shown in Figure 3.6, the workpiece structural compliance at the fixture-workpiece contact (assumed to be zero in Chapter 3) is approximated by three linear springs and is incorporated into the overall compliance of the system by placing them in series with other springs representing the contact and fixture element compliances. This approach enables the dynamic model to remain compact and efficient, which is especially desirable in fixture design that involves parameter optimization. Note that the validity of this approach is based on the assumption that small-area contacts result in highly localized system deformation and stress. For highly flexible parts, however, this may not be true.

The spring constants for the workpiece structural stiffness are obtained using a finite element (FE) method (ANSYS® 10.0 is used in this work). The method involves the following steps: i) create a meshed model of the workpiece with all fixture-workpiece

contacts defined as keypoints; 2) fix degrees of freedom of all but one contact; 3) apply a unit load in the x direction at the free contact and calculate the resulting workpiece displacement at that point in the same direction; 4) obtain the workpiece local stiffness (i.e., the spring constant), k_{ixw}, which is equal to the reciprocal of the displacement; 5) repeat steps 3 and 4 for the y and z directions at the same contact to obtain k_{iyw} and k_{izw}; and 6) repeat steps 2 to 5 for each of the remaining contacts.

For example, the FE model and deformation for the 25th (last) level of the pocketing operation is shown in Figure 5.5. Figure 5.6 compares the three compliance sources of the system (fixture, contact, and workpiece) at the 25th level. Contact compliance is seen to be dominant because the fixture element stiffness is high due to their stubby geometry.

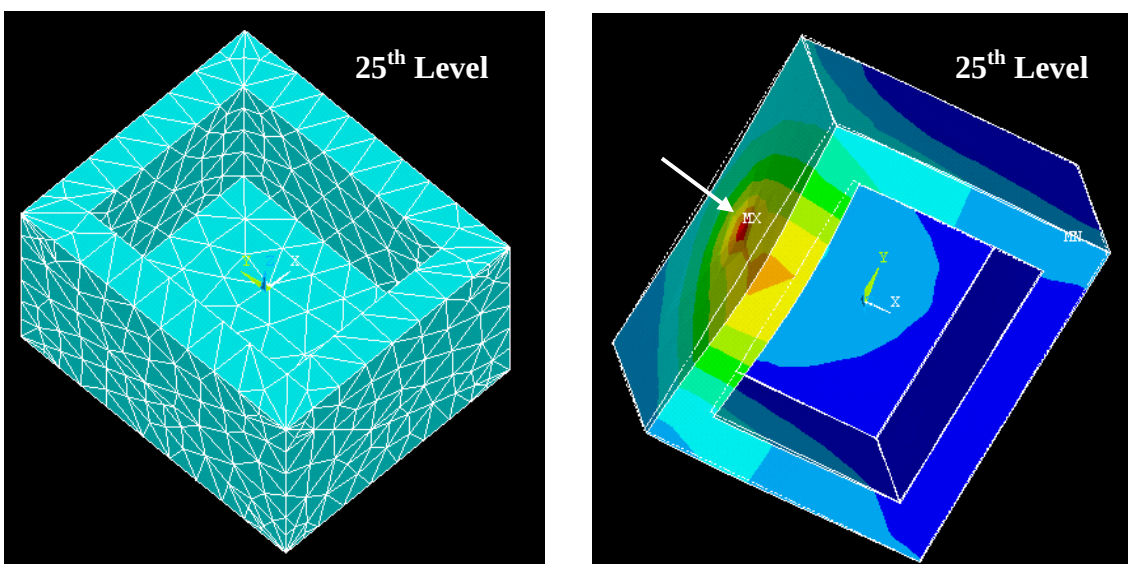

a) Meshed model b) Deformation due to a unit load at C2

Figure 5.5 FE modeling of workpiece compliance

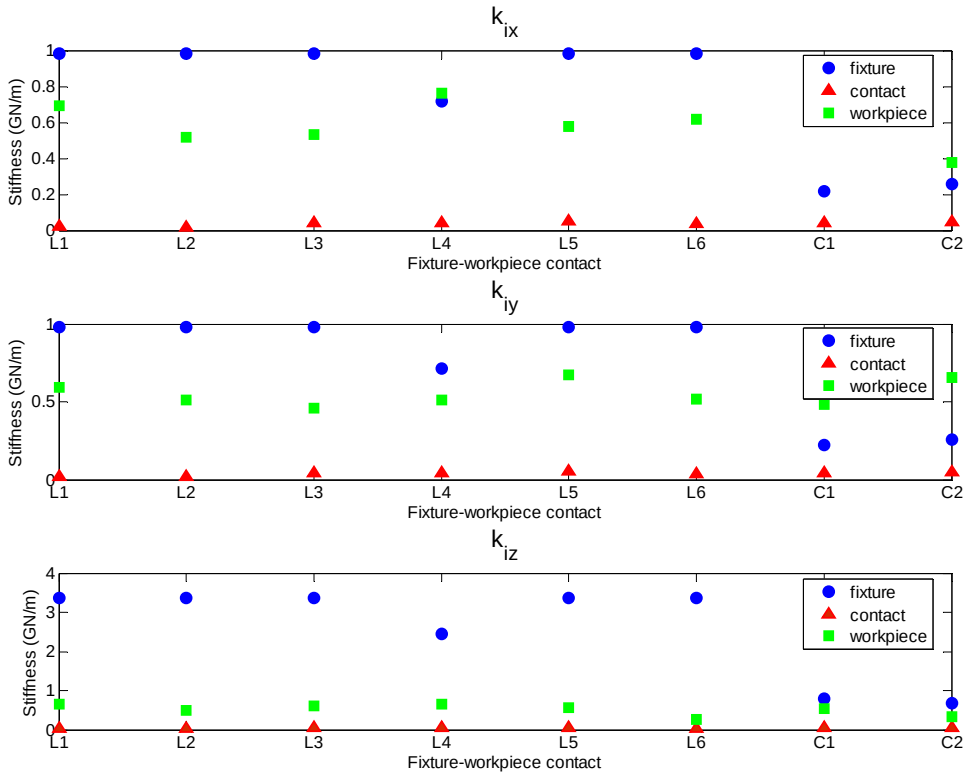

Figure 5.6 Stiffness: fixture vs. contact vs. workpiece (25th level)

5.5 Predicted vs. Measured Dynamics

As mentioned earlier, the pocket was cut one *Z* level at a time and there are 25 levels in all. Each level includes a contour pass and six straight passes. Experimental data (cutting forces and accelerations) were collected at selected levels in the straight passes only. Information about the tool path and data collection is given in Table 5.4.

Table 5.4 Tool path and data collection information

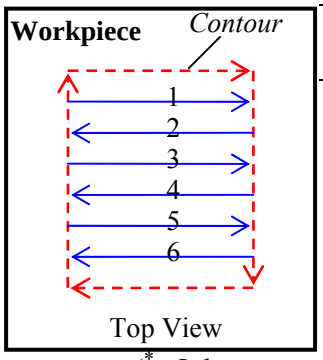

Dataset (or Point)	Level	Pass	Radial Depth* (mm)	Volume Removed (%)
1	1	1	6.35	1.31
2	8	4	12.7	13.64
3	13	1	6.35	22.02
4	19	2	12.7	32.46
5	25	1	6.35	42.72

(*: Other experimental conditions are the same as listed in Table 5.1.)

The measured cutting forces, matrices [M], [$\dot{M}$], and [K], and other information such as the C.G. of the workpiece, orientation of the (xyz) frame were then fed to the dynamic model, which was coded in Matlab® 7.0 and solved using the Newmark-beta method, to obtain $\bar{q}(t)$. Differentiating $\bar{q}(t)$ twice yields the translational accelerations of the C.G. of the workpiece, $\bar{a}_G(t) \in R^3$. The accelerations of the point where the accelerometer was mounted, denoted as $\bar{a}_A(t) \in R^3$, is given by [71],

$$\bar{a}_A = \bar{a}_G + \bar{\alpha} \times \bar{r}_{A/G} + \bar{\omega} \times (\bar{\omega} \times \bar{r}_{A/G}) \tag{5.1}$$

where, $\bar{\omega}$ and $\bar{\alpha}$ represent the angular velocities and accelerations of the workpiece, respectively; and $\bar{r}_{A/G}$ is the displacement vector from the C.G. of the workpiece to the accelerometer position in the (xyz) frame. Note that $\bar{\omega}$ and $\bar{\alpha}$ are obtained from $\bar{q}(t)$ via differentiation.

The acceleration vector $\bar{a}_A$ is referenced to the (xyz) frame while the measured accelerations are referenced to the global (XYZ) frame. To enable comparison, $\bar{a}_A$ is transformed from (xyz) to (XYZ). Note that this transformation is time-dependent as the

origin (the C.G. of the workpiece) and the orientation of (*xyz*) vary with time due to the MRE.

The following six types of simulations were performed for each of the five selected points given in Table 5.4.

1) MRE0: MRE is not considered.
2) MRE1: only changes of mass and moments of inertia of the workpiece are considered.
3) MRE2: in addition to MRE1, changes in the workpiece C.G. and the orientation of the (*xyz*) frame are also taken into account.
4) MRE3: in addition to MRE2, the rate of change of system inertia is included;
5) MRE4: in addition to MRE3, change in the contact compliance is considered;
6) MRE5: in addition to MRE4, the workpiece structural compliance and its change during machining are incorporated.

Note that the degree of sophistication of the model increases from MRE0 to MRE5.

Again, the root mean square (RMS) values of the simulated and measured steady-state acceleration signals are compared. The results of the comparison on RMS accelerations are summarized in Table 5.5 and Figure 5.7. Table 5.5 reports the measured RMS acceleration vector components at each of the five selected points and their comparison with results from the six types of simulations (MRE0 to MRE5). Figure 5.7 compares the percentage error in prediction for each simulation type at different points of the pocketing process (see last column of Table 5.4). Note that numbers in Table 5.5 are

rounded to two decimal places and hence two numbers of the same value in the table are not necessarily the same in their actual values.

It is seen from Table 5.5 that consideration of the MRE on the fixture-workpiece dynamics, regardless of the simulation type (MRE1-MRE5), improves the model prediction accuracy at all points of the pocketing process. At any point, the more sophisticated the model, the smaller the prediction error. This is indicated by Figure 5.7, where the MRE0 line is the highest, followed by MRE1, MRE2, MRE3, and MRE4 while the MRE5 line is the lowest (smallest error).

Table 5.5 Predicted vs. measured RMS accelerations (m/s^2)

Volume Removed		Exp	**MRE0**		**MRE1**		**MRE2**		**MRE3**		**MRE4**		**MRE5**	
			Sim	Diff (%)	Sim	Diff (%)	Sim	Diff (%)	Sim	Diff (%)	Sim	Diff (%)	Sim	Diff (%)
1.31%	a_x	2.97	2.73	-8.28	2.73	-8.01	2.74	-7.84	2.74	-7.84	2.74	-7.70	3.03	1.81
	a_y	6.52	5.61	-13.96	5.63	-13.66	5.85	-10.29	5.85	-10.29	5.95	-8.72	6.17	-5.33
	a_z	11.20	10.47	-6.53	10.64	-5.07	10.66	-4.89	10.66	-4.89	10.70	-4.51	10.90	-2.73
13.64%	a_x	4.55	3.70	-18.60	3.93	-13.64	4.07	-10.36	4.07	-10.36	4.09	-10.02	4.31	-5.13
	a_y	13.11	10.71	-18.31	11.10	-15.31	11.51	-12.21	11.51	-12.21	11.60	-11.52	11.86	-9.54
	a_z	7.66	6.54	-14.73	6.57	-14.33	6.90	-10.02	6.90	-10.02	6.95	-9.30	7.10	-7.39
22.02%	a_x	2.98	2.15	-27.97	2.49	-16.28	2.61	-12.34	2.61	-12.34	2.62	-12.14	2.74	-8.09
	a_y	7.39	5.37	-27.28	5.95	-19.40	6.27	-15.13	6.27	-15.13	6.29	-14.84	6.87	-7.00
	a_z	8.28	6.21	-25.01	6.77	-18.18	7.36	-11.04	7.36	-11.04	7.49	-9.55	7.82	-5.55
32.46%	a_x	3.98	2.66	-33.16	3.13	-21.54	3.40	-14.69	3.40	-14.69	3.41	-14.28	3.67	-7.83
	a_y	13.09	8.85	-32.36	10.08	-23.03	10.85	-17.08	10.85	-17.08	10.90	-16.74	11.76	-10.14
	a_z	12.70	7.63	-39.91	9.43	-25.69	10.92	-14.03	10.92	-14.03	10.97	-13.57	12.05	-5.10
42.74%	a_x	1.56	0.83	-46.77	1.14	-27.43	1.20	-23.52	1.20	-23.52	1.27	-18.79	1.42	-9.11
	a_y	4.20	2.38	-43.23	3.13	-25.38	3.30	-21.45	3.30	-21.45	3.39	-19.29	3.82	-9.07
	a_z	8.51	4.53	-46.77	6.06	-28.75	6.61	-22.29	6.61	-22.29	6.94	-18.40	7.81	-8.18

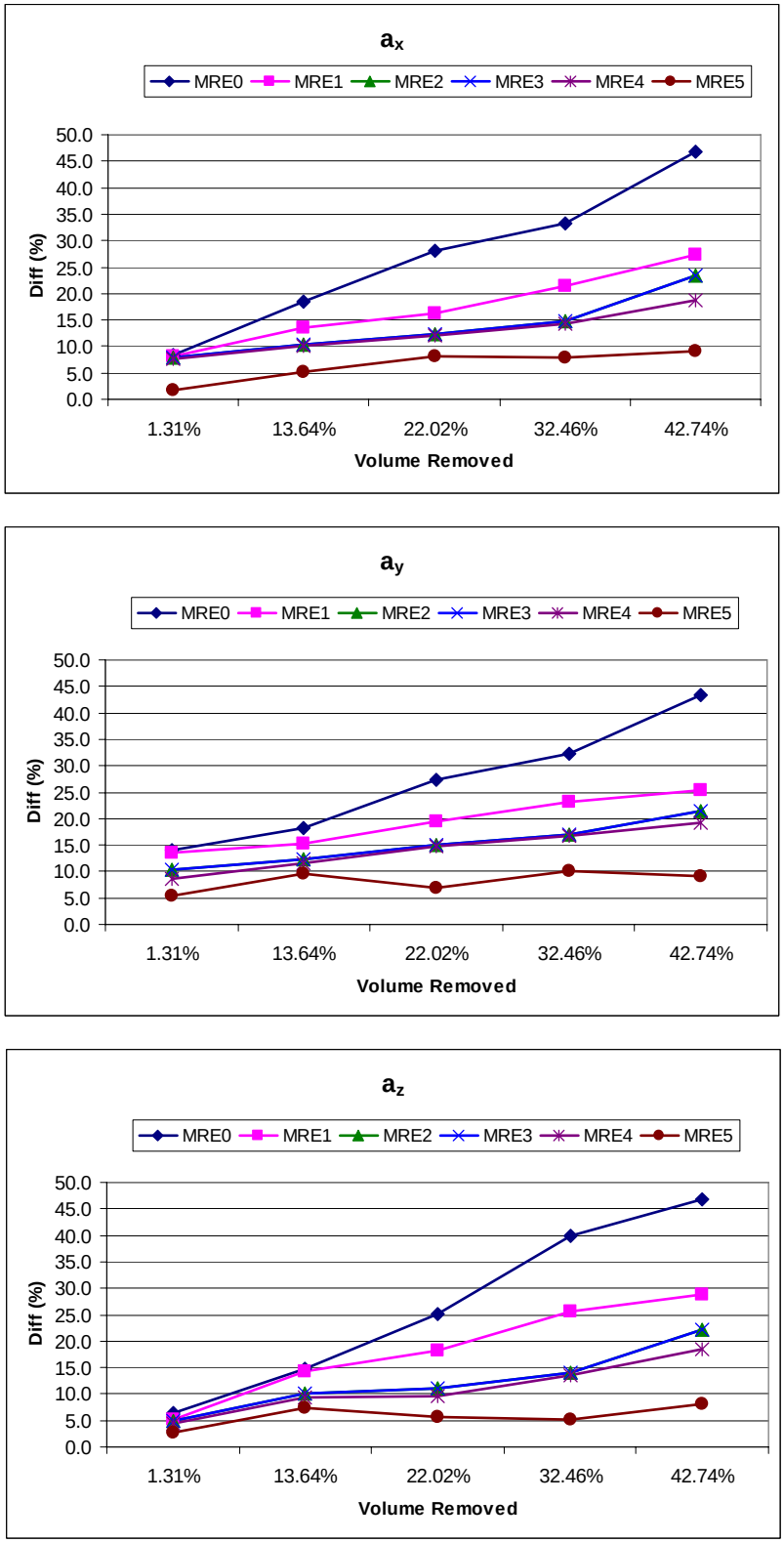

Figure 5.7 Prediction errors of MRE0-MRE5 at different points of pocketing

All but one of the lines (MRE5) in Figure 5.7 are monotonic, indicating that the prediction error of MRE0 or any incomplete MRE simulation (MRE1, MRE2, MRE3, or MRE4) increases with the percentage of volume removed. The average percentage error in prediction for MRE0 are 9.59%, 17.21%, 26.75%, 35.15%, and 45.59% for 1.31%, 13.63%, 22.02%, 32.46%, and 42.74% material removal, respectively. These errors decrease to 3.29%, 7.39%, 6.88%, 7.69%, and 8.79%, respectively, for MRE5. This result indicates the importance of considering MRE in dynamic modeling of a machining fixture-workpiece system especially when a significant portion of volume is removed. Furthermore, the complete model (MRE5) appears to work well (average prediction error for all five points is 6.81%).

As the MRE has been broken down into five sub-effects captured by the cases MRE1-MRE5 respectively, it is possible to investigate the relative significance of the different material removal sub-effects. The significance of a sub-effect is indicated in Figure 5.7 by the distance between its representative line and the one immediately above it. The larger this distance, the greater the improvement in prediction accuracy of the simulation of that sub-effect and the more significant is this sub-effect as far as the system dynamics is concerned.

Of the different sub-effects, the change in system inertia (MRE1), change in workpiece structural compliance (MRE5), and the change in system geometry (MRE2) are seen to have the most prominent effect on the fixture-workpiece dynamics. The average improvement in prediction accuracy for MRE1, compared with its immediate predecessor (i.e., MRE0), for all five points of the pocketing process is 8%, and is 4.9%, 4.72%, 1.94%, and 0% for MRE5, MRE2, MRE4, and MRE3, respectively.

The direct effect of change in workpiece mass on the system dynamics, captured by MRE1, is seen to be the most significant. Its indirect effect on the dynamics via change in the fixture-workpiece contact stiffness, captured by MRE4, is somewhat insignificant because the 1.94% improvement also includes the effect of change in the (*xyz*) frame. This can be explained by looking at the static model given by Equation (3.19) in which the workpiece weight plays a role in the first constraint representing the equilibrium condition of the system under clamping loads. In the pocketing example, the weight of the workpiece is about 40 N while the clamping force is around 900 N. Therefore, change in workpiece weight has very little effect on the solution to Equation (3.19) and the subsequent contact stiffness calculation.

The system inertia change (8% improvement) seems more influential than the stiffness change (4.9% improvement) because, as seen from Figure 5.6, the contact compliance (due to spherical-tipped fixture elements) is dominant even at the end of the process with 42.72% material removed. For more rigid contacts (e.g., planar-tipped fixture elements), however, the effect of stiffness change on the system dynamics may be equally or more influential.

Consideration of the rate of change of system inertia in the model, captured by MRE3, is found to generate negligible improvement in model prediction accuracy for the pocketing example. To explain this result, a rough single degree of freedom (DOF) analysis of the pocketing operation is performed for comparing the inertial, anti-damping due to rate of change of inertia, and elastic force terms on the left hand side of the dynamic model given in Equation (3.8), and the results are shown in Table 5.6. Note that $[\dot{M}]\dot{\bar{q}}$ in Equation (3.8) produces an anti-damping effect on the fixture-workpiece system

because $[\dot{M}]$ is negative (the system inertia decreases during machining). The matrix $[\dot{M}]$ can be approximated by $\Delta[M]/\Delta t$ for small Δt and hence is determined by the material removal rate (MRR) of the machining process.

Therefore, the term $\dot{m}$ in Table 5.6 (equivalent to $[\dot{M}]$ for a multiple DOF analysis) is derived from the MRR of the pocketing process given by (feed)*(radial depth)*(axial depth). The acceleration $\ddot{x}$, a dummy variable in this rough analysis, is assumed to be 100 m/s^2. The velocity $\dot{x}$ and the displacement x are approximated to be $\ddot{x} \cdot \Delta t$ and $\dot{x} \cdot \Delta t$, respectively, and Δt is the reciprocal of the sampling rate (12,000 Hz) used in the pocketing experiment. As seen in Table 5.6, the anti-damping force $\dot{m}\dot{x}$ is negligible compared to the inertial force $m\ddot{x}$ and the elastic force kx for the pocketing process. Although this is a very rough analysis, it can explain why consideration of $[\dot{M}]$ (MRE4) does not seem to improve the model prediction accuracy at all. However, this result is specific to the example, which is characterized by a rather low MRR, a relatively heavy workpiece, and a relatively rigid system configuration. For aggressive machining on light, flexible systems, the anti-damping effect due to change of system inertia may play a more significant role in determining the system dynamics.

Table 5.6 Inertia vs. rate of change of inertia vs. elasticity

m (kg)	4	$\ddot{x}$ (m/s^2)	100	$m\ddot{x}$ (N)	400
$\dot{m}$ (kg/s)	-7.4×10^{-4}	$\dot{x}$ (m/s)	8.3×10^{-3}	$\dot{m}\dot{x}$ (N)	-6.14×10^{-6}
k (N/m)	1×10^{8}	x (m)	7×10^{-7}	kx (N)	70

5.6 Modal Impact Test

Modal impact tests were conducted at all five selected points in the pocketing process. A picture taken from the actual test is shown in Figure 5.8, where an impulse hammer (Kistler® 9722A2000) with a medium-hard rubber tip was used to impact the fixtured workpiece that has lost a portion of material due to pocketing and the excitation (impact) and response (acceleration) data were collected.

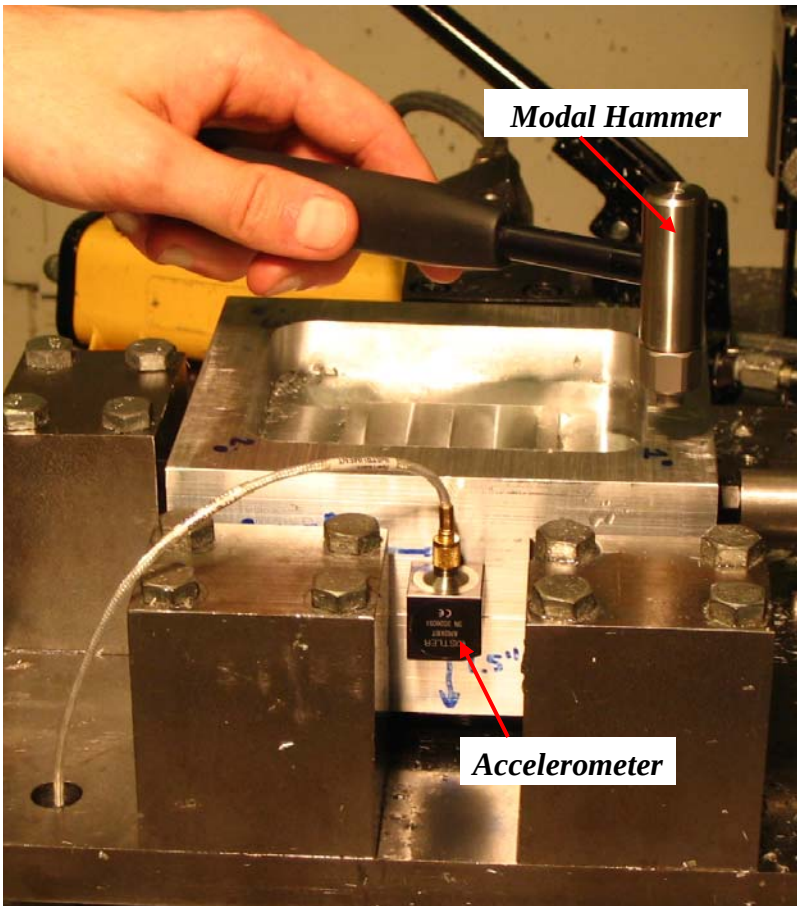

Figure 5.8 Modal impact test in pocketing

Table 5.7 Predicted vs. measured system modal frequencies (Hz)

Mode	Depth Level/Volume Removed														
	1/1.31%			8/13.64%			13/22.02%			19/32.46%			25/42.74%		
	Exp	Sim	Diff (%)	Exp	Sim	Diff (%)	Exp	Sim	Diff (%)	Exp	Sim	Diff (%)	Exp	Sim	Diff (%)
1	1700	1631	-4.09	1720	1699	-1.20	1770	1708	-3.49	1785	1768	-0.93	1800	1814	0.80
2	1895	1885	-0.53	1960	1959	-0.07	2013	2013	-0.01	2040	2074	1.67	2112	2038	-3.52
3	1970	1960	-0.49	2180	2047	-6.08	2370	2113	-10.84	2435	2184	-10.30	2440	2149	-11.94
4	-	-	-	-	-	-	4555	-	-	3419	-	-	2956	-	-
5	-	-	-	-	-	-	-	-	-	5230	-	-	4400	-	-
6	-	-	-	-	-	-	-	-	-	5830	-	-	5880	-	-

The Complex Mode Indicator Function (CMIF) technique [77] was used to estimate the modal frequencies of the system from the raw data. Shown in Figure 5.9 are the CMIF plots for the five selected levels of the process (see Table 5.4). In each plot of Figure 5.9, the modal frequencies are indicated by the large peaks of the first (or highest) singular value curve and double or multiple modes are indicated by simultaneously large values of the other two curves. The predicted and measured modal frequencies of the fixture-workpiece system at the five instants of the pocketing process are compared in Table 5.7. Note that the predicted frequencies are obtained from the MRE5 simulation.

It is observed from Figure 5.9 and Table 5.7 that the system modal frequencies are divided into two groups – modes 1-3 lie between 1,500 and 2,500 Hz while modes 4-6 lie between 2,900 and 6,000 Hz. The first group of modes is attributed to the fixture-workpiece contact compliance while the second group is thought to result from the structural compliance of the workpiece. The first group appears throughout the pocketing process (at all five levels) while the second group does not show up until the 13th level (corresponding to 22.02% material removal) because in the 1st and 8th levels the volume removed is relatively small (up to 13.64%) and the structural stiffness of the workpiece is still relatively high.

As more material is cut away and the workpiece becomes compliant, a new mode of 4,555 Hz appears in the 13th level as seen in its CMIF plot. In the 19th level, a further decrease in workpiece rigidity reveals two more new modes (5,230 Hz and 5,830 Hz) while the one shown in the 13th level now decreases to 3,419 Hz. This modal frequency decreases further to 2,956 Hz in the 25th level and the 5,230 Hz mode now decreases to 4,400 Hz. The 5,830 Hz mode seems to disappear in the 25th level. It is possible that a

mode is not adequately excited in the test if the hammer impacts a node or a position near a node of that mode. In the 25th level a new mode of 5880 Hz is seen. It is expected that, if more material is removed, additional modes will appear and the existing modes will further decrease and eventually become mixed with the modes attributable to the contact compliance. Note that the decrease in workpiece mass and the increase in workpiece compliance due to material removal are two competing factors in determining the system natural frequencies. In the pocketing example, the change in compliance seems to influence more significantly the modal response of the fixtured workpiece at higher frequencies.

It is also observed that the frequencies in the first group slightly increase and become separated as material is removed. This is thought to be because the system inertia decreases during machining while the contact compliance (contributing to the first group) changes only slightly (see analysis in Section 5.5).

It can be seen from Table 5.7 that the model predicts the first group of frequencies well (average percentage error = 3.73%) but is unable to predict the second group. This is because the size of the dynamic model given in Equation (3.8) remains 6×6 after incorporation of the workpiece structural compliance by assuming that the workpiece deformations are highly localized (see Section 5.4). As a result, only low order modes can be predicted by the dynamic model because it captures only three translational modes. The dynamic model, as shown earlier, still performed quite well in predicting the workpiece motion because the high order modes (second group) of the fixture-workpiece system were not excited in the pocketing operation. A Fourier analysis of the cutting

force data shows that no major harmonic is higher than 2,000 Hz while the lowest mode in the second group of modes in the CMIF plots is 2,956 Hz.

The Complex Exponential (CE) algorithm [76] was used to estimate the damping of the fixture-workpiece system. The three damping ratios (corresponding to modes 1-3 in Table 5.7) for the 1st level are found to be 7.68%, 5.84%, and 4.51% and they are 5.63%, 6.66%, and 4.87% for the 25th level. This indicates that the system is lightly damped.

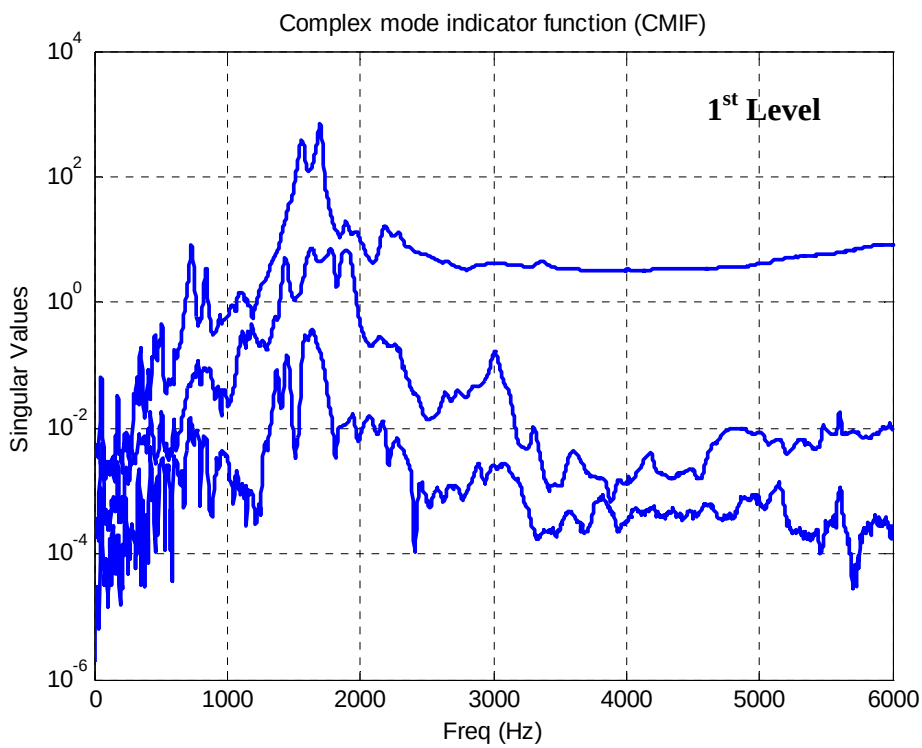

(a)

Figure 5.9 CMIF plots for identification of modal frequencies

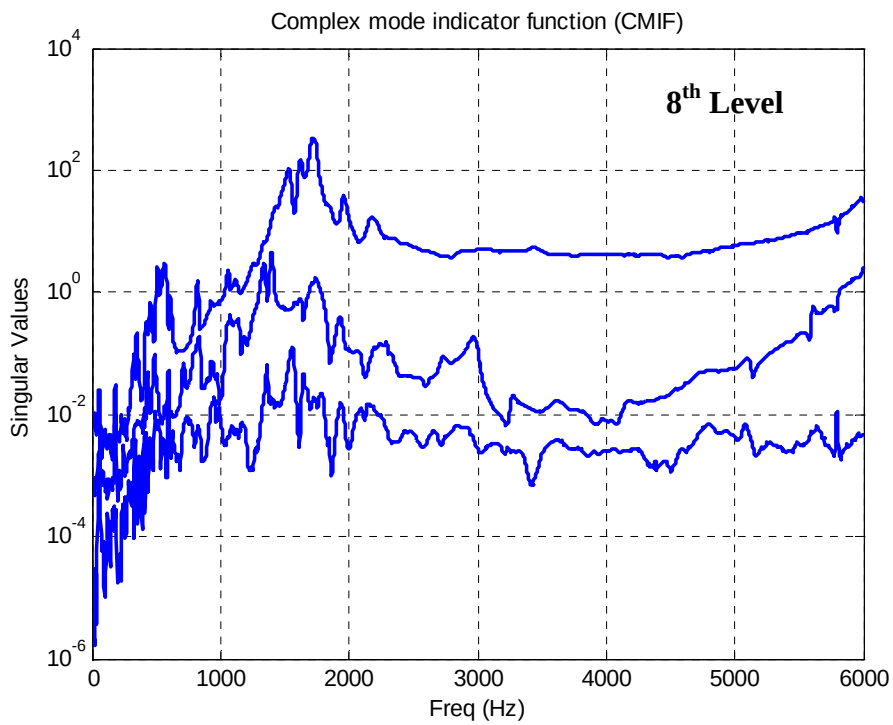

(b)

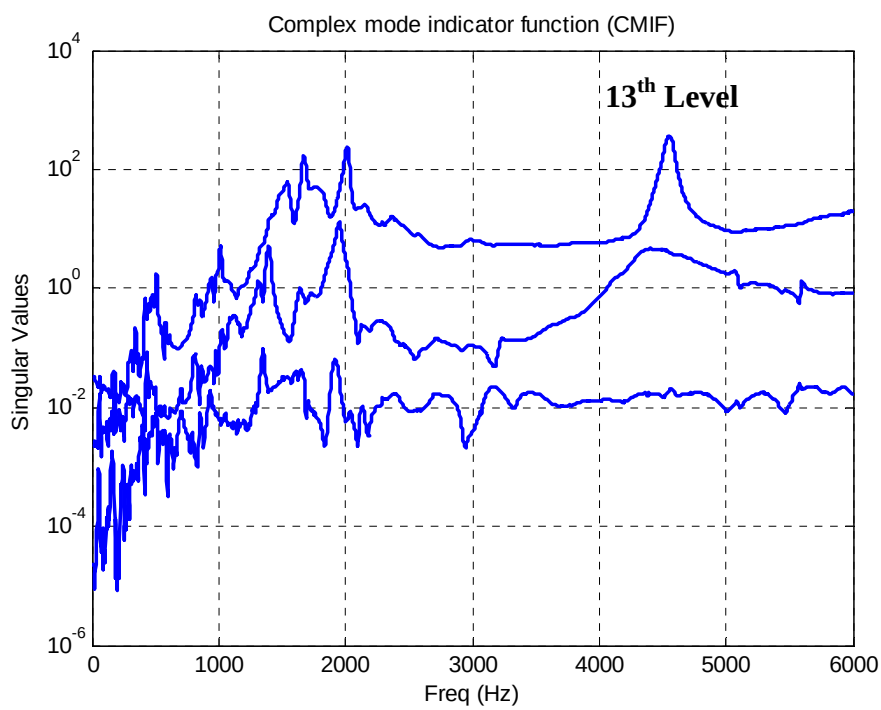

(c)

Figure 5.9 Continued

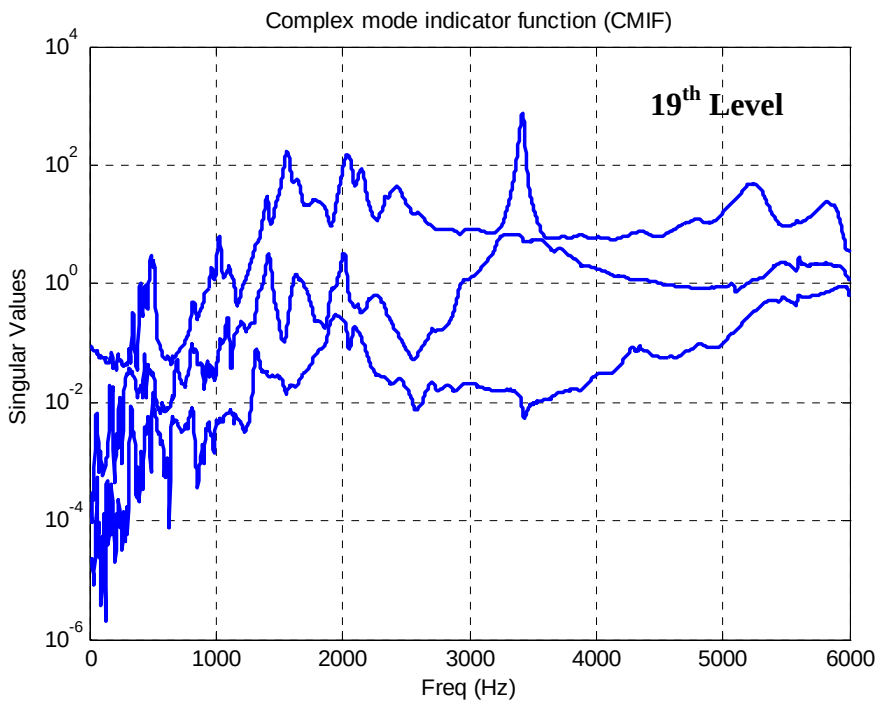

(d)

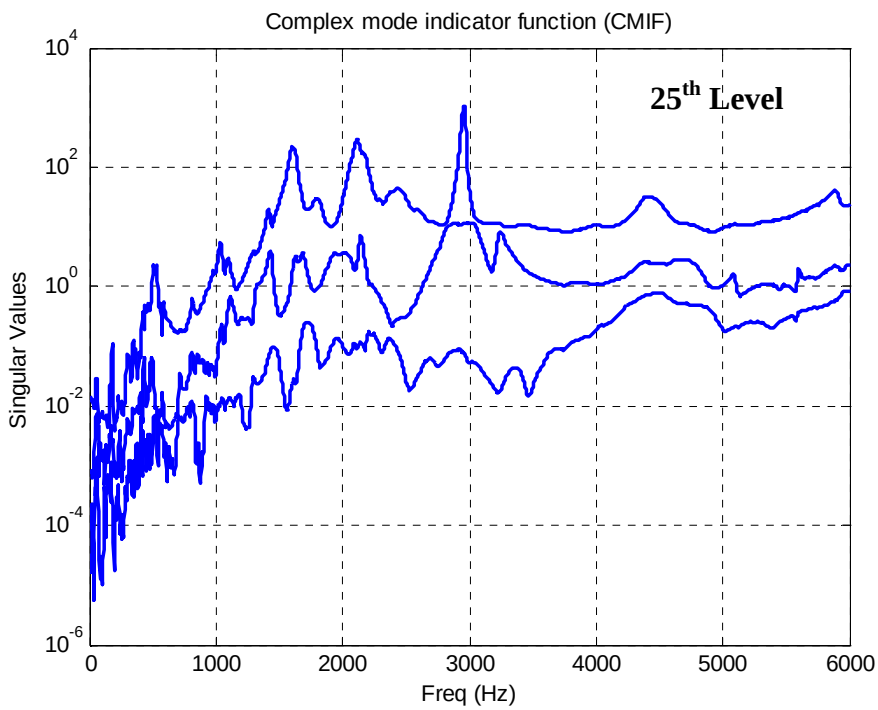

(e)

Figure 5.9 Continued

5.7 Summary

A systematic study, featuring both theoretical and experimental investigations, of the material removal effect (MRE) on the dynamic behavior of a fixture-workpiece system in machining has been presented in this chapter. A finite element approach was developed to calculate the structural compliance of the workpiece as well as its change during machining. The workpiece compliance was then incorporated into the overall compliance of the fixture-workpiece system.

Data collected in a pocket milling operation were used to validate the theoretical models and to investigate the significance of MRE as well as the relative importance of influences of different MRE induced phenomena (e.g., change of system inertia, geometry, and stiffness and rate of change of system inertia) on the system dynamics. Modal impact tests were conducted at different points of the pocketing process, corresponding to different percentages of volume removed, to further validate theoretical models and to experimentally investigate the MRE on the modal properties of the fixture-workpiece system.

Major conclusions from the study in this chapter are as follows:

- Consideration of MRE is crucial for an accurate analysis of the fixture-workpiece system dynamics when a significant portion of volume is removed in the machining operation. For the pocketing process presented in this chapter, the average prediction errors of the RMS acceleration of the workpiece were 9.59%, 17.21%, 26.75%, 35.15%, and 45.59% for 1.31%, 13.63%, 22.02%, 32.46%, and 42.74% material removal, respectively, when

the MRE was not considered. After accounting for the MRE, these errors decreased to 3.29%, 7.39%, 6.88%, 7.69%, and 8.79%, respectively. The average prediction error after accounting for the MRE completely is 6.81%.

- The MRE can be broken down into several sub-effects resulting from the change in system inertia, stiffness, geometry, etc. The relative significance of the sub-effects is case-specific and requires individual analysis. For the pocketing operation in this chapter, the average improvements in prediction accuracy of MRE1 (change of inertia), MRE2 (change of geometry), MRE3 (rate of change of inertia), MRE4 (change of contact compliance), and MRE5 (change of workpiece compliance), compared with MRE0 (no consideration of MRE), are 8%, 4.72%, 0%, 1.94%, and 4.9%, respectively.
- For the example system analyzed in this chapter, as material is removed, the modal frequencies resulting from the fixture-workpiece contact compliance grow slightly and become separated while those arising from the structural compliance of the workpiece decrease significantly. The theoretical model is able to predict the low order system natural frequencies well (average error is 3.73%).

CHAPTER 6

PARAMETER EFFECT AND SENSITIVITY ANALYSES

The fixturing dynamic stability, defined and discussed in Chapter 3, is an important performance measure of a machining fixture and is affected by a variety of factors such as the excitation frequencies, fixture layout, clamping forces, the static coefficient of friction at the fixture-workpiece contact, percentage of material removed, fixture-workpiece contact geometry, fixture element design, workpiece material, etc. This chapter presents parameter effect and a sensitivity analyses of fixturing dynamic stability in machining based on the stability analysis procedure developed in Chapter 3. In the parameter effect analysis, critical fixture design and machining process parameters are selected and their effects on the fixturing dynamic stability are studied to understand their roles and relative significance in determining machining fixture performance. In the sensitivity analysis, changes in fixturing (in)stability due to imprecision in the selected parameters is examined.

The chapter is organized as follows. The approaches used in the parameter effect and sensitivity analyses are described first; then, a numerical example is given and the results are presented and discussed; finally, the chapter is summarized and major conclusions drawn.

6.1 Parameter Effect Analysis

In the parameter effect analysis, four parameters – spindle speed, static coefficient of friction, fixture layout, and clamping forces – are selected for investigation of their roles and relative importance in affecting the fixturing dynamic stability of a fixture-workpiece system in machining.

The spindle speed of the machine tool is chosen because it is an important machining process parameter and directly determines the dominant frequency in the machining force, which provides the external excitation to the fixture-workpiece system. The dominant excitation frequency in a milling process, which is of particular interest to this study, is equal to the tooth passing frequency and is given by,

$$f_t = (N)(SS/60) \quad (Hz) \tag{6.1}$$

where N is the number of flutes in the cutting tool and SS is the spindle speed of the machine tool in rpm.

When f_t (or $2\,f_t$, $3\,f_t$, $4\,f_t$, and so on) is in the vicinity of a natural frequency of the fixture-workpiece system, a system with light damping will undergo serious vibrations due to resonance and thus degrade the operational safety and part quality. As analyzed later in this chapter, there exist critical spindle speeds that induce resonance in a fixture-workpiece system in milling.

The static coefficient of friction at the fixture-workpiece interface, denoted as μ_S, appears in the second fixturing stability criterion given in Equation (3.1) and the static model given in Equation (3.19) and hence plays a role in determining the fixturing dynamic stability in machining. The parameter μ_S, which depends mainly on the

materials and surface properties of the workpiece and the fixture element, can be possibly modified to achieve certain fixture design goals.

The last two selected parameters, fixture layout and clamping forces, are known to be the most important fixture design parameters. They have paramount influence on the fixture performance and clamping forces are generally easy to change. In the procedure for fixturing dynamic stability analysis established in Chapter 3, the fixture layout and clamping forces directly determine the solution of the static model given in Equation (3.19) and thus the elastic deformation of the system due to clamping as well as the system stiffness. Therefore, it is of great interest to perform an in-depth investigation of these two parameters.

The method used in the parameter effect analysis in this work is described as follows:

1) Each of the four selected parameters is assigned two values. One value is designed to result in a more stable fixturing configuration (based on standard practice) than the other. For example, the first value for the spindle speed is selected to generate an excitation frequency near a natural frequency of the fixture-workpiece system and hence expected to result in weak fixturing dynamic stability while the second value is chosen such that the excitation frequency is away from the resonance regions. As another example, the two fixture layouts used differ in the level of spacing of locators in the primary datum. For a typical 3-2-1 locator layout, it is generally believed [1] that the larger the triangle formed by the three locators in the primary datum (illustrated in Figure 6.1), the more stable the fixturing configuration.

2) A full factorial combination of the eight values (two for each parameter) generated in the previous step is analyzed, resulting in a total of sixteen cases.
3) For each case, the onset of fixturing dynamic instability of the system during machining as well as the degree of the (in)stability are analyzed using the procedure developed in Chapter 3.
4) The fixturing dynamic stability analysis results of all sixteen cases are compared.

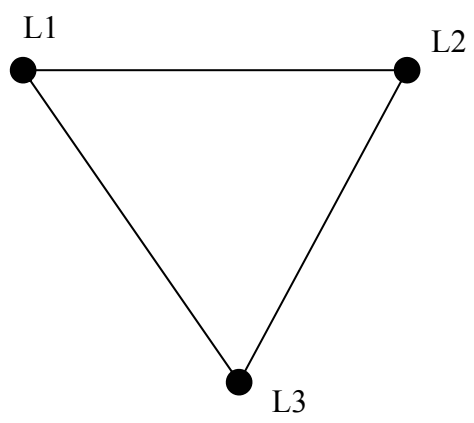

Figure 6.1 Locators in the primary datum for a 3-2-1 fixture layout

6.2 Sensitivity Analysis

In practice, fixture design parameters are subject to imprecision arising from the imperfection of equipment and operations. For example, position deviations may exist when the fixture elements are placed around the workpiece; errors may occur in measurements of the static coefficient of friction at the fixture-workpiece interfaces. It is

then desirable to understand the sensitivity of fixturing dynamic stability to such imprecision in the fixture design parameters.

In the sensitivity analysis described in this chapter, a stable case is selected from the sixteen cases generated in the parameter effect analysis. Further selected fixture design parameters are assigned a number of levels of imprecision. For each imprecision level, the fixturing dynamic stability of the system is analyzed. The results for all levels are then compared.

6.3 Numerical Example

The following numerical example is used to perform the parameter effect and sensitivity analyses.

6.3.1 Problem Data

The example considers an end milling operation. The operation, as illustrated in Figure 6.2, involves milling a slot on the top face of a prismatic workpiece. The slot is formed in multiple passes. The tool starts cutting at the right end (+X) of the slot and makes a straight pass along the Y axis. Upon finishing a pass, the tool moves along the -X axis to execute the next pass until a depth level is completed, after which the tool travels along the -Z axis to the next depth level. The total volume removed by the tool (i.e., volume of the slot) is 26.58% of the original workpiece volume.

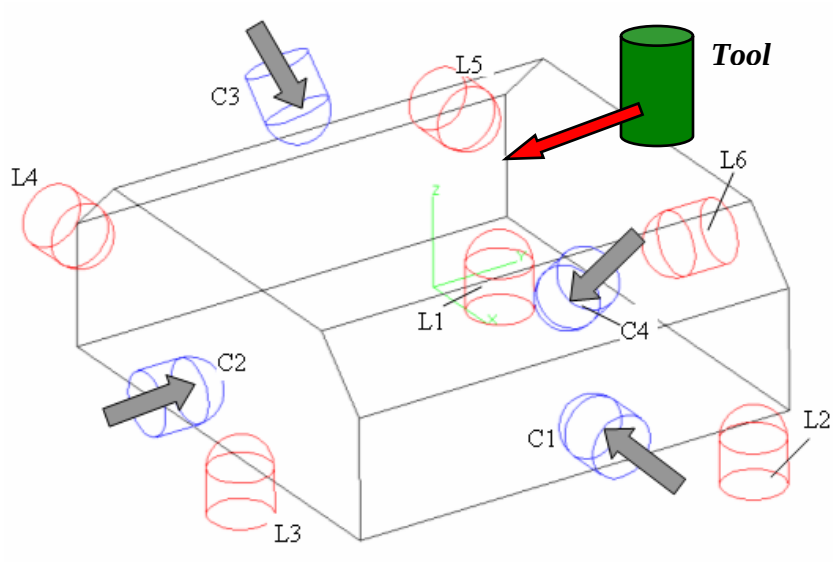

(a) Initial workpiece and fixture layout (L1-L6: locators; C1-C4: clamps)

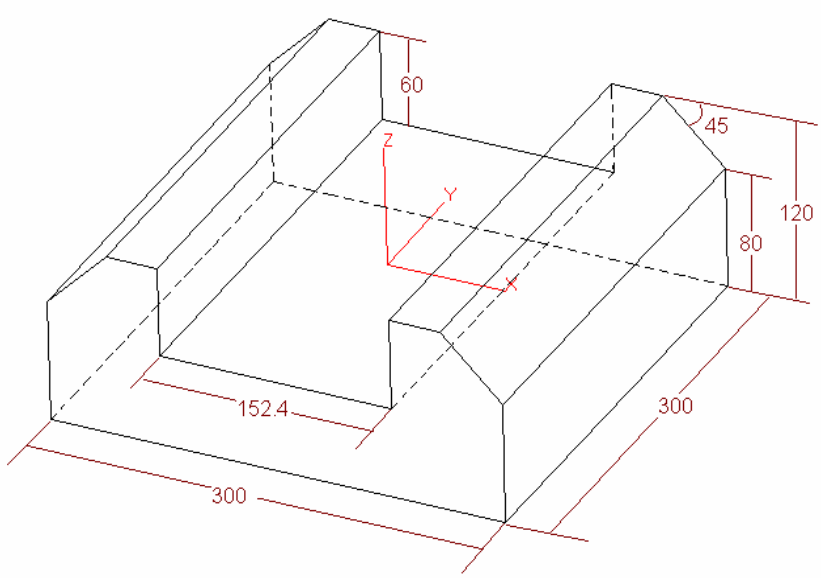

(b) Final part and dimensions (in mm)

Figure 6.2 End milling operation used in the example

A 3-2-1 locator layout and four clamps are used to restrain the workpiece, as seen in Figure 6.2 (a). All fixture elements are identical with a cylindrical body (radius=20mm

and length=30mm) and a spherical tip (radius=20mm). The material properties of the workpiece and the fixture elements are given in Table 6.1. The cutting conditions used in this example are summarized in Table 6.2. Note that the spindle speed is not listed here because it is a variable in the parameter effect and sensitivity analyses and will be determined later.

Table 6.1 Material properties

	Workpiece	Fixture Elements
Material	Aluminum 7075-T6	Hardened Steel
Density (kg/m^3)	2700	-
Young's modulus (GPa)	70.3	201
Poisson's ratio	0.354	0.296
Yield strength (MPa)	500	-

Table 6.2 Machining conditions

Feed Rate (mm/rev)	Axial Depth (mm)	Radial Depth (mm)
0.5	5	12.7

(End mill: carbide, 25.4 mm, 3-flute, and 30° helix)

The instantaneous machining forces for this example are obtained from the milling force model mentioned in Chapter 3 and derived from [75]. The spindle speed does not play a role in this force model. The cutting forces in three orthogonal directions are shown for a single tool revolution (360°) in Figure 6.3.

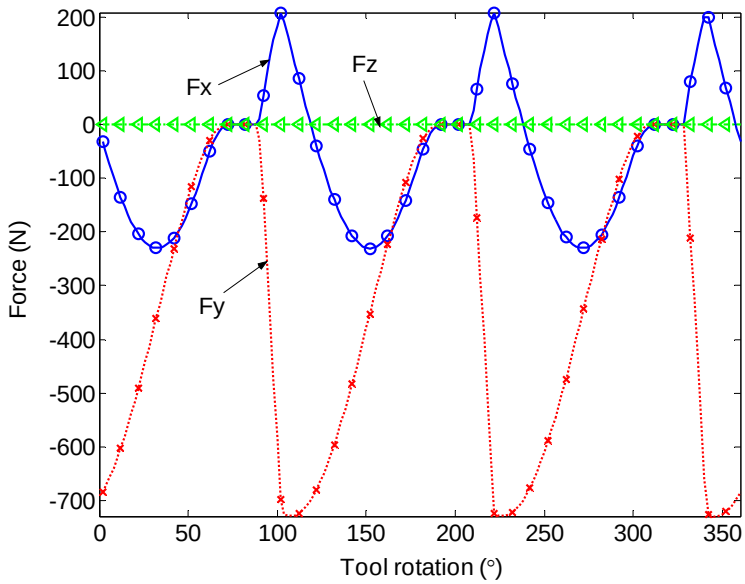

Figure 6.3 Simulated milling forces

6.3.2 Parameter Effect Analysis

As mentioned earlier, four parameters – spindle speed (SS), static coefficient of friction (μ_S), fixture layout, and clamping forces (F_c) – are selected for parameter effect analysis and each parameter is assigned two values. Table 6.3 lists the values of SS, μ_S, and F_c. The information for the two selected fixture layouts is given in Figure 6.4 and Table 6.4. Note that the coordinates of L6 and all clamps are identical for the two layouts.

Table 6.3 Assigned values of selected parameters

Variation	SS (rpm)	μ_S	F_c^* (N)
1	12,000	0.25	3,000
2	15,000	0.35	5,000

(*: all clamps apply the same force.)

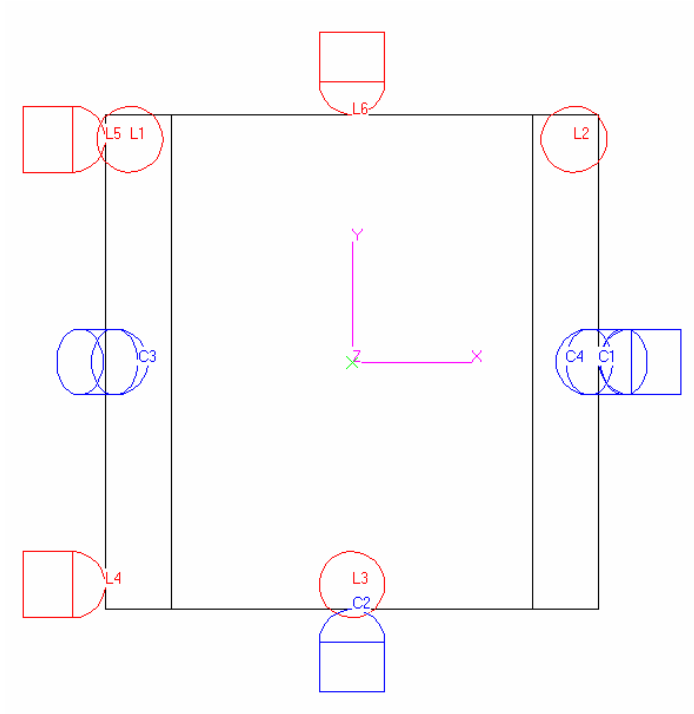

(a) Layout #1

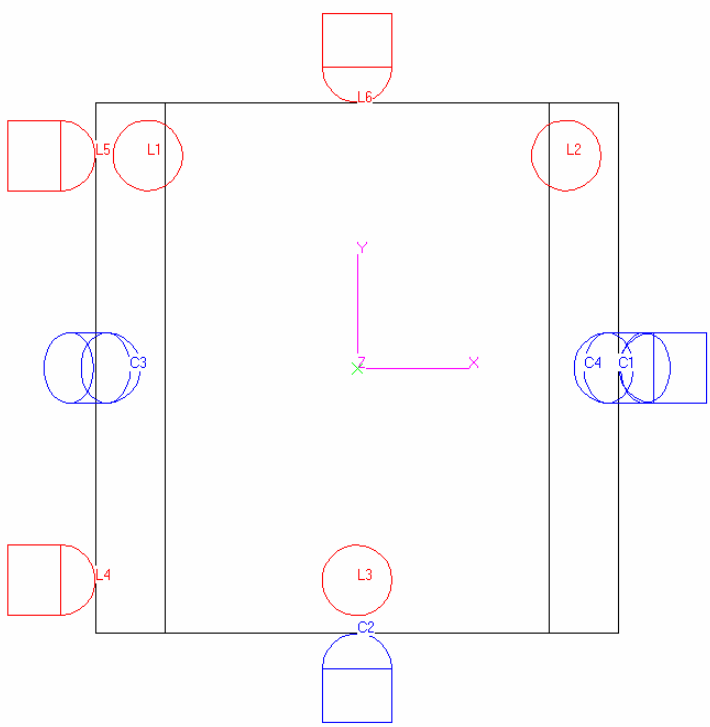

(b) Layout #2

Figure 6.4 Two selected fixture layouts

Table 6.4 Coordinates of fixture-workpiece contacts

	Locator	Coordinate (x, y, z) (mm)	Clamp	Coordinate (x, y, z) (mm)
Layout #1	L1	(-135, 135, -60)	C1	(150, 0, -20)
	L2	(135, 135, -60)	C2	(0, -150, -20)
	L3	(0, -135, -60)	C3	(-130, 0, 40)
	L4	(-150, -135, 0)	C4	(130, 0, 40)
	L5	(-150, 135, 0)		
	L6	(0, 150, -20)		
Layout #2	L1	(-120, 120, -60)	C1	(150, 0, -20)
	L2	(120, 120, -60)	C2	(0, -150, -20)
	L3	(0, -120, -60)	C3	(-130, 0, 40)
	L4	(-150, -120, 0)	C4	(130, 0, 40)
	L5	(-150, 120, 0)		
	L6	(0, 150, -20)		

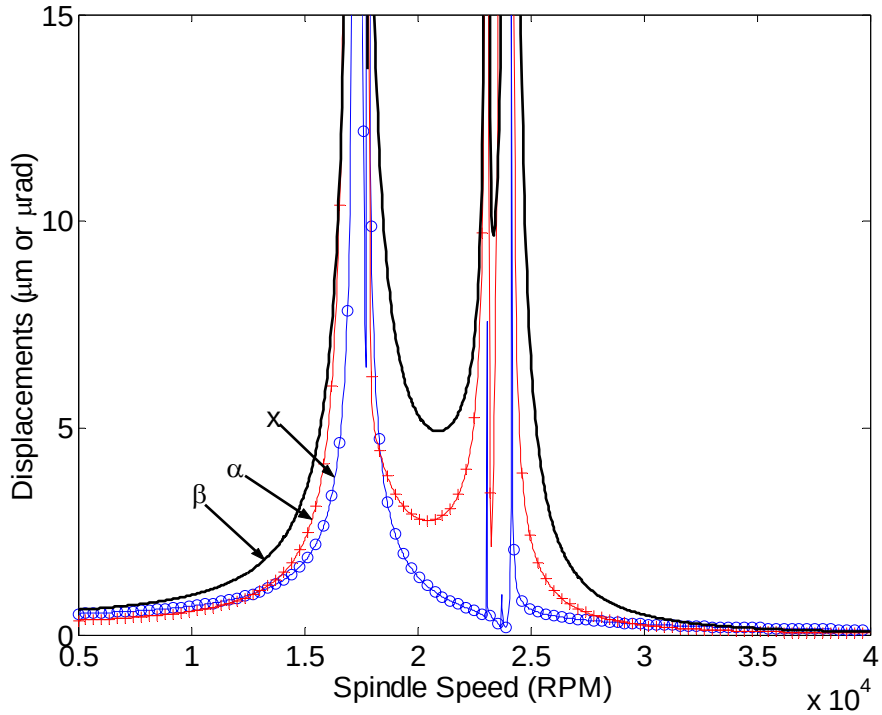

Figure 6.5 Workpiece vibrations vs. spindle speed

The two spindle speeds, 12,000 rpm and 15,000 rpm, are selected based on a harmonic analysis of the example system. The harmonic analysis results are shown in Figure 6.5, from which it is seen that 15,000 rpm is closer to the first resonance region than 12,000 rpm and hence is expected to result in higher system vibration and weaker fixturing dynamic stability. Note that, for purposes of clarity, the workpiece vibration in Figure 6.5 is shown in only three degrees of freedom – translation along the *x* axis (*x*) and rotations about the *x* and *y* axes (α and β, respectively).

A full factorial combination of the eight assigned values (two for each parameter) results in sixteen machining cases, which are summarized in Table 6.5.

Table 6.5 Sixteen machining cases in parameter effect analysis

					Degree of Instability	
Case	SS (rpm)	μ_S	Layout	F_c (N)	Lift-off (μm)	Macro-slip (N)
1	**12000**	**0.25**	**1**	**3000**	**-19.87**	**90.83**
2	12000	0.35	1	3000	-21.02	-188.78
3	12000	0.25	1	5000	-28.92	-298.67
4	12000	0.35	1	5000	-31.13	-723.65
5	**12000**	**0.25**	**2**	**3000**	**-19.35**	**164.30**
6	12000	0.35	2	3000	-20.38	-199.88
7	12000	0.25	2	5000	-28.45	-250.06
8	12000	0.35	2	5000	-30.01	-775.70
9	**15000**	**0.25**	**1**	**3000**	**-19.87**	**91.22**
10	15000	0.35	1	3000	-21.02	-190.68
11	15000	0.25	1	5000	-28.91	-298.78
12	15000	0.35	1	5000	-31.12	-723.41
13	**15000**	**0.25**	**2**	**3000**	**-19.35**	**167.32**
14	15000	0.35	2	3000	-20.39	-194.20
15	15000	0.25	2	5000	-28.45	-250.87
16	15000	0.35	2	5000	-30.00	-776.27

The fixturing dynamic stability of each of the sixteen machining cases in Table 6.5 is then analyzed and the results for all cases are shown in Figures 6.6 and 6.7 with

Figure 6.6 showing the lift-off check results and Figure 6.7 showing the macro-slip check results.

The vertical axis in Figure 6.6 represents the maximum total workpiece displacement in the $+z_i$ direction (i.e., away from the ith fixture element) due to the combined effect of clamping and machining loads, i.e., the left hand side of the first fixturing dynamic stability criterion given in Equation (3.1). Therefore, a positive (above the zero horizontal plane) bar in Figure 6.6 means that lift-off occurs at a fixture-workpiece contact. A negative bar implies that lift-off does not occur. In addition, the height of the bar represents the degree of fixturing dynamic instability (if positive) or stability (if negative) in terms of lift-off. It is seen from Figure 6.6 that none of the cylinders is positive and hence no lift-off occurs at any fixture-workpiece contact in any of the sixteen cases.

The vertical axis in Figure 6.7 represents the maximum violation of the Coulomb friction law at a fixture-workpiece contact during machining, i.e., the left hand side of the second fixturing dynamic stability criterion given in Equation (3.1). Therefore, a positive bar in Figure 6.7 means that macro-slip occurs at a fixture-workpiece contact. A negative bar means that macro-slip does not occur. In addition, the height of the bar represents the degree of fixturing dynamic instability (if positive) or stability (if negative) in terms of macro-slip. It is seen that Figure 6.7 has four positive bars located at the 10th fixture-workpiece contact (i.e., C4 in Figure 6.2) in cases #1, #5, #9, and #13, respectively.

The four unstable cases are highlighted in Table 6.5. Also listed in Table 6.5 is the degree of fixturing dynamic instability for each case, represented by the shortest negative (if stable) or tallest positive (if unstable) bar.

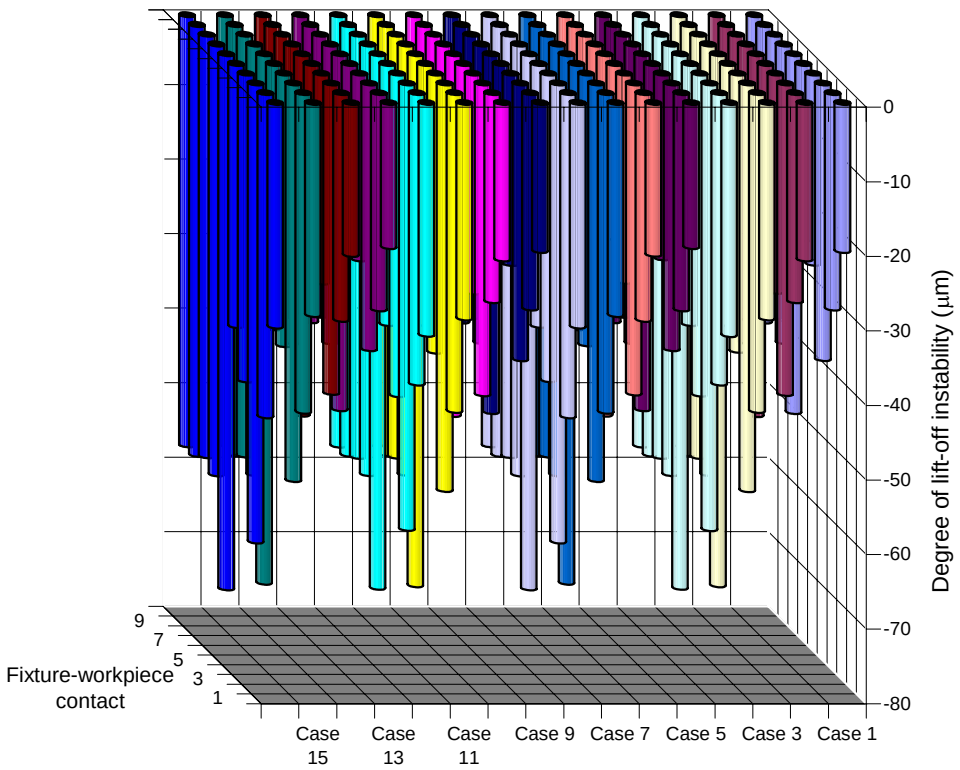

Figure 6.6 Results of lift-off check in parameter effect analysis

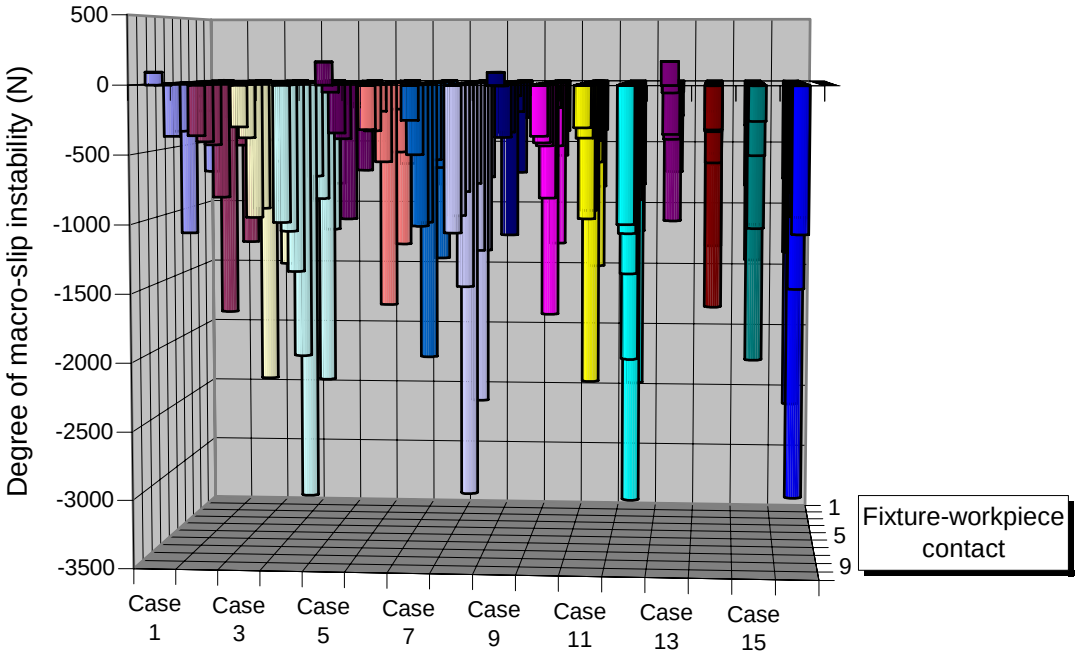

Figure 6.7 Results of macro-slip check in parameter effect analysis

For the effect of a single parameter (SS, μ_S, fixture layout, or F_c) on the fixturing dynamic stability in the example milling operation, the stability analysis results generally match one's intuition and are summarized as follows:

1) The effect of spindle speed on fixturing dynamic stability can be examined by comparing cases #1 and #9, which differ only in spindle speed. As seen in Table 6.5, both cases are unstable (highlighted) but case #9 is slightly more unstable (degree of macro-slip = 91.22 N) than case #1 (degree of macro-slip = 90.83 N). This is because the spindle speed used in case #9 (15,000 rpm) is closer to the resonance region shown in Figure 6.5 than in case #1 (12,000 rpm).
2) The effect of μ_S can be seen by comparing cases #1 and #2. As shown in Table 6.5, case #1 has a lower μ_S and is unstable while case #2 is stable because higher μ_S generally helps stabilize the workpiece dynamics according to the second fixturing dynamic stability criterion in Equation (3.1).
3) Based on common fixture design rules employed in practice, case #1 has a better primary datum surface locator layout than case #5 (see Figure 6.4) while all other parameters in the two cases are the same. Both cases turn out to be unstable as indicated in Table 6.5. However, case #1 with a better layout is less unstable (degree of macro-slip = 90.83 N) than case #5 (degree of macro-slip = 164.30 N).
4) Comparing cases #1 and #3 reveals the effect of the clamping force (F_c) on fixturing dynamic stability. Case #1 has an F_c of 3,000 N and is unstable. With an increase in F_c (5,000 N), case #3 turns out to be stable.

It is also seen that the clamping force (F_c) and the static coefficient of friction (μ_S) have a more prominent impact on the fixturing dynamic stability than the spindle speed and the fixture layout in this example. Specifically:

1) Compared to case #1, case #14 has a 25% higher (less stable) SS, an inferior (less stable) layout (26.6% smaller area of the triangle formed by the three locators in the primary datum), the same F_c, but a 40% higher (more stable) μ_S. Case #1 turns out to be unstable while case #14 is stable as seen in Table 6.5.
2) Compared to case #2, case #16 has a 25% higher (less stable) SS, a 26.6% smaller primary locator area (less stable), the same μ_S, but a 66.7% higher (more stable) F_c. Case #16 turns out to be 311.2% more stable (in terms of macro-slip) than case #2.

6.3.3 Sensitivity Analysis

A stable case, case #14 in Table 6.5, is selected to investigate the sensitivity of fixturing dynamic stability to imprecision in the static coefficient of friction, μ_S. The parameter μ_S is chosen for sensitivity analysis because: i) the previous parameter effect analysis shows that μ_S has a significant effect on the fixturing dynamic stability; ii) it is generally difficult to measure μ_S accurately; and iii) μ_S may change during machining due to the system dynamics and thus has a higher degree of uncertainty than the other parameters.

A total of five levels of imprecision in μ_S are considered: -10%, -5%, 0%, 5%, and 10%, which correspond to static coefficients of friction of 0.315, 0.3325, 0.35, 0.3675, and 0.385, respectively. The resulting five machining cases are summarized in Table 6.6.

Table 6.6 Five machining cases in sensitivity analysis

					Degree of Instability	
Case	SS (rpm)	μ_S	Layout	F_c (N)	Lift-off	Macro-slip
1	15000	0.315	2	3000	-20.60	-2.81
2	15000	0.3325	2	3000	-20.54	-166.33
3	15000	0.35	2	3000	-20.39	-194.15
4	15000	0.3675	2	3000	-20.34	-70.42
5	**15000**	**0.385**	**2**	**3000**	**-20.04**	**58.36**

The fixturing dynamic stability of each of the resulting five machining cases is evaluated and the results for all five cases are shown in Figures 6.8 and 6.9 with Figure 6.8 showing lift-off check results and Figure 6.9 showing the macro-slip check results. Interpretations of the positive and negative bars and the heights of the bars are the same as before (see the previous subsection). In addition, the degrees of fixturing instability (lift-off and macro-slip) for the five cases are listed in Table 6.6 and the unstable case (case #5 here) is highlighted.

It is seen from Figure 6.8 that no negative bars exist and hence no lift-off occurs at any fixture-workpiece contact in any of the five cases. However, macro-slip occurs in case #5 at the 4th (L4) and 5th (L5) contacts as seen in Figure 6.9 and the degree of instability is 58.36 N.

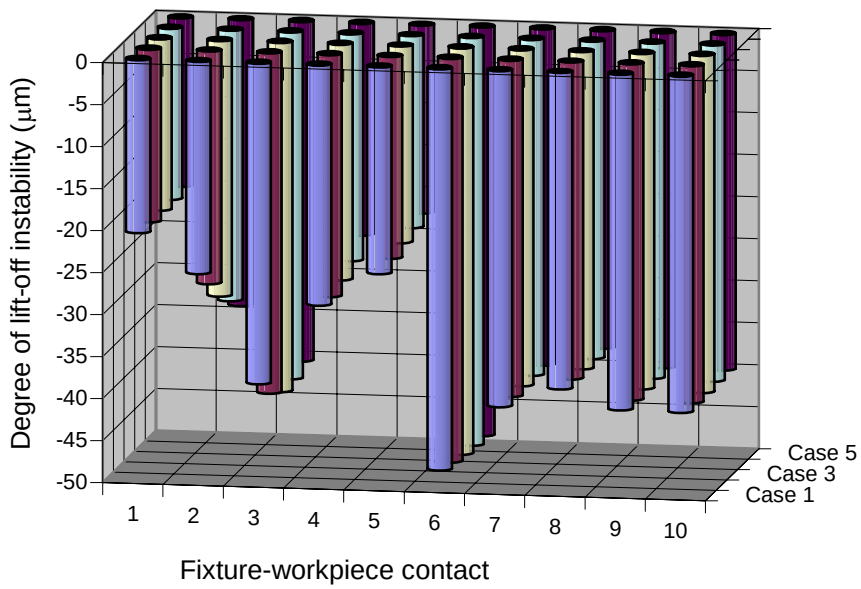

Figure 6.8 Results of lift-off check in sensitivity analysis

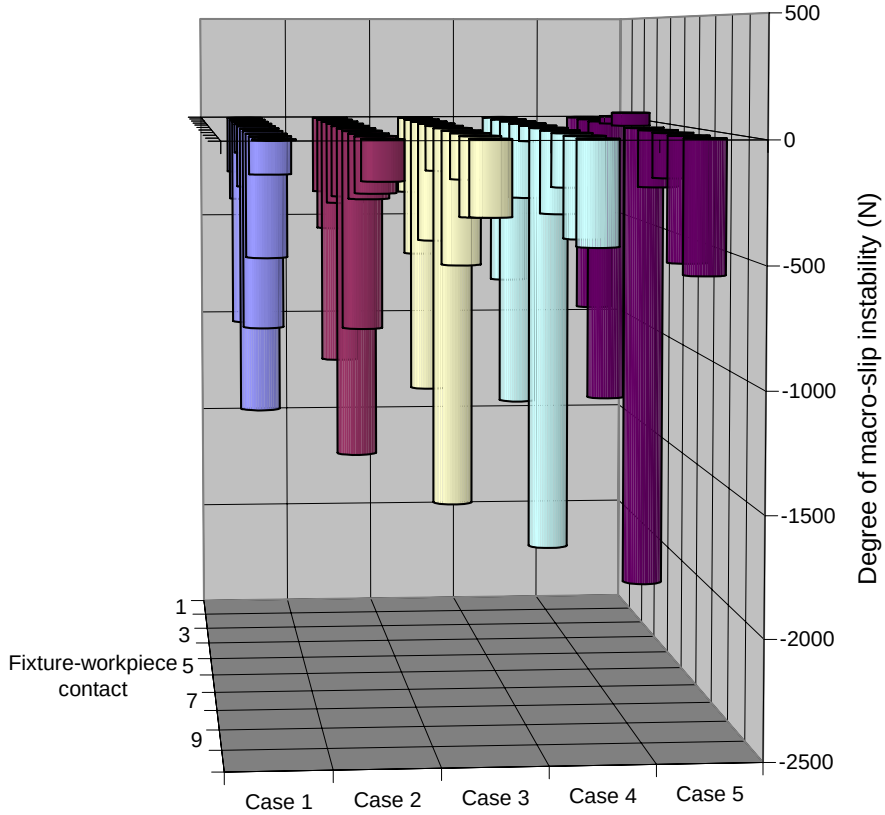

Figure 6.9 Results of macro-slip check in sensitivity analysis

From the results, it is found that:

1) The lift-off instability seems insensitive to the imprecision in μ_S, as seen in the second to last column of Table 6.6. This is because μ_S does not play a role in the lift-off stability criterion given in Equation (3.1). The small difference between the degrees of lift-off instability for the five machining cases is due to the fact that μ_S slightly affects the calculation of the clamping force induced system deformations, δ_{ij}, by appearing in the third constraint in the static model given in Equation (3.19). The deformation δ_{ij} directly affects lift-off instability.
2) The macro-slip instability, however, is quite sensitive to the imprecision in μ_S, as seen in the last column of Table 6.6. Small deviations result in significant changes in the degree of macro-slip instability.
3) Both positive and negative deviations from the nominal μ_S (0.35 in case #3) seem to increase the macro-slip instability (i.e., weaken the fixturing dynamic stability). Comparing cases #2 and #4 with case #3, a positive/negative 5% deviation of μ_S leads to 63.7%/14.3% increase of macro-slip instability. Comparing cases #1 and #5 with case #3, a positive/negative 10% deviation of μ_S leads to 130.1%/98.5% increase of macro-slip instability. The high sensitivity of macro-slip instability to variations in μ_S is because μ_S plays a direct role in the macro-slip stability criterion given in Equation (3.1). In addition, it also affects the solution of the static model.

It is contrary to one's intuition that a positive deviation in μ_S also degrades the fixturing dynamic stability. According to the macro-slip stability criterion, an increase in μ_S directly helps stabilize the workpiece dynamics. This counter-intuitive observation may be explained as follows:

1) An increase in μ_S results in lower normal reaction force, P, at the fixture-workpiece contact (except at the clamps which are assumed to hold constant forces) because the total energy of the system always tends to stay at its minimum when all constraints are satisfied. The decrease in P, in turn, results in a decrease of the normal contact stiffness, k_{zc}, and also a decrease in the normal contact deformation, δ_z.
2) The decreases in k_{zc} and δ_z directly weaken the ability of the system to prevent macro-slip, as noted in the macro-slip stability criterion. In addition, a lower k_{zc} results in lower fixture-workpiece system stiffness and thus leads to higher workpiece vibration, which implies lower stability.
3) Therefore, an increase in μ_S results in competing factors that affect the fixturing dynamic stability. The overall effect is case-specific.

Based on the results and insights obtained from the sensitivity analysis, it is recommended that other fixture design parameters (e.g., fixture layout and clamping forces) be adjusted accordingly to incorporate the imprecision (or uncertainty) in μ_S in order to realize a proper fixture design.

6.4 Summary

The roles of four critical fixture design and machining process parameters (spindle speed, static coefficient of friction μ_S at the fixture-workpiece interface, fixture layout, and clamping forces) in affecting the fixturing dynamic stability in machining have been investigated in this chapter. In addition, sensitivity analysis has been performed to examine the sensitivity of fixturing dynamic stability to the imprecision (or uncertainty) in μ_S.

The following conclusions can be drawn from this study:

- Generally, higher clamping forces and μ_S, spindle speeds farther away from the resonance regions of the fixture-workpiece system, and larger spacing of fixture elements help improve the fixturing dynamic stability in machining.
- Clamping forces and the static coefficient of friction have a more pronounced impact on fixturing dynamic stability than the spindle speed and the fixture layout.
- The lift-off instability seems insensitive to the imprecision in μ_S, but the macro-slip instability is quite sensitive to deviations in μ_S. Both positive and negative deviations in μ_S degrade the fixturing dynamic stability.
- An increase in μ_S results in competing factors that affect the fixturing dynamic stability. The overall effect is case-specific. Therefore, a safe fixture design requires consideration of parameter imprecision whether it is positive or negative.

CHAPTER 7

CLAMPING OPTIMIZATION

In industrial practice, workpieces are often inappropriately clamped due to lack of reliable scientific tools for fixture synthesis, resulting in unsafe operations or poor part quality. Using the procedure developed in Chapter 3 for modeling and analysis of fixturing dynamic stability with consideration of material removal effect, this chapter presents an approach for determination of the minimum required clamping forces that ensure the fixturing dynamic stability of a fixture-workpiece system in machining. The clamping force optimization problem is formulated as a bilevel nonlinear programming problem and solved using the Particle Swarm Optimization (PSO) technique. Through a simulation example, insight into the effects of fixture-workpiece system dynamics and its continuous change due to material removal on fixturing dynamic stability and the minimum required clamping forces is obtained.

This chapter is organized as follows. First, the problem of clamping optimization is described and the overall approach is described. Then, a mathematical model is developed and its solution technique is discussed for determination of the minimum required clamping forces that achieve a dynamically stable fixturing configuration. Subsequently, an application example is given and the results are discussed. Finally, the chapter is summarized and major conclusions are drawn.

7.1 Problem Description and Approach

As discussed in Chapter 3, a fixture fails to fully restrain a workpiece when lift-off or macro-slip occurs at one or more fixture-workpiece contacts at any instant of the machining process. Such fixturing instabilities must be eliminated through proper fixture design. An important controllable fixture design parameter is the clamping force applied to the workpiece prior to the cutting operation. This parameter needs be chosen carefully since insufficient clamping forces cannot provide fixturing stability while unnecessarily high clamping forces will cause excessive workpiece elastic/plastic deformation.

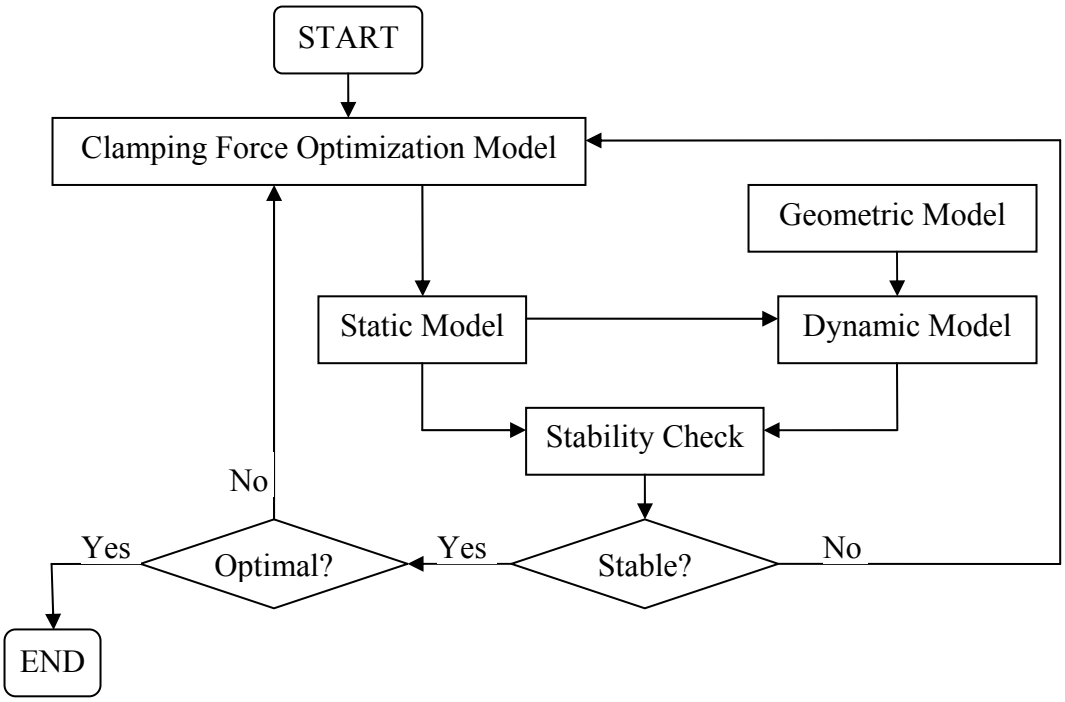

Figure 7.1 Overview of the clamping force optimization procedure

The overall approach used in this thesis to determine the minimum required clamping forces that ensure the fixturing dynamic stability of a fixture-workpiece system in machining is summarized in the flowchart shown in Figure 7.1. It is seen that the approach is based on the fixturing dynamic stability analysis procedure presented in Chapter 3 and an optimization method to perform the task of searching for the minimum set of clamping forces. Development of the clamping force optimization model is presented in the next section.

7.2 Bilevel Nonlinear Optimization Model

The objective function to be minimized is the 2-norm of the clamping force vector, denoted as $\overline{F}_c$. The number of components of this vector depend on the number of clamps C used in the fixture and thus $\overline{F}_c \in R^C$. The task here is to search in a C-dimensional hyperbox for an $\overline{F}_c$ with minimum length that satisfies the fixturing dynamic stability criteria given in Equation (3.1). This clamping force optimization task is then formulated as a bilievel nonlinear programming problem as follows:

$$\underset{\overline{F}_c}{Minimize} \;\; \theta(\overline{F}_c) = \left\| \overline{F}_c \right\|_2 \tag{7.1}$$

$$\begin{aligned}
&Subject\ to: \\
&\qquad \Delta_{ij}(t) = d_{ij}(t) - \delta_{ij} \qquad for\ \ j = x,\ y,\ z \\
&\qquad \max_t \{\Delta_{iz}(t)\} \le 0 \\
&\qquad \max_t \ \{\sqrt{[k_{ix}\,\Delta_{ix}(t)]^2 + [k_{iy}\,\Delta_{iy}(t)]^2} - \mu_S^i [k_{iz} \left|\Delta_{iz}(t)\right|]\} \le 0 \\
&\qquad \overline{L}_b \le \overline{F}_c \le \overline{U}_b
\end{aligned}$$

where, i = 1 to (L+C); $d_{ij}(t)$, the dynamic displacement of the workpiece at the ith fixture-workpiece contact in the jth direction (j = x, y, z) during machining, is obtained from $\overline{d}(t) = [S]^T \overline{q}(t)$ (see Equations (3.20) and (3.21)) and $\overline{q}(t)$ is the solution of the dynamic model given in Equation (3.8); δ_{ij}, the static deformation of the workpiece at the ith contact in the jth direction due to clamping, is obtained from the static model given by Equation (3.19); $\overline{L}_b$ and $\overline{U}_b$ are the upper and lower bounds of $\overline{F}_c$, respectively.

7.3 Solution Technique – PSO

Equation (7.1) includes two optimization tasks at two levels. The upper level is the minimization of the 2-norm of the clamping force vector and the lower level is the minimization of the total complementary energy of the fixture-workpiece system subjected to clamping forces. The constraint regions of the two optimization problems are implicitly dependent on each another. Theoretical approaches are available for certain types of bilievel nonlinear programming problems. Equation (7.1), however, is more complex than a normal bilievel nonlinear problem because the choice at the lower level affects the solution of the dynamic model given in Equation (3.8), which needs to be treated as a black box in the search for the optimal clamping forces.

A heuristic search algorithm, called Particle Swarm Optimization (PSO) [78], is therefore used to solve Equation (7.1). PSO is an evolutionary computation technique developed through simulation of a simplified social model, where an individual member

(i.e., a potential solution) in a group can profit from the discoveries and previous experiences of all other members in the group as well as itself.

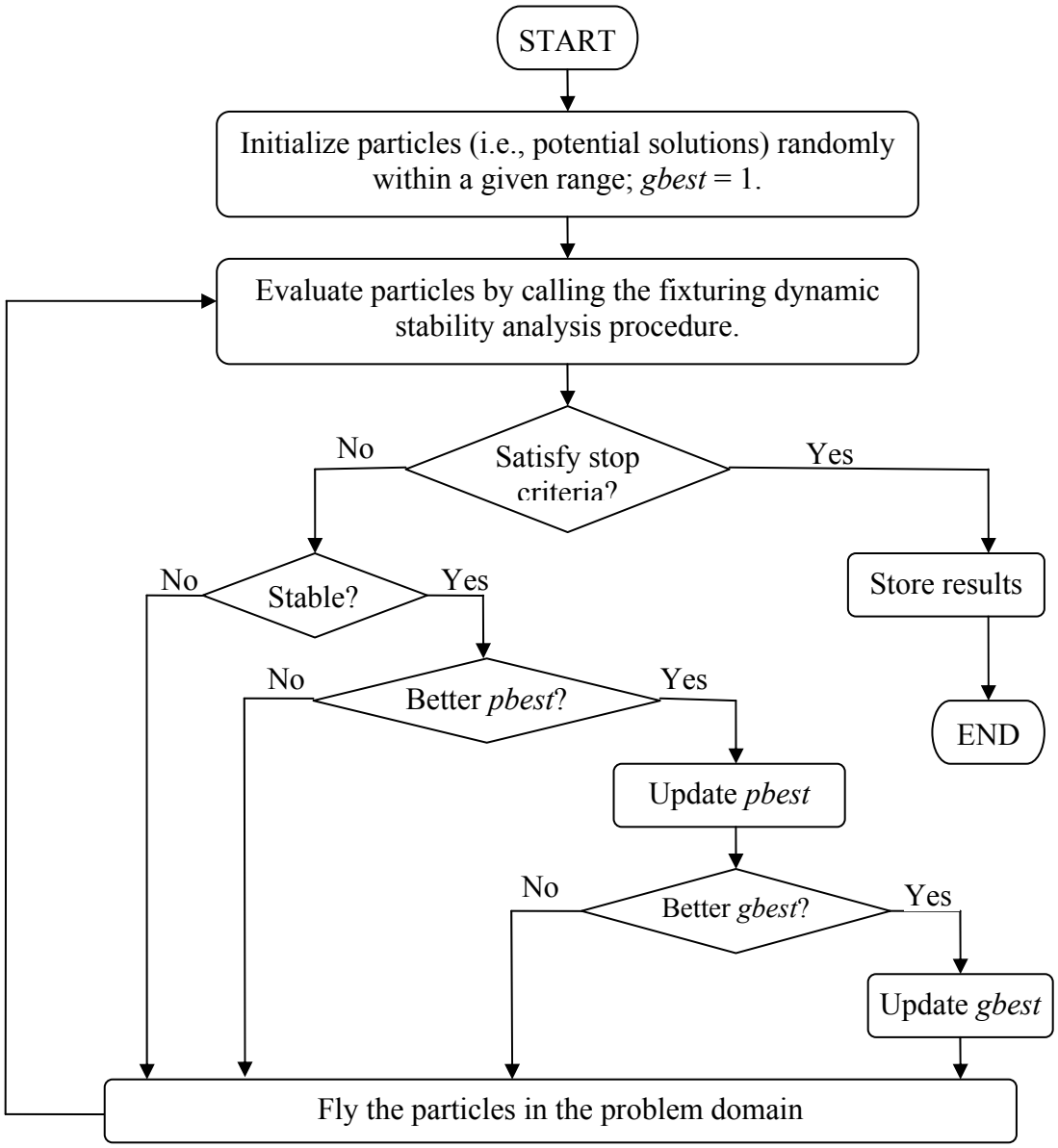

Figure 7.2 Flowchart of PSO approach

The PSO solution technique starts with initialization of a population of random potential solutions represented by particles. The particles are assigned velocities and "flown" through the problem hyperspace. At the kth iteration, the best solution (*pbestx*) and the corresponding objective function value (*pbest*) that each particle has achieved thus far are stored. Also stored is the index (*gbest*) of the particle that has the best performance in the group till that iteration. Equations (7.2) and (7.3) are used to update the velocity (v) and the position (x) of the ith particle at the (k+1)th iteration.

$$\bar{v}_i^{k+1} = w_i^{k+1}\,\bar{v}_i^k + c_1\,rand()\,(pbestx_i^k - \bar{x}_i^k) + c_2\,Rand()\,(pbestx_{gbest}^k - \bar{x}_i^k) \qquad (7.2)$$

where, w is the inertia weight; c_1 and c_2 are positive constants; *rand* and *Rand* are generators of random numbers between 0 and 1.

$$\bar{x}_i^{k+1} = \bar{x}_i^k + \bar{v}_i^{k+1} \qquad (7.3)$$

The flowchart shown in Figure 7.2 summarizes the PSO approach to solve Equation (7.1).

7.4 Application Example

An end milling simulation example is used to illustrate the approach for determination of the minimum required clamping forces that ensure the fixturing dynamic stability of a fixture-workpiece system during machining.

7.4.1 Problem Data

The original workpiece is a solid block with a blind hole (diameter=70 mm; length=150 mm) on the left and four semi-circular grooves (diameter=30 mm) on top (see Figure 7.3). The hole crosses the workpiece from the left side to the center and is located on the center lines of the workpiece in the y and z directions. The grooves are symmetrically located about the x axis and are evenly distributed.

The operation involves end milling a step on the top surface of the workpiece. The cut starts at the right end of the workpiece and the tool travels along the Y axis during each pass. Upon finishing a pass, the tool moves along the X axis to the next pass until a depth level is completed, after which the tool travels down along the Z axis to the next depth level. The total volume removed by the tool is about 30% of the volume of the original workpiece.

A 3-2-1 locator layout (L1-L6) and three clamps (C1-C3) are used to restrain the workpiece (see Figure 7.3). The spatial coordinates of the fixture elements are listed in Table 7.1. All fixture elements are identical with a cylindrical body (radius=19.8 mm; length=30 mm) and a spherical tip (radius=19.8 mm). The material properties of the workpiece and the fixture elements are given in Table 7.2.

The cutting conditions used in this example are summarized in Table 7.3. Note that the spindle speed (6,500 rpm) corresponds to a point on the curved region of the line plot in Figure 7.4, which represents the fixture-workpiece system dynamics vs. spindle speed and is generated from a harmonic analysis of the system as noted in Chapter 3.

The instantaneous machining forces, shown in Figure 7.5, are obtained from the milling force model derived from [75] and discussed in Chapter 3.

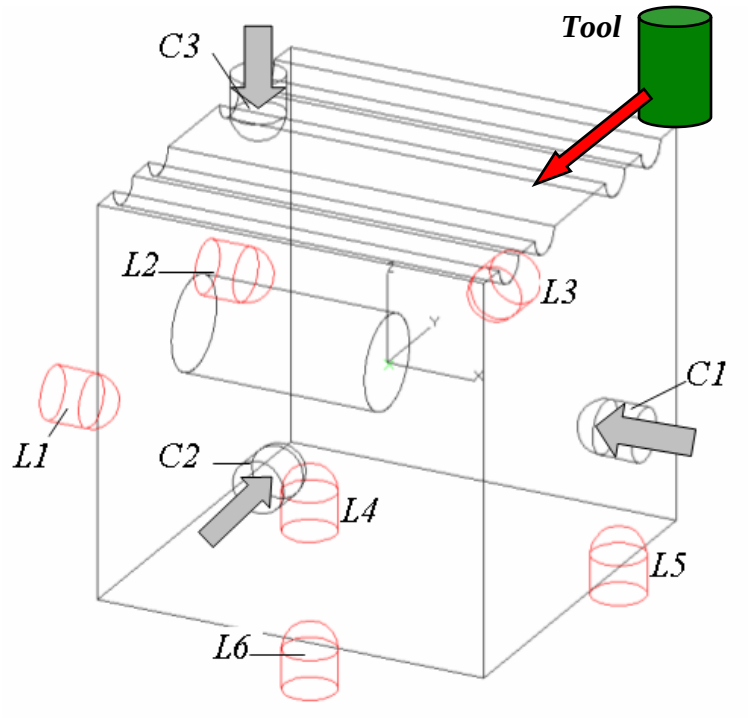

(a) Initial workpiece and fixture layout (L1-L6: locators; C1-C3: clamps)

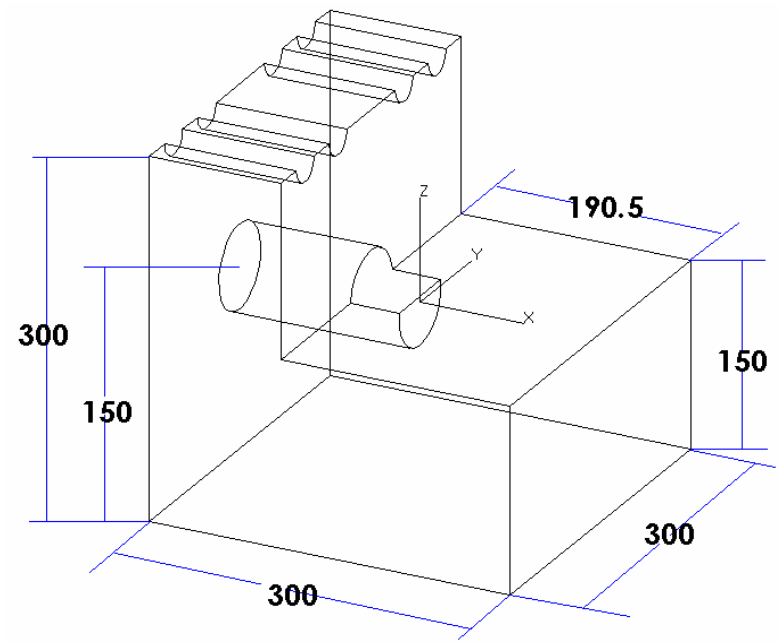

(b) Final part and dimensions (in mm)

Figure 7.3 End milling example for clamping optimization

Table 7.1 Coordinates of fixture-workpiece contacts

Locator	Coordinate (x, y, z) (mm)	Clamp	Coordinate (x, y, z) (mm)
L1	(-150, -120, -15)	C1	(150, 0, -15)
L2	(-150, 120, -15)	C2	(0, -150, -15)
L3	(0, 150, -15)	C3	(-100, 0, 150)
L4	(-120, 120, -150)		
L5	(120, 120, -150)		
L6	(0, -120, -150)		

Table 7.2 Material properties

	Workpiece	Fixture Element
Material	Aluminum 7075-T6	Hardened Steel
Density (kg/m^3)	2700	-
Young's modulus (GPa)	70.3	201
Poisson's ratio	0.354	0.296
Yield strength (MPa)	500	-
Static coefficient of friction	0.35	

Table 7.3 Cutting conditions

Feed Rate (mm/sec)	Axial Depth (mm)	Radial Depth (mm)	Spindle Speed (rpm)
100	5	12.7	6500

(End mill: HSS, 25.4 mm, 4-flute, and 30º helix)

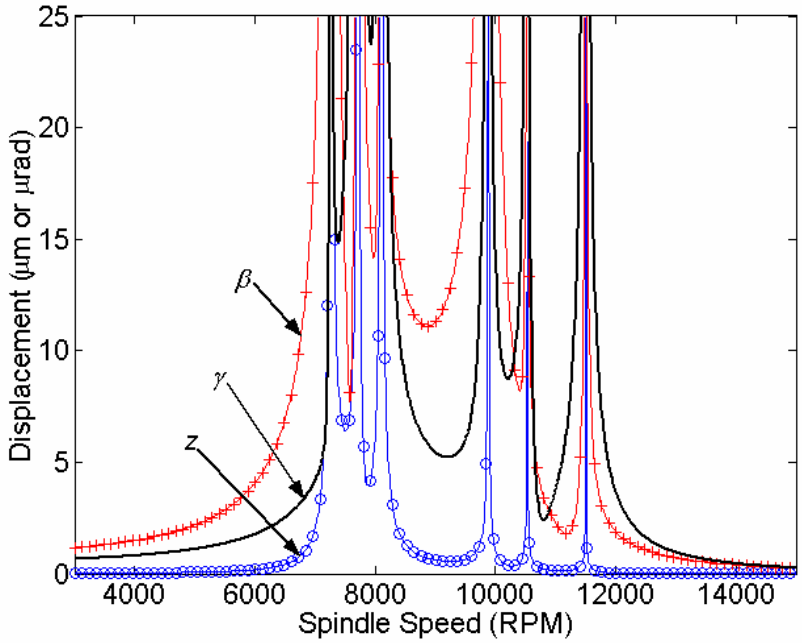

Figure 7.4 Workpiece dynamics vs. spindle speed

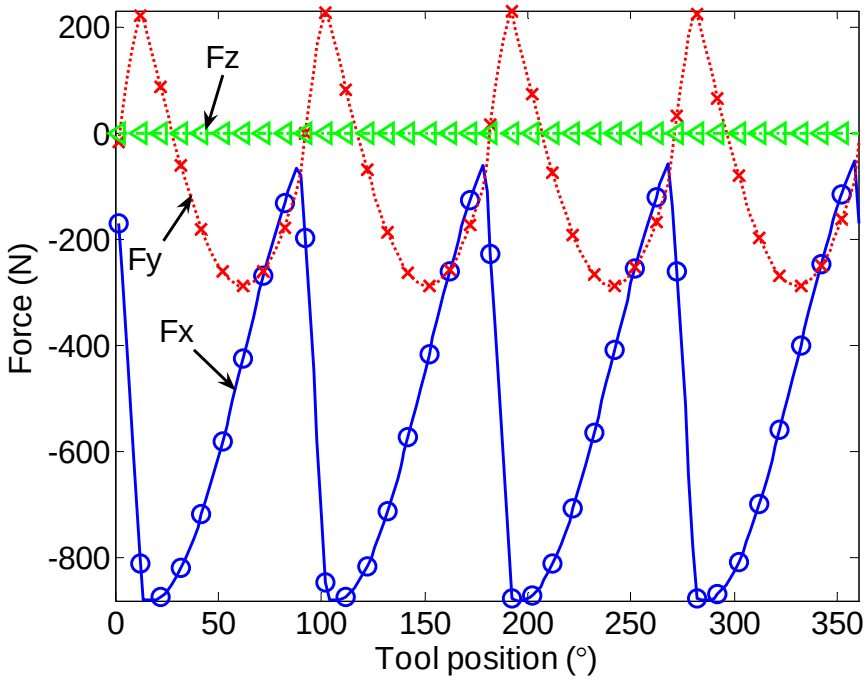

Figure 7.5 Simulated milling forces

7.4.2 PSO

The design parameters used in the PSO search are listed in Table 7.4. At the beginning of the search, the particle population (i.e., potential solutions) is initialized randomly but within the bounded solution space. The particles are then evaluated and flown through the problem domain until either of the stop criteria is satisfied. In the end, *pbestx(gbest, :)* is the "optimal" solution and *pbest(gbest)* is the corresponding "minimum" objective function value. Note that, PSO, as a search algorithm, does not guarantee a globally optimal solution. Hence, the "optimal" solution here refers to the best solution that the PSO technique can find.

7.4.3 Results and Discussion

Figure 7.6 shows the convergence of the PSO search for the example machining operation. The two plots are for the first and last tool passes, respectively. The optimal clamping forces found for the two passes are given below the plots. It is observed that,

1) The objective value decreases quickly during the search and the solution converges fast (the total numbers of iterations are 21 and 16 for the first and last passes, respectively); and
2) The "optimal" solutions for the first and last passes are quite different.

The first observation confirms the search power of the PSO algorithm and the appropriateness of the values of the design parameters listed in Table 7.4. The second observation indicates the significance of the material removal effect on the fixture-workpiece dynamics and consequently the minimum required clamping forces. It suggests the need for time-varying clamping forces during machining.

Table 7.4 Parameter values used in the PSO model

Parameter	**Value**		**Comments**
Dimension of the solution space	3		Three clamps.
Size of the solution space	Lower bound	1000 N	i) Specified by the user; ii) Can be updated during search; iii) If feasible, smaller upper bound is desirable.
	Upper bound	6000 N	
Population Size	30		Depending on the size of the solution space.
Inertia weight w	0.4~0.9		Case specific.
Coefficients c_1, c_2	1.0, 1.0		Case specific.
Stop criteria	i) $maxIt = 50$; ii) $m = 8$.		i) $maxIt$ – maximum # of iterations. ii) m: # of consecutive iterations without considerable improvement in the solution.

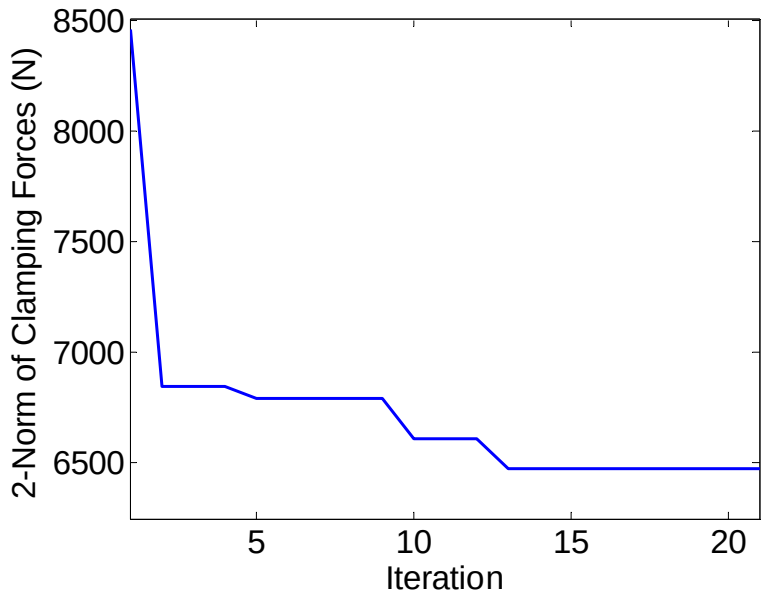

(a) First pass: ${}^{1}\overline{F}_c^{opt}$ = [4144.0 3860.1 3143.5] (N)

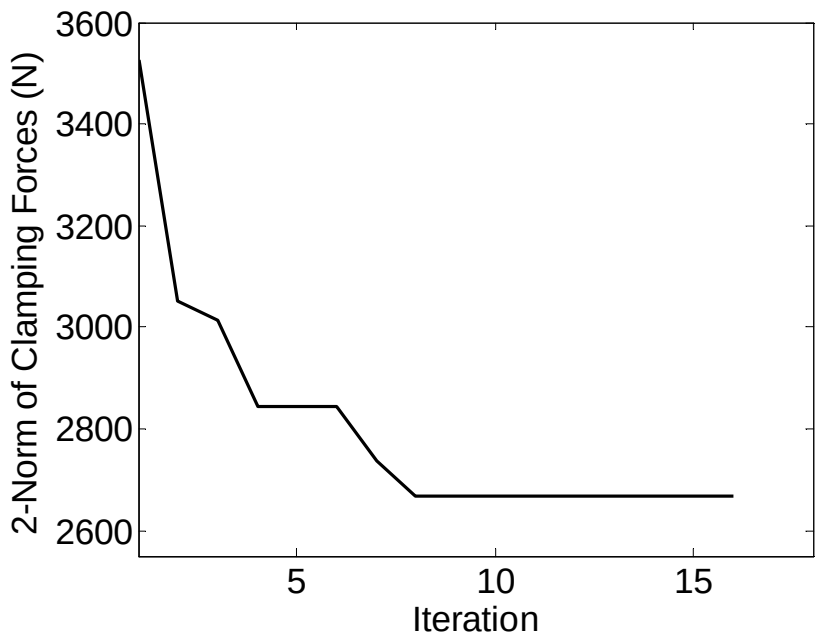

(b) Last pass: ${}^{2}\overline{F}_c^{opt}$ = [1523.7 1837.5 1191.4] (N)

Figure 7.6 Convergence of PSO search and solutions

Figure 7.7 compares the dynamic motions of the fixture-workpiece system during the first and last passes when their corresponding "minimum" clamping forces (see Figure 7.6) are used. It is seen that the dynamic motion of the fixtured workpiece during the first tool pass is larger than during the last pass. This says that the workpiece experiences smaller motion as it loses material. The reason for this may be found by examining the change in the system natural frequencies as the material is cut away. The lowest natural frequency of the system is 454.90 Hz during the first pass and 502.39 Hz during the last pass. Although the change is not very large, the system inertia decreases significantly. The small change in the natural frequency is because the system stiffness also decreases as lower "minimum" clamping forces are used for the last pass. The dominant excitation frequency (i.e., tooth passing frequency) for this simulation example is 433.33 Hz, which is near the lowest natural frequency of the initial fixture-workpiece system. As the workpiece loses material, the machining operation moves away from resonance and thus produces smaller system dynamic motion.

The stability check results for the first and last pass operating with their corresponding "minimum" clamping forces are shown in Figure 7.8. At each fixture-workpiece contact, lift-off and macro-slip are checked by applying the fixturing dynamic stability criteria given in Equation (3.1). The left hand sides of the two inequalities in Equation (3.1) must be non-positive, as is the case in Figure 7.8, to achieve a dynamically stable fixturing configuration. It is also seen from Figure 7.8 that macro-slip can occur more easily than lift-off since the former is just barely avoided (see the shortest stem in the macro-slip check plots). The marginal satisfaction of the fixturing dynamic stability criteria indicates the "optimality" of the clamping forces found by the PSO approach.

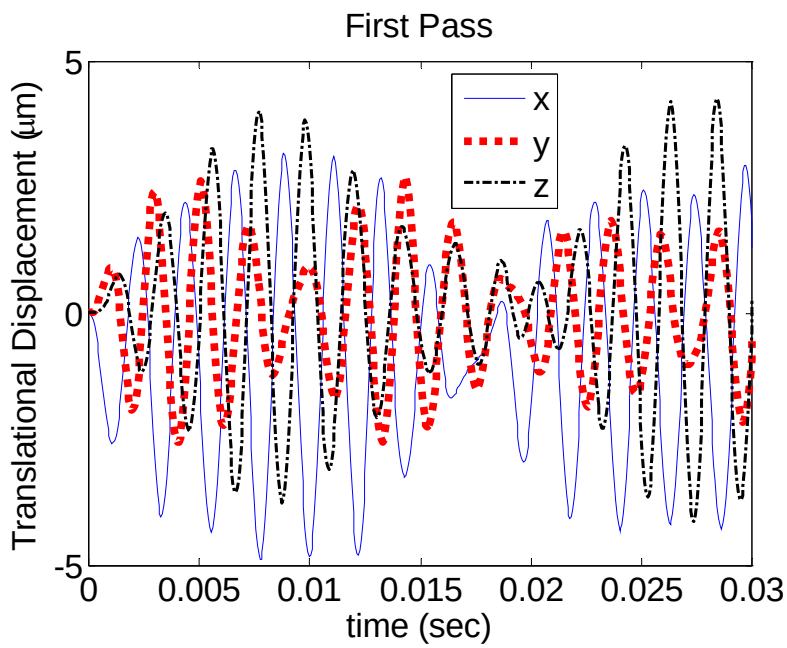

(a) Translations during the first pass

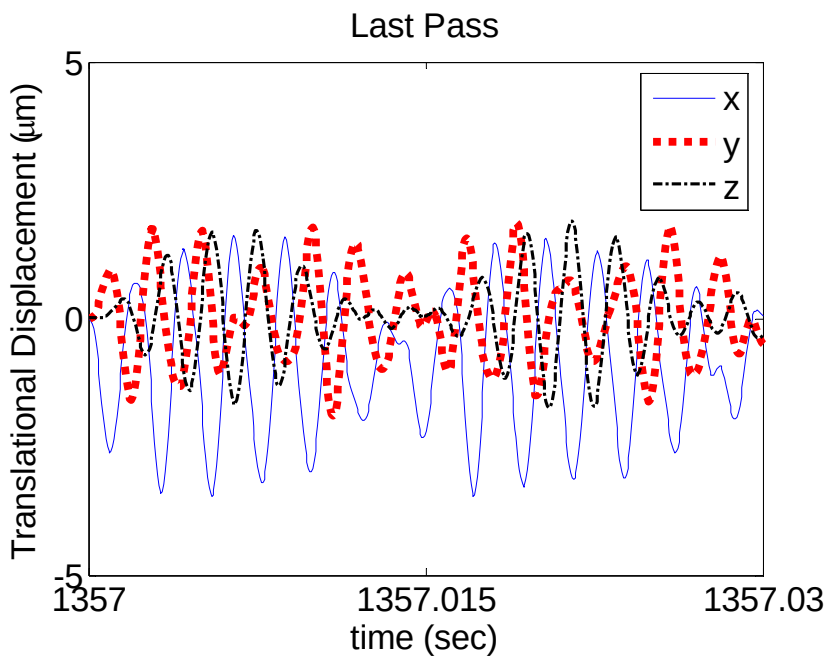

(b) Translations during the last pass

Figure 7.7 Workpiece dynamic motions during the first and last passes

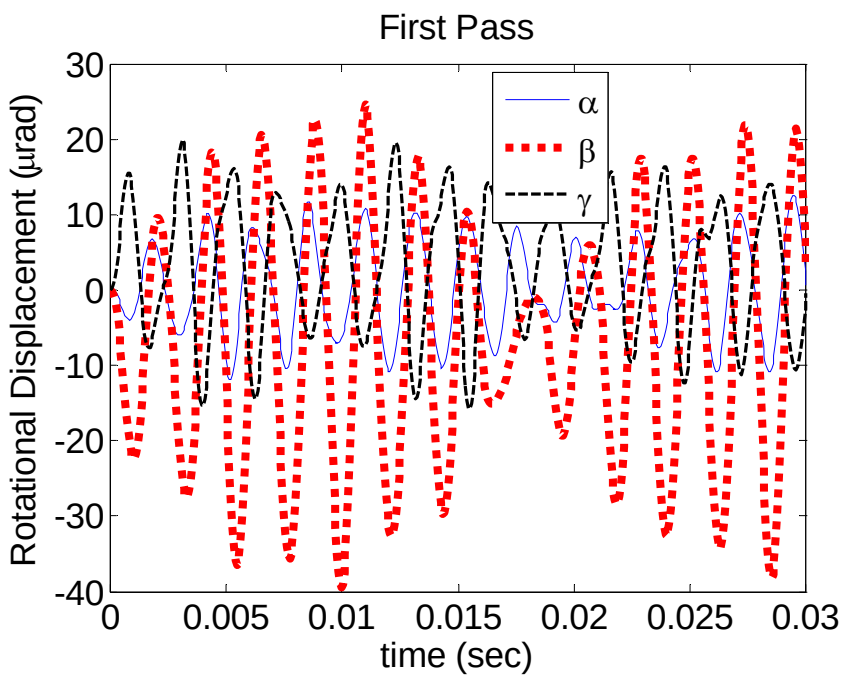

(c) Rotations during the first pass

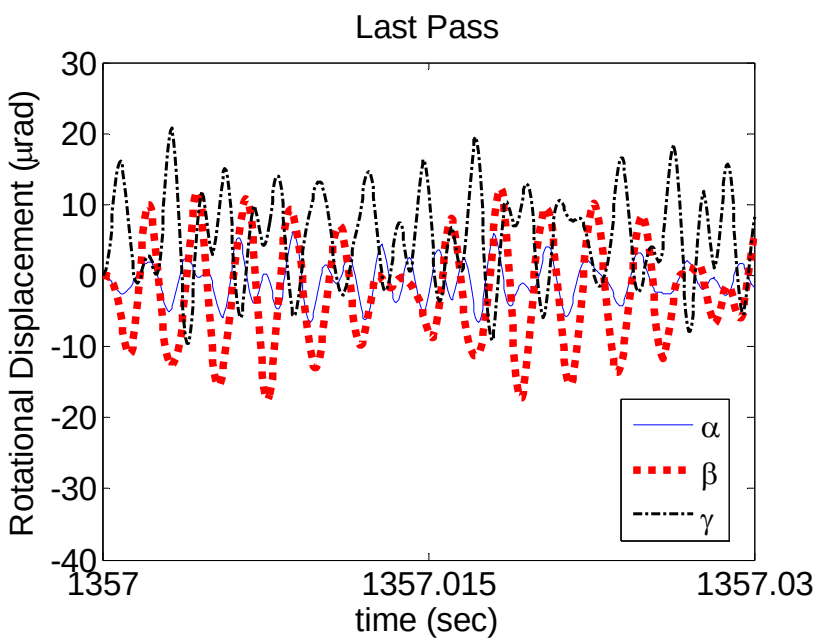

(d) Rotations during the last pass

Figure 7.7 Continued

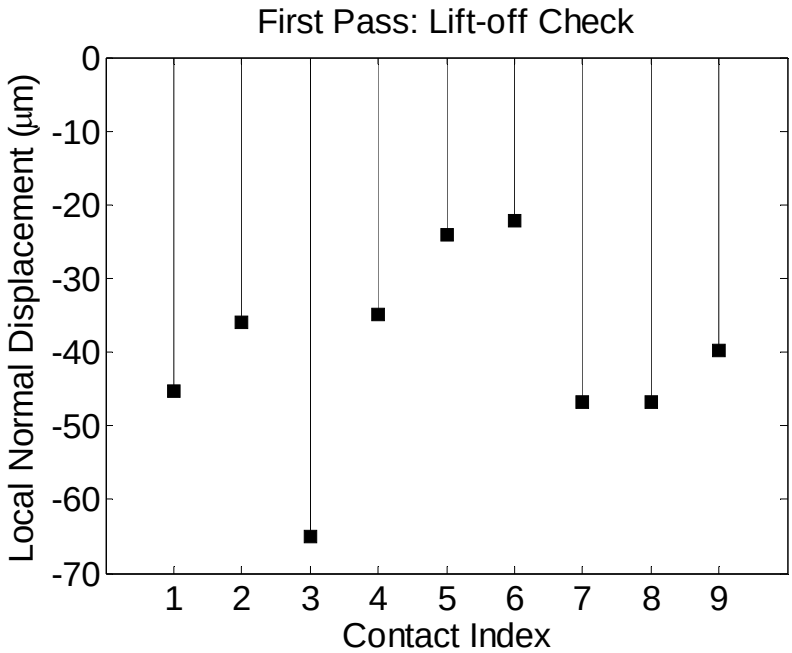

(a) Lift-off check for the first pass

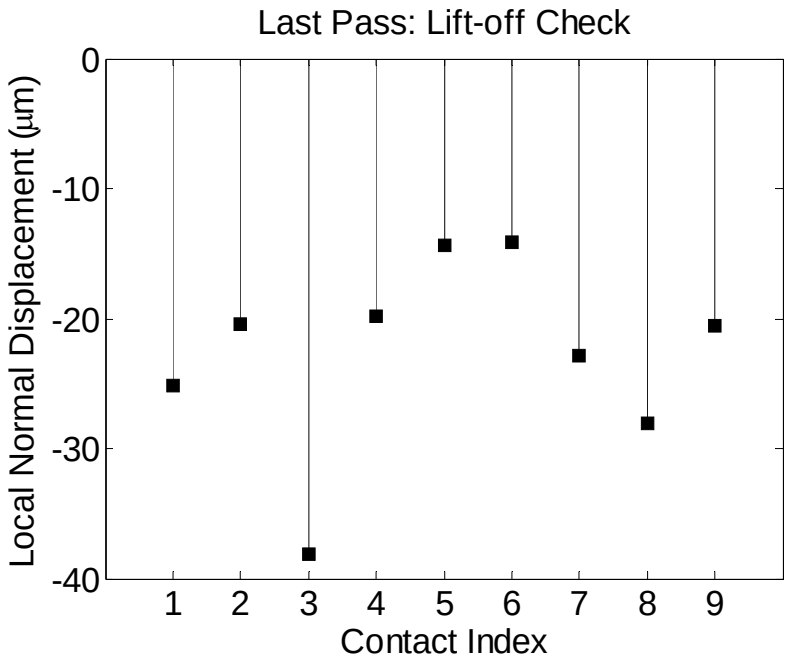

(b) Lift-off check for the last pass

Figure 7.8 Fixturing dynamic stabilities during the first and last passes

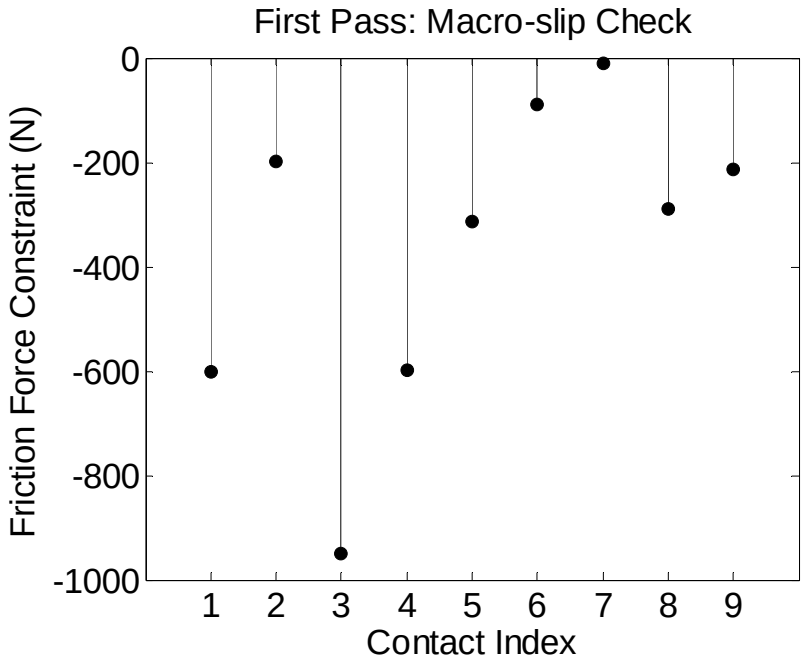

(c) Macro-slip check for the first pass

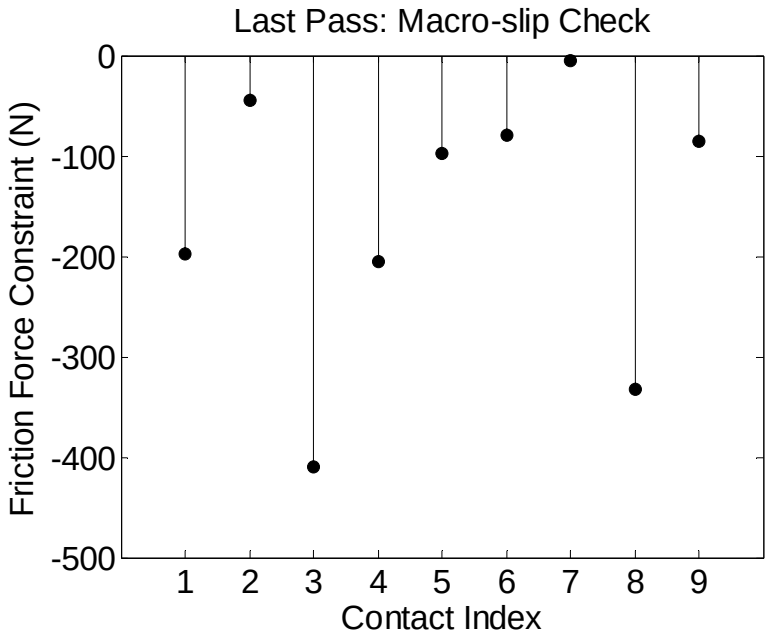

(d) Macro-slip for the last pass

Figure 7.8 Continued

7.5 Summary

A generic approach for determination of the minimum required clamping forces to ensure the fixturing dynamic stability of a fixture-workpiece system in machining has been developed in this chapter. The clamping force optimization problem was formulated as a bilevel constrained nonlinear programming problem and was successfully solved using a novel swarm intelligence technique.

The major observations from the simulations performed in this chapter are as follows:

- The Particle Swarm Optimization technique is capable of finding the "best" set of clamping forces quickly (search iterations are 21 and 16 for the first and last tool passes, respectively, in the simulation example).
- In determination of the minimum required clamping forces to ensure the fixturing dynamic stability of the fixture-workpiece system in the example milling operation, consideration of fixture-workpiece system dynamics is found to be crucial when the excitation frequency is in the vicinity of the natural frequency of the system. In the simulation example presented in this chapter, the excitation frequency (i.e., tooth passing frequency) is 433.33 Hz, which is quite close to the lowest natural frequency of the system (454.90 Hz).
- Material removal significantly affects the fixture-workpiece system dynamics and subsequently the minimum clamping forces required for achieving fixturing dynamic stability. The minimum required clamping forces are found to decrease as material is removed from the workpiece. For the simulation

example presented in the chapter, a clamping force vector of {4144.0; 3860.1; 3143.5} N is found to be optimal for the first pass while {1523.7; 1837.5; 1191.4} N is found to be optimal for the last pass (after about 30% material is removed). This suggests the need for implementing dynamically varying clamping forces during machining to achieve better fixture performance. Note that, when implementing the clamping optimization solution, one may round up the clamping forces according to the resolution of his or her clamping devices. Rounding up clamping forces, as shown in Chapter 6, increases fixturing dynamic stability and hence leads to a safer fixture design. In addition, fixturing dynamic stability is not very sensitive to clamping force variations (see Table 6.5).

CHAPTER 8

CONCLUSIONS AND RECOMMENDATIONS

8.1 Conclusions

The primary goal of this thesis was to establish a model-based framework for analysis and synthesis of the dynamic behavior (emphasizing the fixturing dynamic stability) of an arbitrarily configured fixture-workpiece system in machining accounting for the material removal effect. The five major accomplishments of this thesis are as follows:

1) A systematic, mathematical procedure for modeling and analysis of fixturing dynamic stability of an arbitrarily configured machining fixture-workpiece system with consideration of the material removal effect has been developed.
2) Models and approaches for simulation of fixture-workpiece dynamics and analysis of fixturing dynamic stability have been validated using machining experiments and modal impact tests. Good agreement between the predictions and the measurements has been found.
3) An in-depth theoretical and experimental investigation of the effect of material removal on the fixture-workpiece dynamics has been performed.
4) The roles of important fixture design and machining process parameters in affecting fixturing dynamic stability have been studied via a parameter effect

analysis, and the sensitivity of fixturing dynamic stability to imprecision in a critical parameter has been examined.

5) A generic approach for the determination of the minimum clamping forces that ensure fixturing dynamic stability in machining has been developed.

The main conclusions in each of the above areas of accomplishment are summarized below:

8.1.1 Modeling and Analysis of Fixturing Dynamic Stability in Machining

- The fixture-workpiece system during machining (e.g., milling) exhibits significant dynamics when the excitation frequency is in the vicinity of a natural frequency of the system. In such a case, consideration of dynamics is critical for an accurate analysis of the system.
- Material removal in machining continuously changes the properties of the fixture-workpiece system, e.g., inertia and geometry. As material is removed from the workpiece, the fixture-workpiece system behaves differently. As a result, dynamic clamping may be an option to achieve the best possible system performance.
- Allowing different forces at different clamps with a good combination of the clamping forces can improve the overall fixture performance.
- For structurally rigid workpieces (e.g., solid blocks), the structural compliance of the workpiece can be considered to be negligible compared to other sources of compliance in the system such as fixture-workpiece contacts and fixture elements

especially when spherical-tipped contacts and long, slim fixture elements are used to constrain the workpiece.

8.1.2 Experimental Validation

- The vibratory behavior of a fixtured workpiece during machining simulated by the dynamic model given in Equation (3.8) agrees reasonably with the experimental results obtained for a variety of fixturing and machining scenarios. The average prediction error of the root mean square (RMS) acceleration for the ten machining cases presented in Chapter 4 is 15.58%. This indicates that the simulation is able to capture the majority of the workpiece motion, although whether a model is accurate enough depends on the requirements of a specific application.
- The procedure for fixturing dynamic stability analysis is able to predict well both the onset of lift-off and the degree of fixturing (in)stability, which can serve as a guideline for improving an existing fixture design.
- Modeling of dynamics is crucial for a correct analysis of the fixture-workpiece system subjected to a machining operation when any harmonic in the excitation is near a natural frequency of the system. For the experimental system presented in Chapter 5, the dominant frequencies (1,332 Hz and 1,655 Hz) of the workpiece response (acceleration) signal were found to be four and five times the dominant frequency (333 Hz = tooth passing frequency) of the excitation (cutting force), respectively, because 1,332 Hz and 1,665 Hz are near two natural frequencies (1,315 Hz and 1,690 Hz) of the system and the corresponding harmonics are greatly

magnified. This dynamic amplification feature cannot be revealed by a static or quasi-static analysis.

- Higher clamping forces result in a stiffer fixture-workpiece system and therefore the system stiffness should be modeled as being clamping force dependent.

8.1.3 Investigation of Material Removal Effect

- Consideration of the material removal effect (MRE) is crucial for an accurate analysis of the fixture-workpiece system dynamics when a significant volume of material is removed in the machining operation. For the pocketing process presented in Chapter 5, the average prediction errors of the RMS acceleration of the workpiece were 9.59%, 17.21%, 26.75%, 35.15%, and 45.59% for 1.31%, 13.63%, 22.02%, 32.46%, and 42.74% material removal, respectively, when the MRE was not considered. After accounting for the MRE, these errors decreased to 3.29%, 7.39%, 6.88%, 7.69%, and 8.79%, respectively. The average model prediction error with consideration of MRE is 6.81%.
- The MRE can be broken down into several sub-effects resulting from the change in system inertia, stiffness, geometry, etc. The relative significance of the sub-effects is case-specific and requires individual analysis. For the pocketing operation in Chapter 5, the average improvements in prediction accuracy of MRE1 (change in inertia), MRE2 (change in geometry), MRE3 (rate of change of inertia), MRE4 (change in contact compliance), and MRE5 (change in workpiece compliance), compared with MRE0 (no consideration of MRE), are 8%, 4.72%, 0%, 1.94%, and 4.9%, respectively.

- For the example system analyzed in Chapter 5, as material is removed, the modal frequencies resulting from the fixture-workpiece contact compliance grow slightly and become separated while those arising from the structural compliance of the workpiece decrease significantly. The theoretical model is able to predict the low order system natural frequencies well (average percentage error is 3.73%).

8.1.4 Parameter Effect and Sensitivity Analyses

- Generally, higher clamping forces and μ_S, spindle speeds farther away from the resonance regions of the fixture-workpiece system, and larger spacing of fixture elements help improve the fixturing dynamic stability in machining;
- Clamping forces and the static coefficient of friction have a more pronounced impact on fixturing dynamic stability than the spindle speed and the fixture layout.
- The lift-off instability seems insensitive to the imprecision in μ_S, but the macro-slip instability is quite sensitive to deviations in μ_S. Both positive and negative deviations in μ_S degrade the fixturing dynamic stability.
- An increase in μ_S results in competing factors that affect the fixturing dynamic stability. The overall effect is case-specific. Therefore, a safe fixture design requires consideration of parameter imprecision whether it is positive or negative.

8.1.5 Clamping Optimization

- The Particle Swarm Optimization (PSO) technique employed in this thesis is able to quickly find the "best" set of clamping forces that ensure the fixturing dynamic stability of a fixture-workpiece system in machining.

- Consideration of dynamics is again crucial in determination of the minimum required clamping forces.
- Material removal significantly affects the fixture-workpiece system dynamics and consequently the minimum required clamping forces for achieving fixturing dynamic stability. For the simulation example presented in Chapter 7, a clamping force vector of {4144.0; 3860.1; 3143.5} N is found to be optimal for the first pass while {1523.7; 1837.5; 1191.4} N is found to be optimal for the last pass. This suggests the need for implementing dynamically varying clamping forces during machining to achieve better fixture performance. Note that, when implementing the clamping optimization solution, one may round up the clamping forces according to the resolution of his or her clamping devices. Rounding up clamping forces, as shown in Chapter 6, increases fixturing dynamic stability and hence leads to a safer fixture design. In addition, fixturing dynamic stability is not very sensitive to clamping force variations (see Table 6.5).

8.2 Recommendations

Several issues and areas for future work are discussed in this section.

First, it would be worthwhile to model the impact dynamics resulting from the initial plunging of the cutting tool into the workpiece at the beginning of a machining operation. The dynamic model developed in this thesis is for simulation of steady state dynamics. Although the model is found to be capable of capturing the major variations of

workpiece motion when the initial impact dynamics is present (see Chapter 4), the prediction errors in the amplitude of workpiece motion are generally larger than when the impact dynamics dies out (i.e., steady state).

Second, the effect of workpiece vibrations during machining on the fixture-workpiece contact stiffness, which is not considered in this thesis, might be worth some investigation especially when the workpiece dynamic displacements are relatively large. Consequently, the springs used to model the contact compliance would be nonlinear and their constants would be time-varying. This would increase the computational cost of the model and hence a cost vs. improvement analysis would be necessary.

Third, dynamic modeling and analysis of a fixture-workpiece system involving thin components or features appearing at any point of the machining operation would be a good extension of this thesis. Although the current work developed a finite element based approach for consideration of the workpiece structural compliance as well as its change during machining, the approach may not be suitable for highly flexible parts.

Fourth, new approaches would be required to model the dynamics of highly compliant fixture-workpiece systems with thin features. To keep the model compact, a modal model (comprising the natural frequencies and mode shapes) or response model (consisting of a set of frequency response functions) [77] instead of a spatial model (of mass, stiffness, and damping properties, e.g., the dynamic model developed in this thesis) might be a better option as they can be developed from modal testing data to describe the system properties in the range of interest.

Fifth, it is desirable to simultaneously optimize the fixture layout and clamping forces to achieve the fixturing dynamic stability, an important fixture performance measure defined and investigated in this thesis.

Finally, the dynamic model developed in this thesis can be readily used for analysis and synthesis of part quality errors in machining. A preliminary investigation has been performed and shown in Figure 8.1 in which the workpiece vibrates when the tool cuts through, ending up with two rough machined surfaces. The workpiece vibrations are obtained by solving the dynamic model given in Equation (3.8). The rough surfaces can be used to quantify part quality measures such as surface flatness and dimensional deviations.

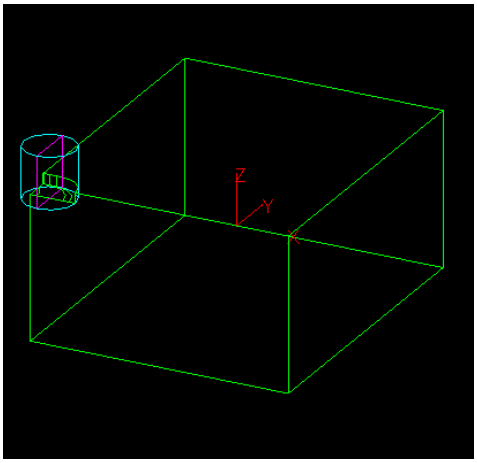

(a)

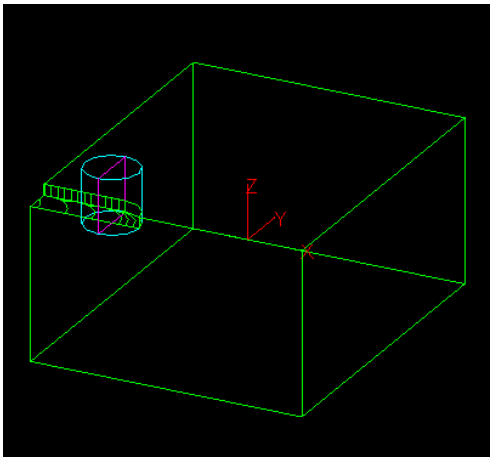

(b)

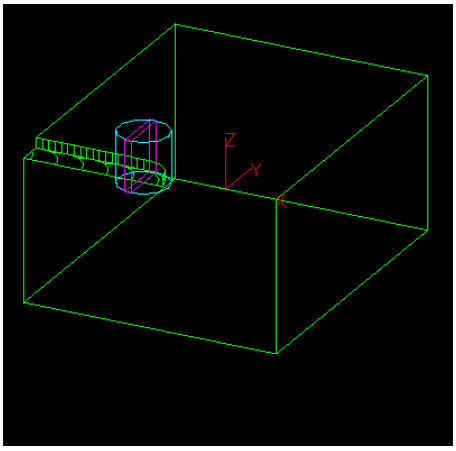

(c)

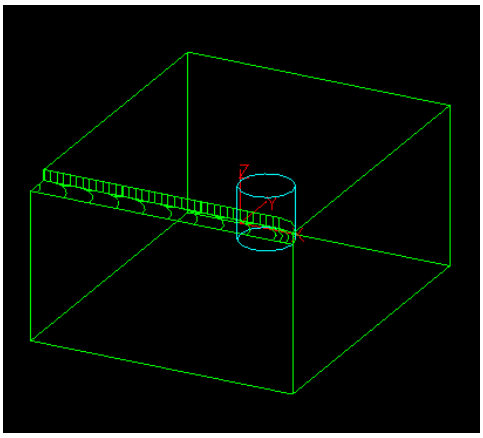

(d)

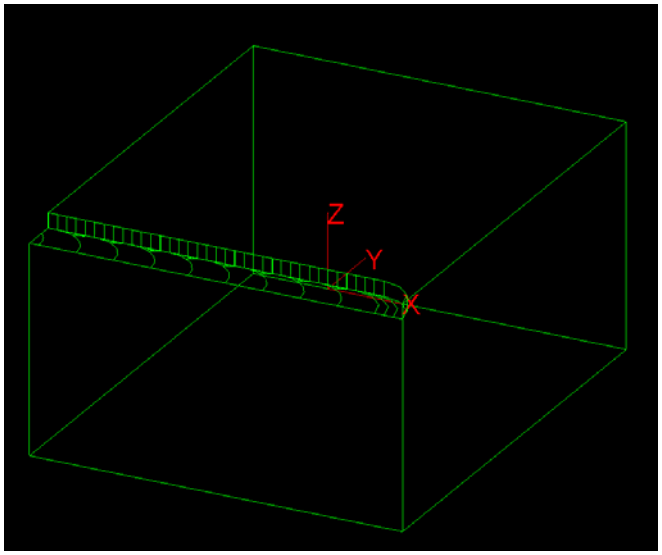

(e)

Figure 8.1 Part quality errors due to fixture-workpiece dynamics

APPENDICES

A.1 Derivation of System Configuration Matrix [*S*]

This appendix shows the derivation process of the configuration matrix, [*S*], of a fixture-workpiece system with multiple frictional contacts (*L* locators and *C* clamps).

The vibration of the fixtured workpiece is characterized by the translational displacement vector, $\Delta\bar{r}$, and the rotational displacement vector, $\Delta\bar{\theta}$, given below,

$$\Delta\bar{r} = \{\Delta x \ \Delta y \ \Delta z\}^T \in R^3 \tag{A.1.1}$$

$$\Delta\bar{\theta} = \{\Delta\alpha \ \ \Delta\beta \ \ \Delta\gamma\}^T \in R^3$$

Let vector $\bar{q}$ represent the generalized coordinates of the fixture-workpiece system. We have,

$$\bar{q} = \{\Delta\bar{r}^T \ \ \Delta\bar{\theta}^T\}^T \in R^6 \tag{A.1.2}$$

Let $\bar{d}_i$ be the displacement vector of the workpiece at the ith contact with respect to the local contact frame ($x_i y_i z_i$). Note that the number of components of $\bar{d}_i$ equals the modeled number of degrees of freedom (DOFs) at the ith contact point, *r*. The quantity *r* is determined as follows:

1) *r*=1, for a frictionless hard fixture element;
2) *r*=3, for a frictional hard fixture element;
3) *r*=4, for a frictional soft fixture element.

To be genetic, the third situation (r=4) is considered here although this thesis focuses on the second situation (r=3). The difference between the second and third situations and the method of reducing the third situation to the second situation are discussed later in this appendix.

The ith fixture element in contact with the workpiece is shown in Figure A.1.1. The four DOFs (r=4) at each contact include three linear DOFs along the x_i, y_i, and z_i directions and one angular DOF along the z_i direction. Therefore, a fixture element can possibly apply a four-component load, denoted as $\overline{F}_i$ and given in Equation (A.1.3), onto the workpiece. In addition, three linear springs and one torsional spring can be used to model the localized elasticity between a fixture element and the workpiece.

$$\overline{F}_i = \{F_{ix}\ F_{iy}\ F_{iz}\ M_{i\theta}\}^T \in R^4 \tag{A.1.3}$$

Note that, if r=3 (the second situation), the torsional load, $M_{i\theta}$, is considered to be negligible and hence the dimension of $\overline{F}_i$ reduces to three.

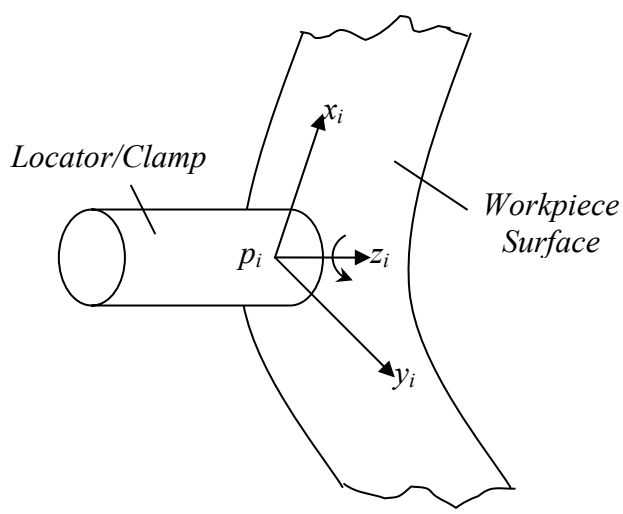

Figure A.1.1 The ith fixture element in contact with the workpiece

Consequently, the displacement vector at the ith fixture-workpiece contact, represented by $\bar{d}_i$, is given by,

$$\bar{d}_i = \{d_{ix}\ d_{iy}\ d_{iz}\ d_{i\theta}\}^T \in R^4 \tag{A.1.4}$$

Note that the last component of $\bar{d}_i$ does not exist if r=3.

Let $\bar{s}_{ix}$, $\bar{s}_{iy}$, and $\bar{s}_{iz}$ be the direction vectors of the x_i, y_i, and z_i axes in the workpiece-fixed frame (xyz) defined in Chapter 3. According to rigid body kinematics, it can be shown that,

$$d_{ix} = \bar{s}_{ix} \cdot (\Delta\bar{r} - \bar{p}_i \times \Delta\bar{\theta}) = s_{ix}^T \Delta\bar{r} + (\bar{p}_i \times s_{ix})^T \Delta\bar{\theta} \tag{A.1.5}$$

$$d_{iy} = \bar{s}_{iy} \cdot (\Delta\bar{r} - \bar{p}_i \times \Delta\bar{\theta}) = s_{iy}^T \Delta\bar{r} + (\bar{p}_i \times s_{iy})^T \Delta\bar{\theta}$$

$$d_{iz} = \bar{s}_{iz} \cdot (\Delta\bar{r} - \bar{p}_i \times \Delta\bar{\theta}) = s_{iz}^T \Delta\bar{r} + (\bar{p}_i \times s_{iz})^T \Delta\bar{\theta}$$

$$d_{i\theta} = \bar{s}_{iz} \cdot \Delta\bar{\theta} = s_{iz}^T \Delta\bar{\theta}$$

where $\bar{p}_i$ represents the position vector from the C.G. of the workpiece to the ith contact in the (xyz) frame.

Referring to Equations (A.1.2) and (A.1.4) and manipulating Equation (A.1.5) yields the relationship between $\bar{d}_i$ and $\bar{q}$ as follows,

$$\bar{d}_i = [S_i]^T \bar{q} \tag{A.1.6}$$

$$[S_i] = \begin{bmatrix} \bar{s}_{ix} & \bar{s}_{iy} & \bar{s}_{iz} & \bar{0} \\ \bar{p}_i \times \bar{s}_{ix} & \bar{p}_i \times \bar{s}_{iy} & \bar{p}_i \times \bar{s}_{iz} & \bar{s}_{iz} \end{bmatrix} \in R^{6\times 4}$$

Let,

$$\bar{d} = [\bar{d}_1^T,\ \bar{d}_2^T,\ \ldots,\ \bar{d}_i^T,\ \ldots,\ \bar{d}_{L+C}^T]^T \in R^{4(L+C)} \tag{A.1.7}$$

The relation between $\overline{d}$ and $\overline{q}$ can be obtained as follows via mathematical manipulation,

$$\overline{d} = [S]^T \ \overline{q} \tag{A.1.8}$$

$$[S] = [[S_1] \ [S_2] \ \cdots \ [S_i] \cdots \ [S_{L+C}]] \in R^{6\times 4(L+C)}$$

The matrix [S] in Equation (A.1.8) is called the configuration matrix of the fixture-workpiece system and it only depends on the fixture layout and the workpiece geometry. This matrix is a critical fixture design parameter that is often manipulated in fixture synthesis.

A.2 Calibration of Hydraulic Hand Pump

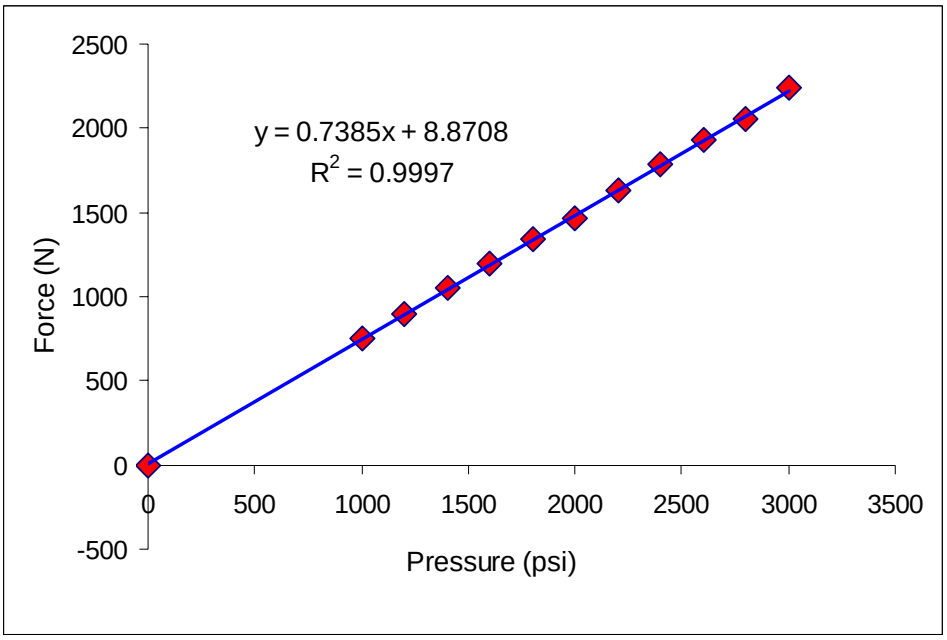

A.2.1 Calibration of clamp C1

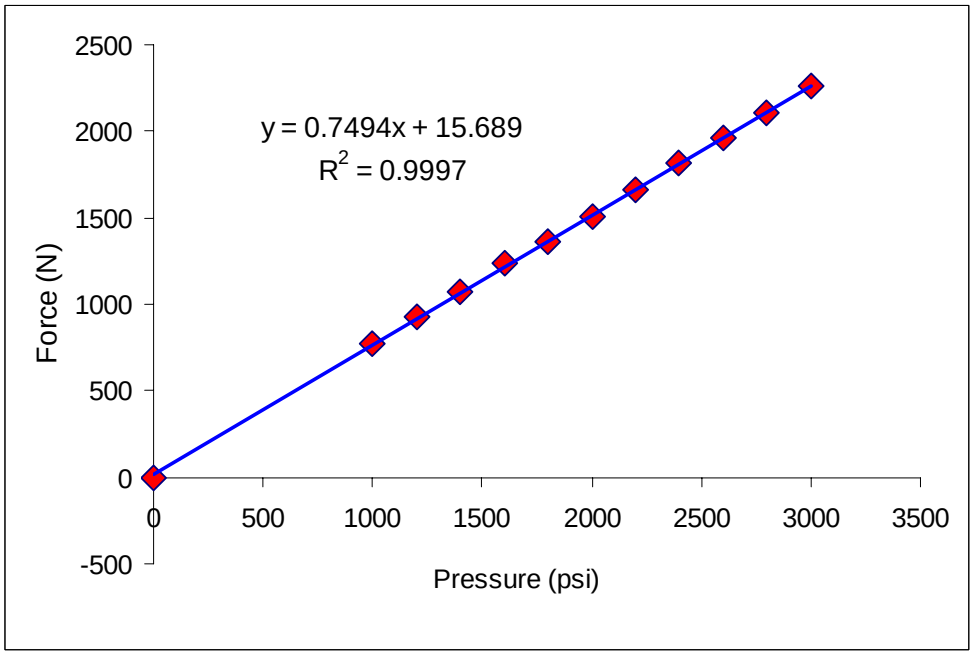

A.2.2 Calibration of clamp C2

A.3 Complete Results for Validation of Dynamic Model in Time Domain

(For the ten machining tests listed in Table 4.1 in Chapter 4)

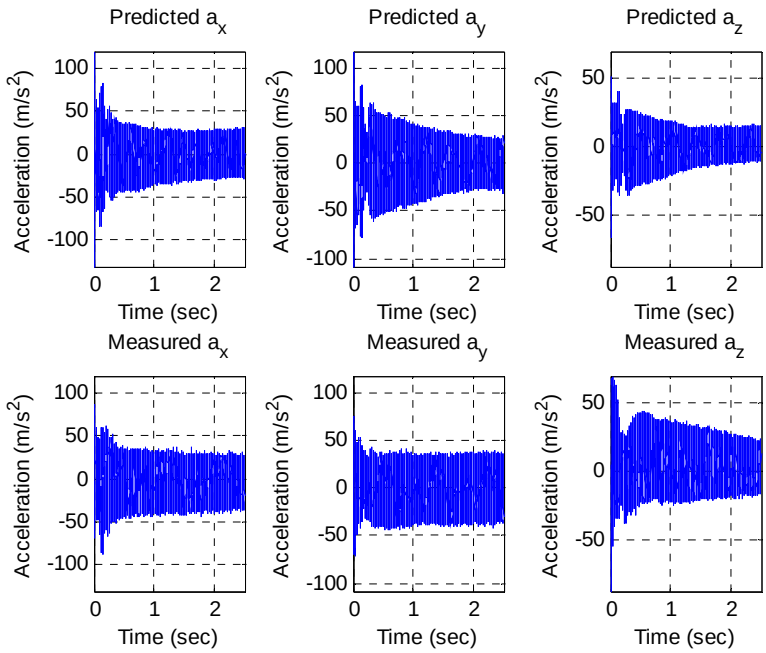

Figure A.3.1 Predicted vs. measured accelerations in time domain (Case #1)

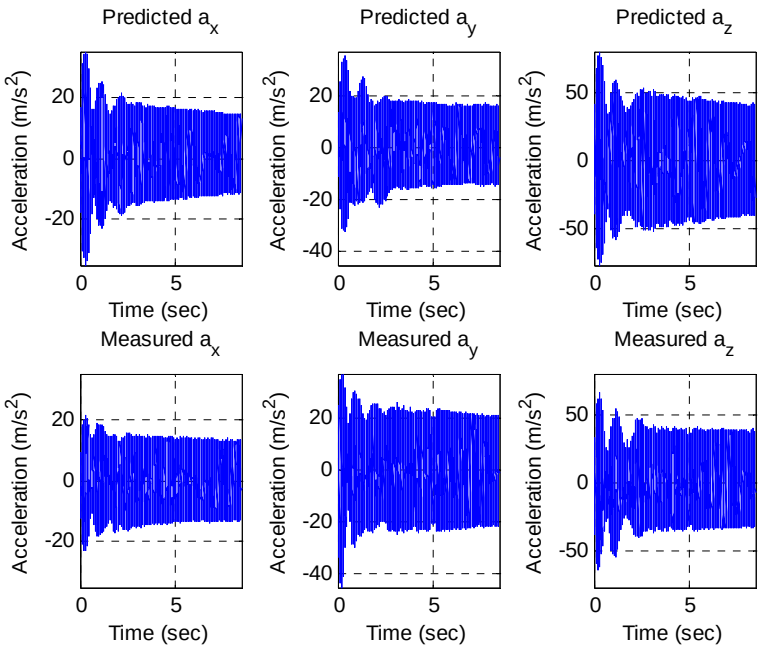

Figure A.3.2 Predicted vs. measured accelerations in time domain (Case #2)

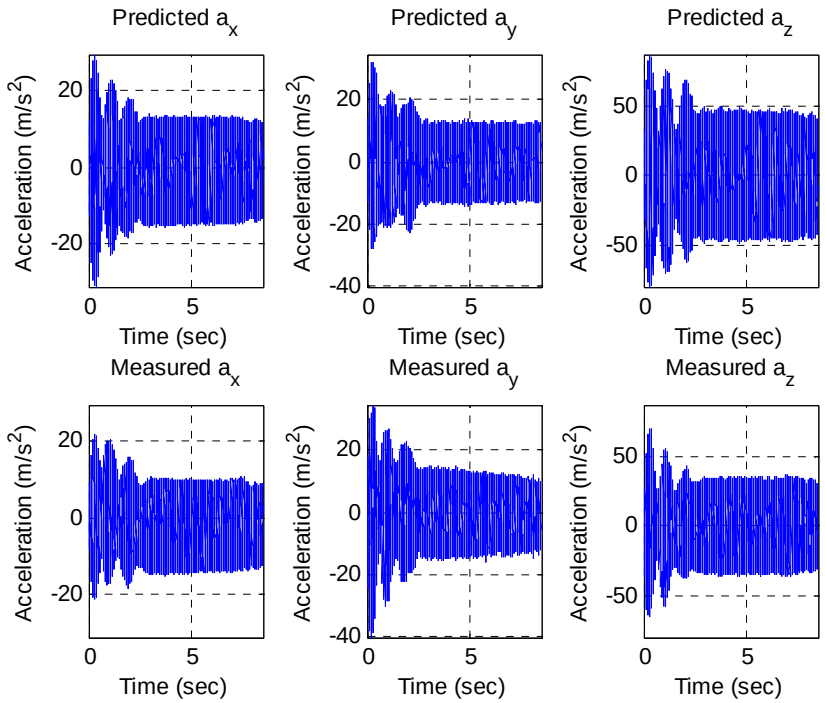

Figure A.3.3 Predicted vs. measured accelerations in time domain (Case #3)

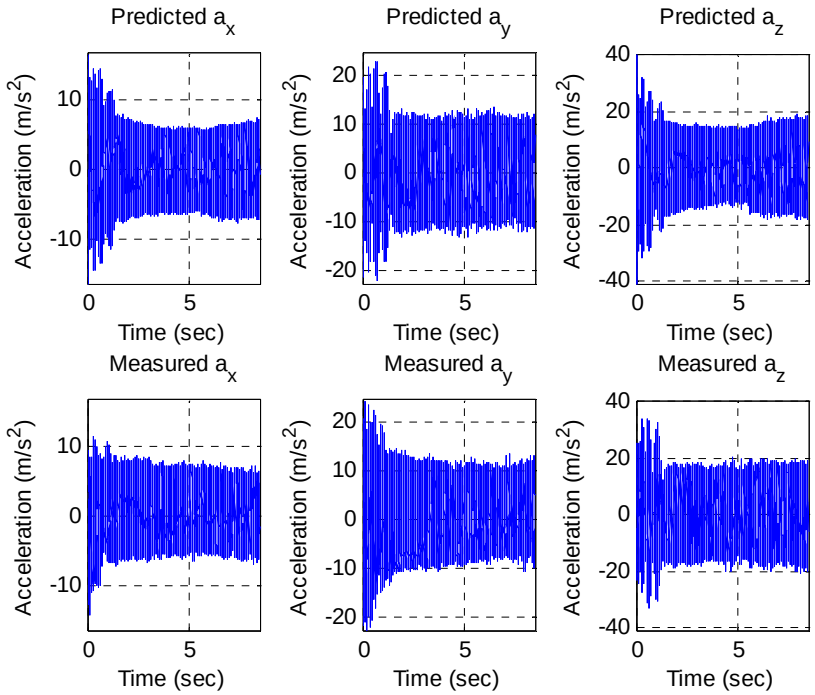

Figure A.3.4 Predicted vs. measured accelerations in time domain (Case #4)

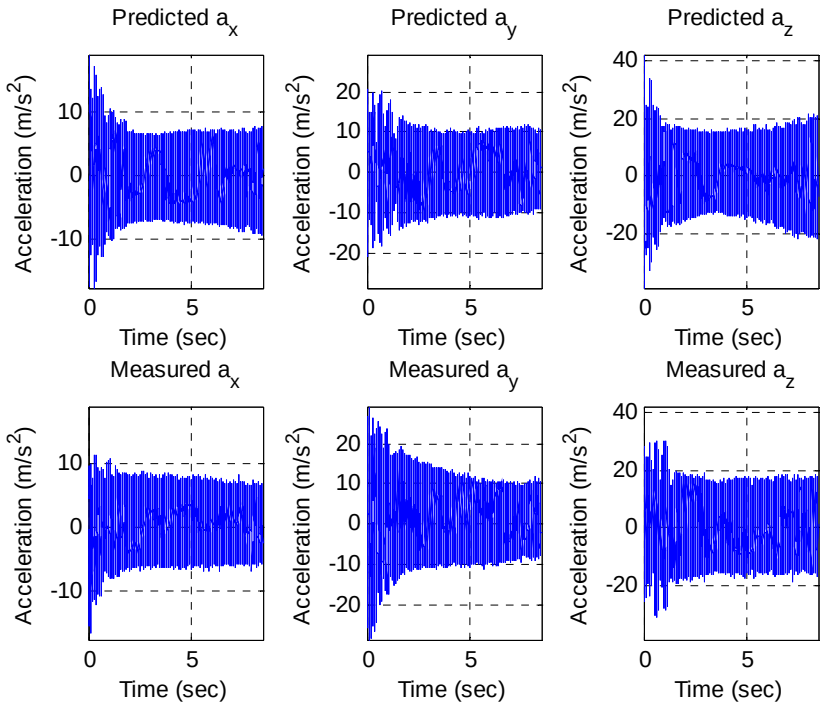

Figure A.3.5 Predicted vs. measured accelerations in time domain (Case #5)

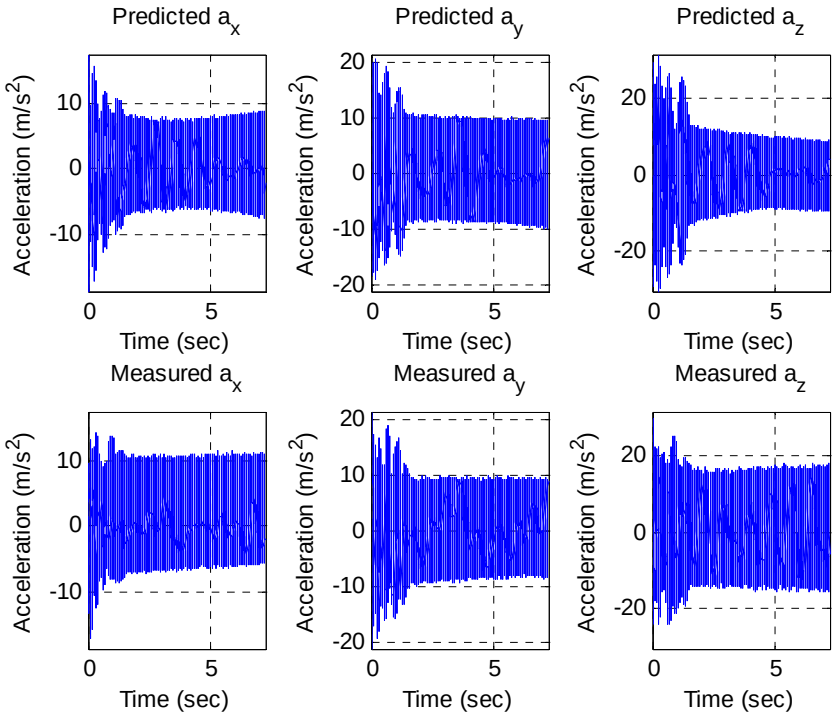

Figure A.3.6 Predicted vs. measured accelerations in time domain (Case #6)

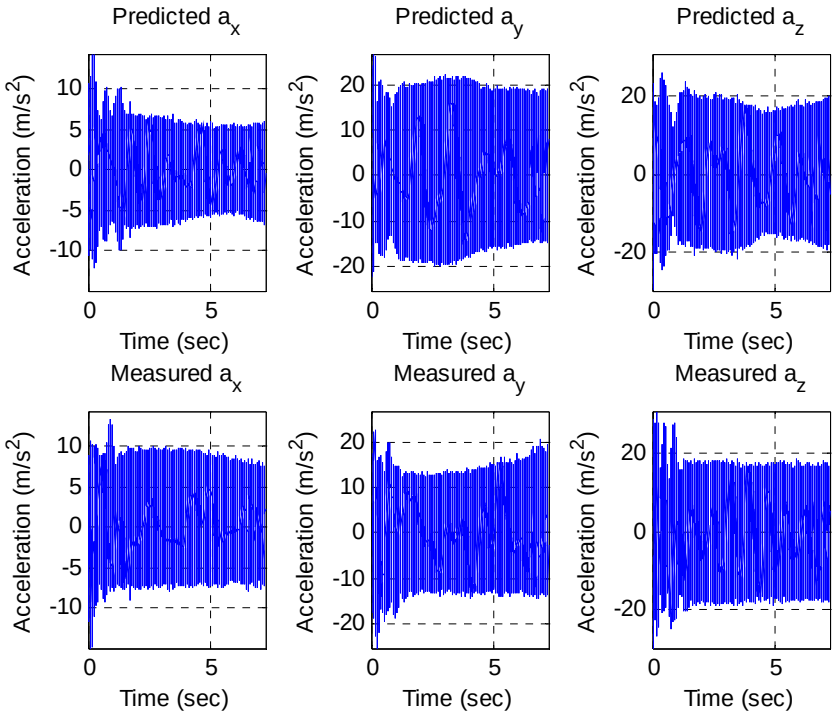

Figure A.3.7 Predicted vs. measured accelerations in time domain (Case #7)

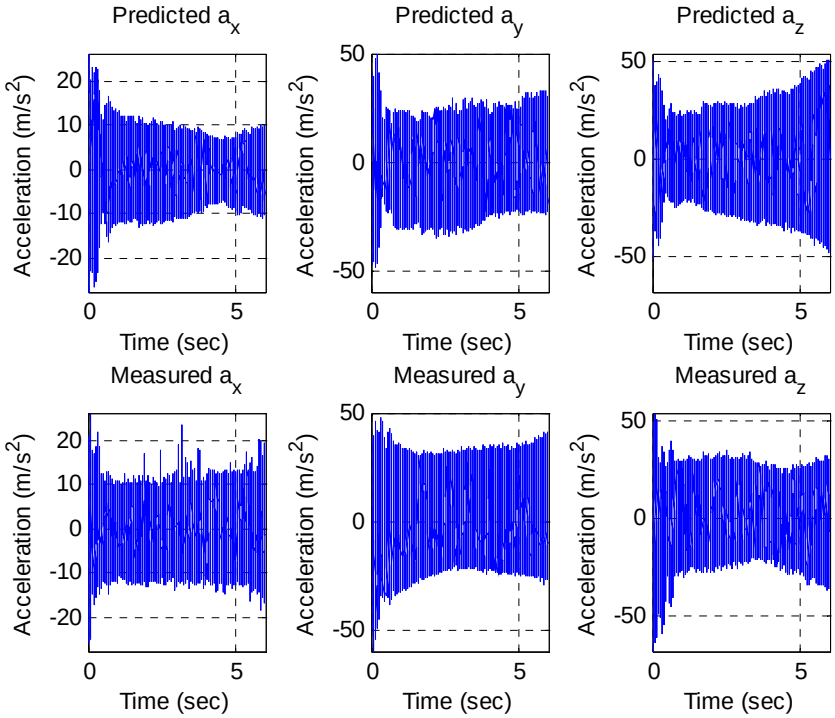

Figure A.3.8 Predicted vs. measured accelerations in time domain (Case #8)

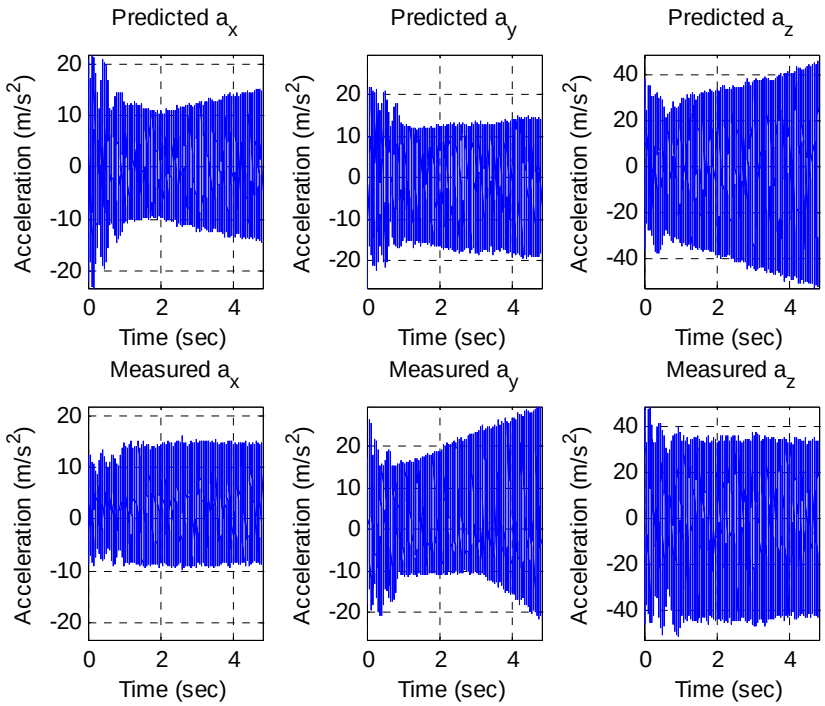

Figure A.3.9 Predicted vs. measured accelerations in time domain (Case #9)

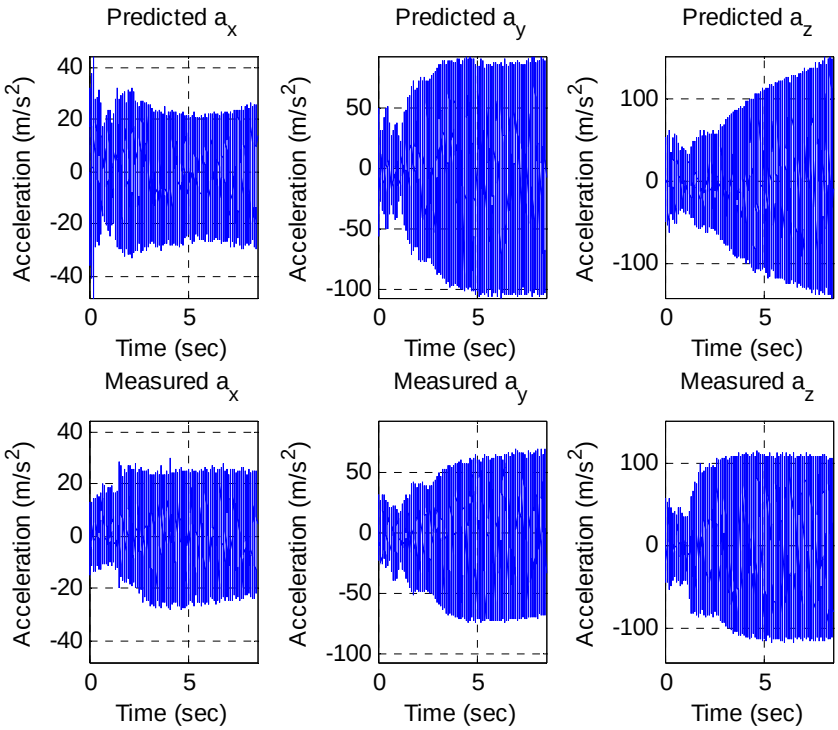

Figure A.3.10 Predicted vs. measured accelerations in time domain (Case #10)

A.4 Complete Results for Validation of Fixturing Stability Analysis Procedure

(For the five machining tests listed in Table 4.5 in Chapter 4)

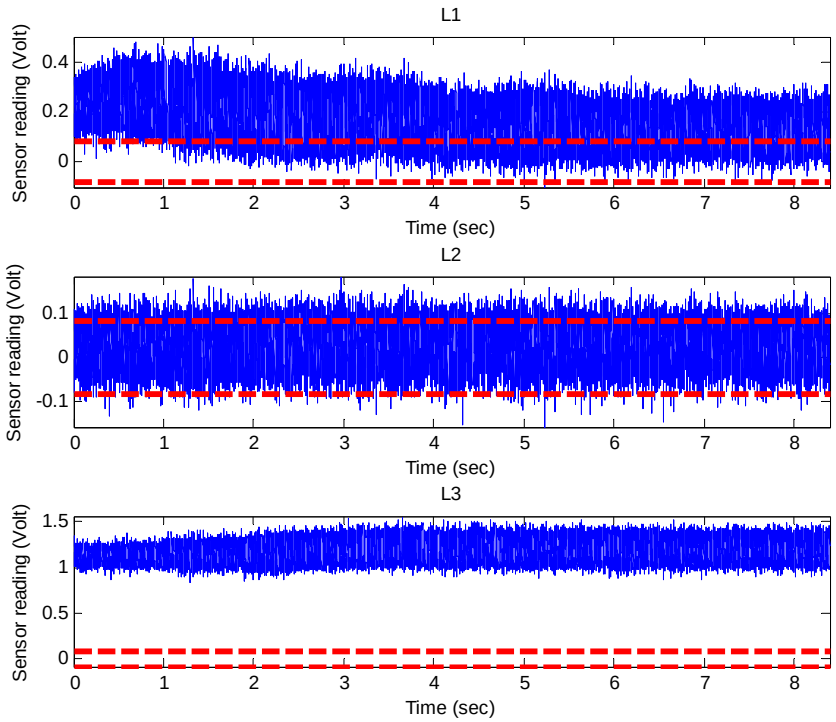

(a) Film sensor readings

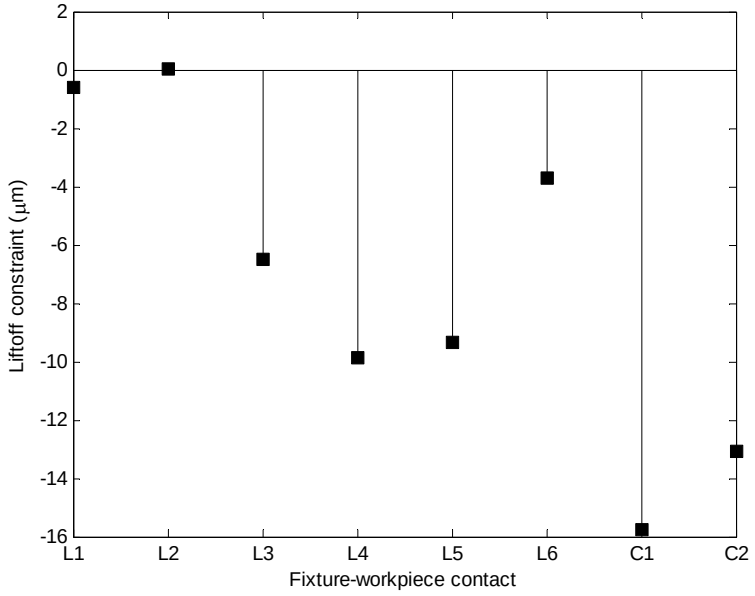

(b) Lift-off check by simulation

Figure A.4.1 Film sensor data and simulation results for case #1

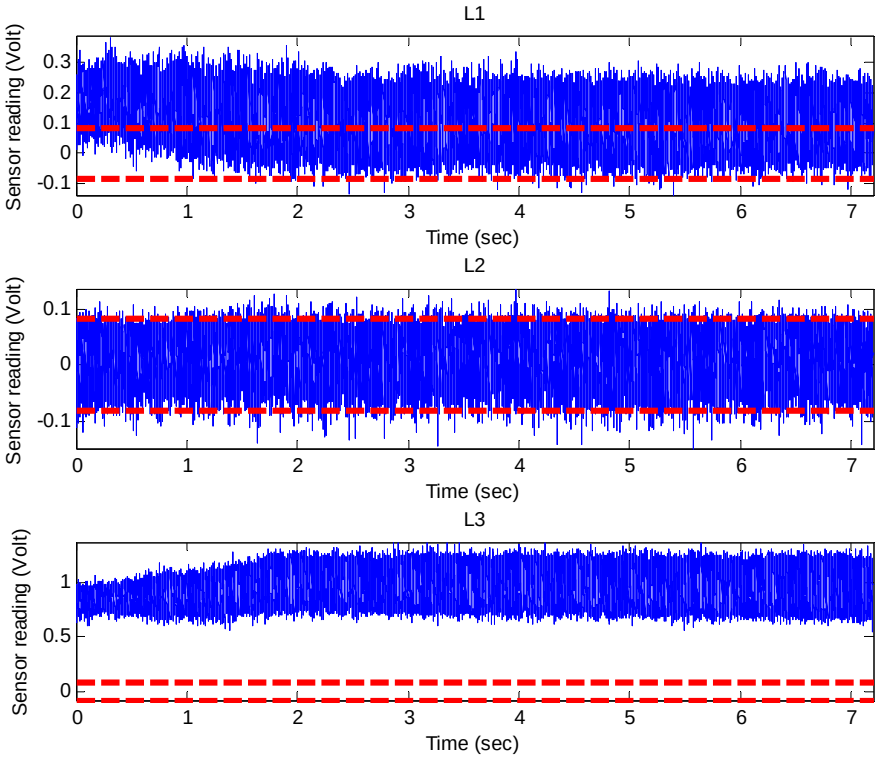

(a) Film sensor readings

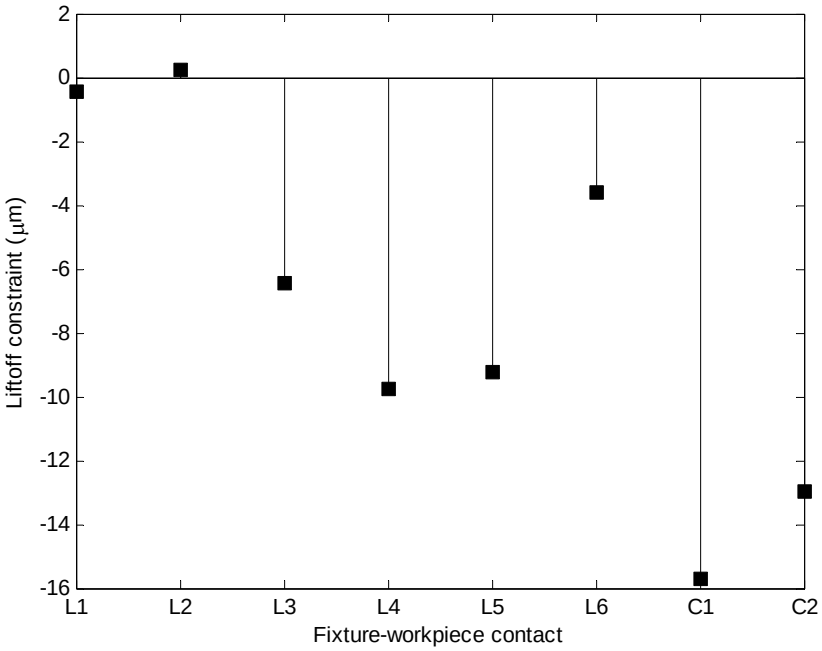

(b) Lift-off check by simulation

Figure A.4.2 Film sensor data and simulation results for case #2

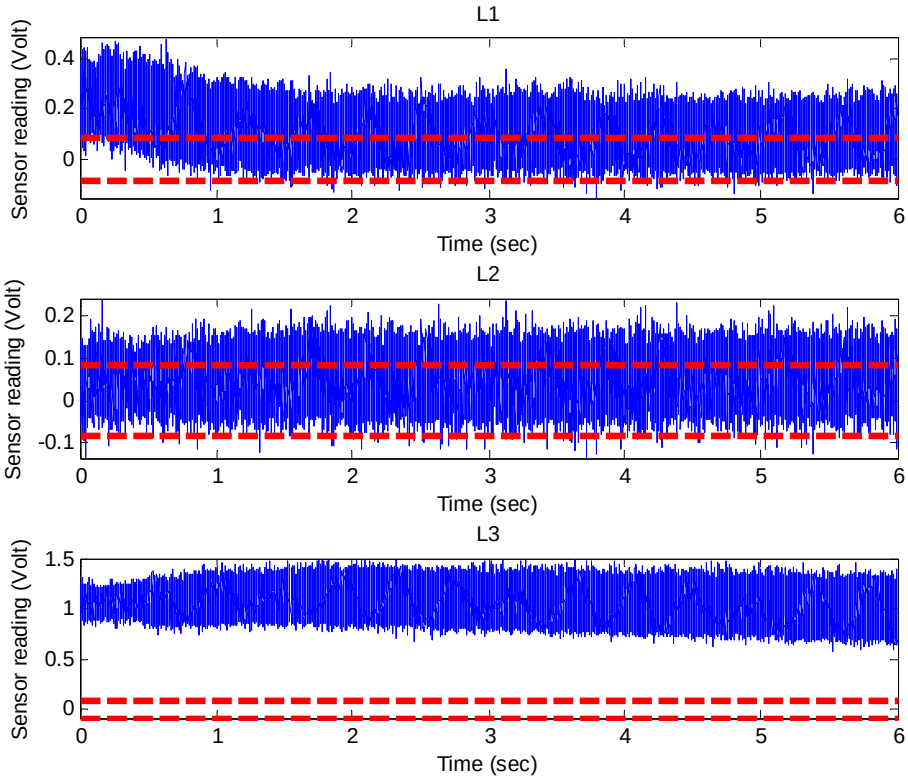

(a) Film sensor readings

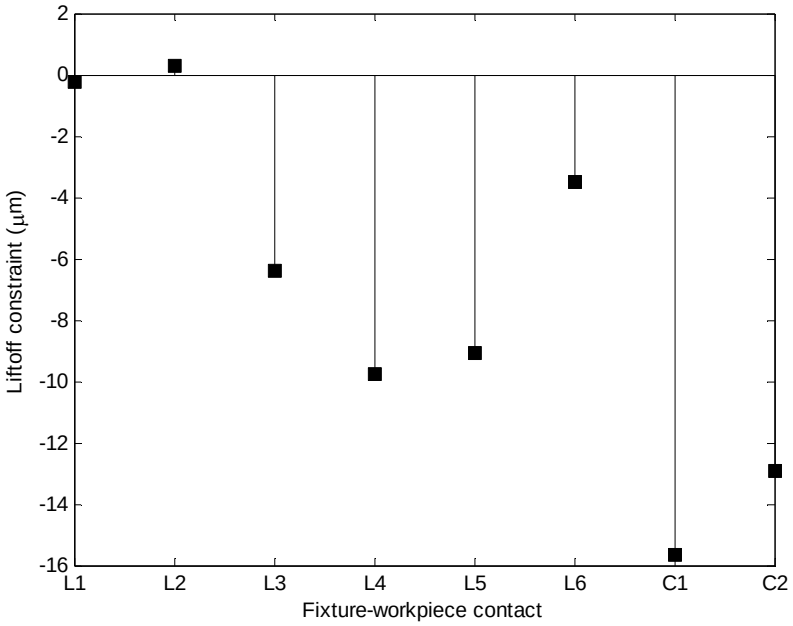

(b) Lift-off check by simulation

Figure A.4.3 Film sensor data and simulation results for case #3

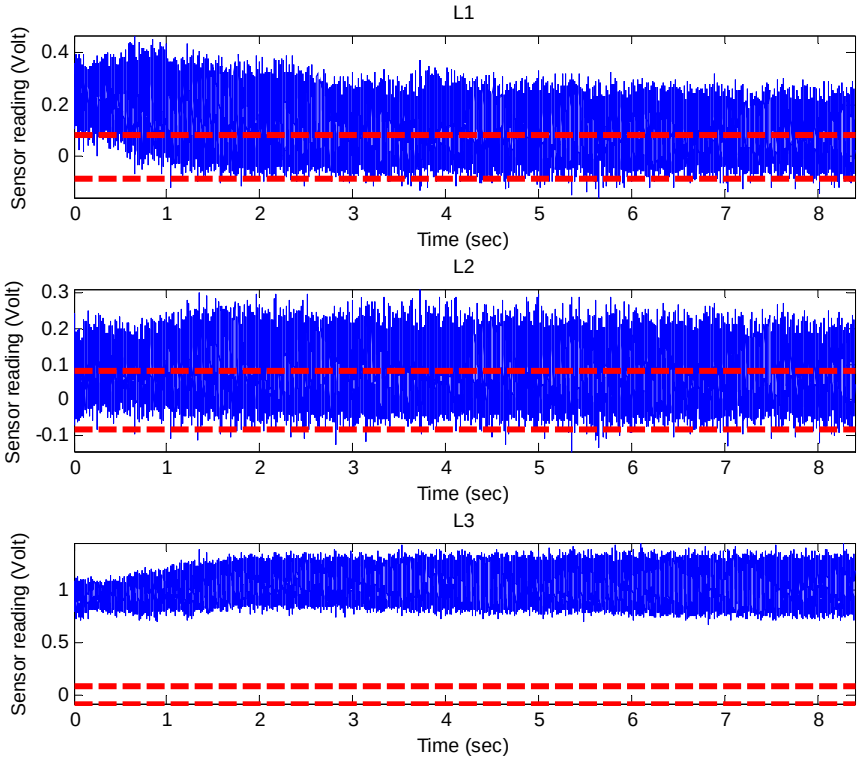

(a) Film sensor readings

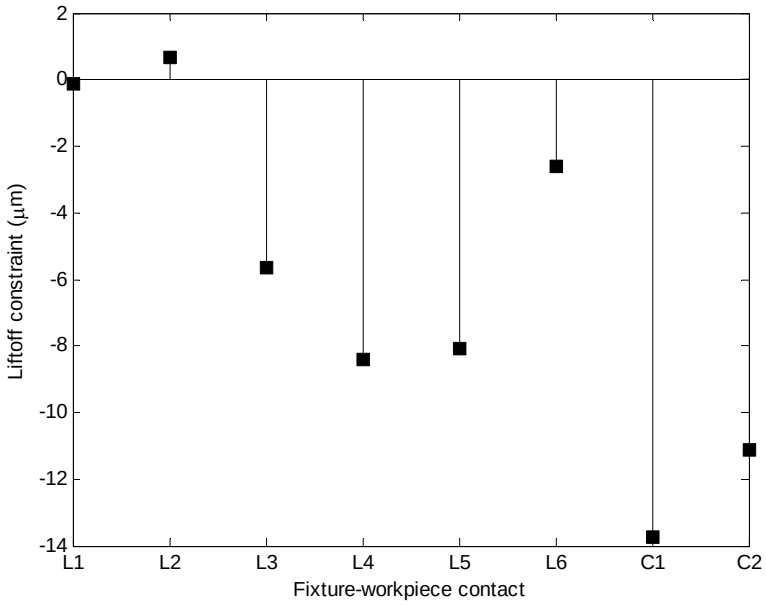

(b) Lift-off check by simulation

Figure A.4.4 Film sensor data and simulation results for case #4

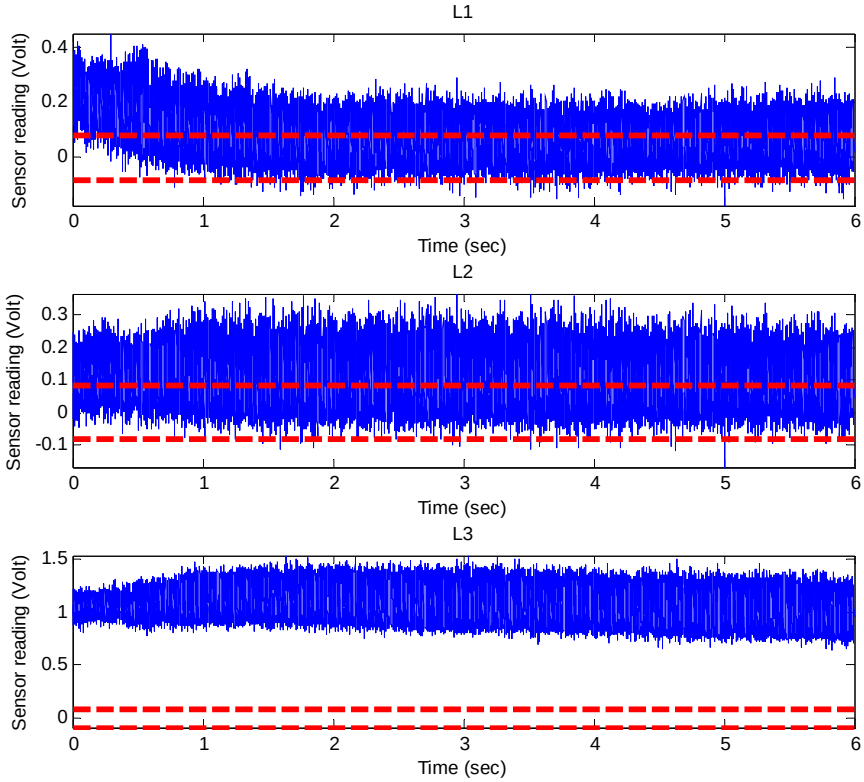

(a) Film sensor readings

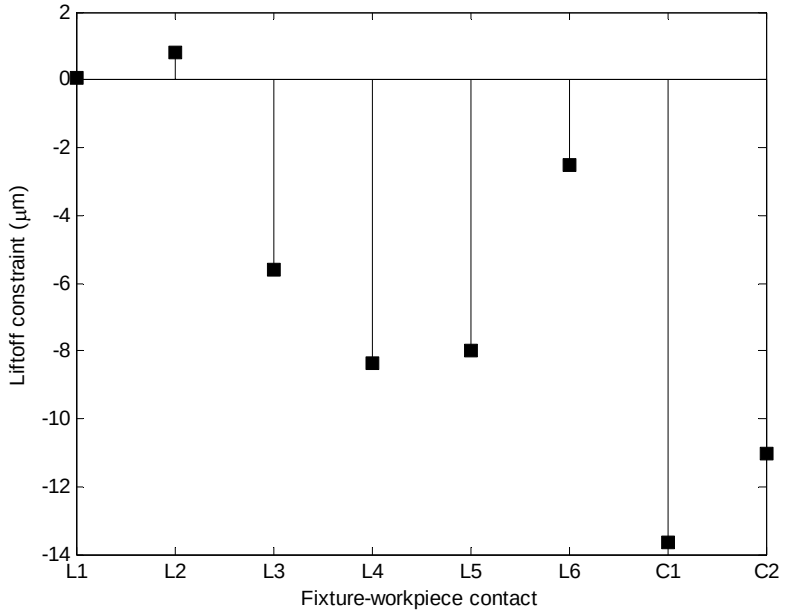

(b) Lift-off check by simulation

Figure A.4.5 Film sensor data and simulation results for case #5

REFERENCES

[1] Carr Lane Manufacturing Co., (1995), *Modular Fixturing Handbook*, 2nd Edition.

[2] Y.C. Chou, V. Chandru, and M.M. Barash, (1989), "A mathematical approach to automatic configuration of machining fixtures: analysis and synthesis," *ASME Journal of Engineering for Industry*, Vol. 111, No. 4, pp. 299-306.

[3] E.C. DeMeter, (1994), "The min-max load criteria as a measure of machining fixture performance," *ASME Journal of Engineering for Industry*, Vol. 116, pp. 500-507.

[4] M.J. Hockenberger and E.C. DeMeter, (1995), "The effect of machining fixture design parameters on workpiece displacement," *ASME*, *Manufacturing Review*, Vol. 8, No. 1, pp. 22-32.

[5] M.J. Hockenberger and E.C. DeMeter, (1996), "The application of meta functions to the quasi-static analysis of workpiece displacement within a machining fixture," *ASME Journal of Manufacturing Science and Engineering*, Vol. 118, pp. 325-331.

[6] B. Li and S.N. Melkote, (1999), "An elastic contact model for the prediction of workpiece-fixture contact forces in clamping," *ASME Journal of Manufacturing Science and Engineering*, Vol. 121, pp. 485-493.

[7] M.Y. Wang and D.M. Pelinescu, (2003), "Contact force prediction and force closure analysis of a fixtured rigid workpiece with friction," *ASME Journal of Manufacturing Science and Engineering*, Vol. 125, pp. 325-332.

[8] Y. Kang, Y. Rong, and J.A. Yang, (2003), "Geometric and kinetic model based computer-aided fixture design verification," *ASME Journal of Computing and Information Science in Engineering*, Vol. 3, pp. 187-199.

[9] G.S.A. Shawki and M.M. Abdel-Aal, (1965), "Effect of fixture rigidity and wear on dimensional accuracy," *International Journal of Machine Tool Design*, Res. 5, pp. 183-202.

[10] G.S.A. Shawki and M.M. Abdel-Aal, (1966), "Rigidity considerations in fixture design – contact rigidity at locating elements," *International Journal of Machine Tool Design*, Res. 6, pp. 31-43.

[11] G.S.A. Shawki and M.M. Abdel-Aal, (1966), "Rigidity considerations in fixture design – rigidity of clamping elements," *International Journal of Machine Tool Design*, Res. 6, pp. 207-220.

[12] G.S.A. Shawki, (1967), "Rigidity considerations in fixture design – contact rigidity for eccentric clamping," *International Journal of Machine Tool Design*, Res. 7, pp. 195-209.

[13] M. Daimon, T. Yoshida, N. Kojima, H. Yamamoto, Komatsu Ltd., and T. Hoshi, (1985), "Study for designing fixture considering dynamics of thin-walled plate and box-like workpieces," *Annals of the CIRP*, Vol. 34, No. 1, pp. 319-324.

[14] A.V. Shuleshkin and N.V. Gromov, (1960), "Setting up of 'body type' work-pieces for increased accuracy," *Russian Engineering Journal*, Vol. 40, No. 6, pp. 45-49.

[15] E.A. Markin, (1968), "Elastic deformations and vibration resistance of the machine-fixture-tool-workpiece system," *Machines Tooling*, Vol. 39, No. 4, pp. 11-14.

[16] L.M. Serdyuk and V.V. Mikityanskii, (1987), "Analyzing the sensitivities of production systems to machine tool fixture dynamic characteristics," *Mashinovedenie*, Vol. 4, pp. 92-96.

[17] R.O. Mittal, P.H. Cohen, and B.J. Gilmore, (1991), "Dynamic modeling of the fixture-workpiece system," *Robotics & Computer-Integrated Manufacturing,* Vol. 8, No. 4, pp. 201-217.

[18] Y.G. Liao and S.J. Hu, (2000), "Flexible multibody dynamics based fixture-workpiece analysis model for fixturing stability," *International Journal of Machine Tools and Manufacture*, Vol. 40, pp. 343-362.

[19] Y.G. Liao and S.J. Hu, (2001), "An integrated model of a fixture-workpiece system for surface quality prediction," *International Journal of Advanced Manufacturing Technology*, Vol. 17, pp. 810-818.

[20] I.M. Deiab, S.C. Veldhuis, and M. Dumitrescu, (2002), "Dynamic modeling of face milling process including the effect of fixture dynamics," *Transactions of NAMRI/SME*, Vol. 30, pp. 461-468.

[21] M.J. Hockenberger and E.C. DeMeter, (1995), "A preliminary investigation into the use of meta-functions for the dynamic analysis of workpiece displacement within a machining fixture," *Transactions of NAMRI/SME*, Vol. 23, pp. 325-330.

[22] Z.J. Tao, A.S. Kumar, A.Y.C. Nee, and M.A. Mannan, (1997), "Modeling and experimental investigation of a sensor-integrated workpiece-fixture system," *International Journal of Computer Application in Technology*, Vol. 10, Nos. 3/4, pp. 236-250.

[23] B. Fang, R.E. DeVor, and S.G. Kapoor, (2001), "An Elastodynamic Model of Frictional Contact ant Its Influence on the Dynamics of a Workpiece-Fixture

System", *ASME Journal of Manufacturing Science and Engineering*, Vol. 123, pp. 481-489.

[24] B. Fang, R.E. DeVor, and S.G. Kapoor, (2002), "Influence of friction damping on workpiece-fixture system dynamics and machining stability," *ASME Journal of Manufacturing Science and Engineering*, Vol. 124, pp. 226-233.

[25] H.E. Motlagh, M. Hamedi, and M.N. Bahramy, (2004), "Application of the Armstrong friction model to study the dynamic transient response in workpiece-fixture systems," *Proceedings of the Institution of Mechanical Engineers, Part B: Journal of Engineering Manufacture*, Vol. 218, pp. 737-747.

[26] J.J.-X. Liu and D.R. Strong, (2002), "Machining fixture verification for linear fixture systems," *International Journal of Production Research*, Vol. 40, No. 14, pp. 3441-3459.

[27] N. Kaya and F. Öztürk, (2003), "The application of chip removal and frictional contact analysis for workpiece-fixture layout verification," *International Journal of Advanced Manufacturing Technology*, Vol. 21, pp. 411-419.

[28] K. Lakshminarayana, (1979), "Mechanics of form closure," ASME Technical Paper, No. 78-DET-32, pp. 1-8.

[29] C.H. Xiong, Y.F. Li, Y.K. Rong, and Y.L. Xiong, (2002), "Qualitative analysis and quantitative evaluation of fixturing," *Robotics and Computer Integrated Manufacturing*, Vol. 18, pp.335-342.

[30] X. Markenscoff, L. Ni, and C.H. Papadimitriou, (1990), "The geometry of grasping," *International Journal of Robotics Research*, Vol. 9, No. 1, pp. 61-74.

[31] E.C. DeMeter, (1993), "Restraint analysis of fixtures which rely on surface contact," *ASME Journal of Engineering for Industry*, Vol. 116, pp. 207-215.

[32] U. Roy and J. Liao, (2002), "Fixturing analysis for stability consideration in an automated fixture design system," *ASME Journal of Manufacturing Science and Engineering*, Vol. 124, pp. 98-104.

[33] J. Hurtado and S.N. Melkote, (2002), "Modeling and analysis of the effect of fixture-workpiece conformability on static stability," *ASME Journal of Manufacturing Science and Engineering*, Vol. 124, pp. 234-241.

[34] V. Nguyen, (1987), "Constructing stable grasps in 3D," *Proceedings of 1987 IEEE International Conference on Robotics and Automation*, pp. 234-239, March, Raleigh, NC.

[35] W.S. Howard and V. Kumar, (1996), "On the stability of grasped objects," *IEEE Transactions on Robotics and Automation*, Vol. 12, No. 6, pp. 904-917.

[36] H. Bruyninckx, S. Demey, and V. Kumar, (1998), "Generalized stability of compliant grasps," *Proceedings of the IEEE International Conference on Robotics and Automation*, pp. 2396-2402.

[37] J. Tlusty, S. Smith, and W. Winfough, (1996), "Techniques for the use of long slender end mills in high-speed milling," *CIRP Annals - Manufacturing Technology*, Vol. 45, No. 1, pp. 393-396.

[38] S. Smith and D. Dvorak, (1998), "Tool path strategies for high speed milling aluminum workpieces with thin webs," *Mechatronics*, Vol. 8, No. 4, pp. 291-300.

[39] W. Cai, S.J. Hu, and J.X. Yuan, (1997), "Variational method of robust fixture configuration design for 3-D workpieces," *ASME Journal of Manufacturing Science and Engineering*, Vol. 119, pp. 593-602.

[40] M. Estrems, H.T. Sánchez, and F. Faura, (2003), "Influence of fixtures on dimensional accuracy in machining processes," *The International Journal of Advanced Manufacturing Technology*, Vol. 21, pp. 384-390.

[41] S.C. Liu and S.J. Hu, (1997), "Variation simulation for deformable sheet metal assemblies using finite element methods," *ASME Journal of Manufacturing Science and Engineering*, Vol. 119, pp. 368-374.

[42] J. Camelio, S.J. Hu, and D. Ceglarek, (2003), "Modeling variation propagation of multi-station assembly systems with compliant parts," *ASME Journal of Mechanical Design*, Vol. 125, pp. 673-681.

[43] W. Zhong, (2004), "Unified modeling of variation propagation and tolerance synthesis for integrated machining-assembly systems part I: modeling variation propagation," *Transactions of NAMRI/SME*, Vol. 32, pp. 541-548.

[44] Y. Shen and N.A. Duffie, (1995), "An uncertainty analysis method for coordinate referencing in manufacturing systems," *ASME Journal of Engineering for Industry*, Vol. 117, pp. 42-48.

[45] K.B. Shimoga and A.A. Goldenberg, (1991), "Grasp admittance center: how sensitive is it to parameter imprecision?" *Proceedings of IEEE International Conference of Robotics and Automation*, pp. 619-624.

[46] K.B. Shimoga and A.A. Goldenberg, (1991), "Grasp admittance center: a concept and its implications," *Proceedings of IEEE International Conference of Robotics and Automation*, April 7-12, Sacramento, CA, pp. 293-298.

[47] M. Hershkovitz and M. Teboulle, (1998), "Sensitivity analysis for a class of robotic grasping quality functionals," *Robotica*, Vol. 16, pp. 227-235.

[48] E.C. De Meter, W. Xie, S. Choudhuri, S. Vallapuzha, and M.W. Trethewey, (2001), "A model to predict minimum required clamp pre-loads in light of fixture-workpiece compliance," *International Journal of Machine Tools and Manufacture,* Vol. 41, pp. 1031-1054.

[49] R.T. Meyer and F.W. Liou, (1997), "Fixture analysis under dynamic machining," *International Journal of Production Research*, Vol. 35, No. 5, pp. 1471-1489.

[50] C.H. Xiong, Y.L. Xiong, and M.Y. Wang, (2003), "Clamping planning in workpiece-fixture systems," Proceedings of ASME International Mechanical Engineering Congress and Exhibition (IMECE), Manufacturing Engineering Division (MED), Vol. 14, pp. 267-272.

[51] B. Li, S.N. Melkote, and S.Y. Liang, (2000), "Analysis of reactions and minimum clamping force for machining fixtures with large contact areas," *The International Journal of Advanced Manufacturing Technology*, Vol. 16, pp. 79-84.

[52] Y.F. Wang, Y.S. Wong, and J.Y.H. Fuh, (1999), "Off-line modeling and planning of optimal clamping forces for an intelligent fixturing system," *International Journal of Machine Tools and Manufacture*, Vol. 39, pp. 253-271.

[53] Z.J. Tao, A.S. Kumar, and A.Y.C. Nee, (1999), "Automatic generation of dynamic clamping forces for machining fixtures," *International Journal of Production Research*, Vol. 37, No. 12, pp. 2755-2776.

[54] J.J. Liu and D.R. Strong, (2003), "Machining fixture verification for nonlinear fixture systems," *International Journal of Advanced Manufacturing Technology*, Vol. 21, pp. 426-437.

[55] X. Gui, J.Y.H. Fuh, and A.Y.C. Nee, (1996), "Modeling of frictional elastic fixture-workpiece system for improving location accuracy," *IIE Transactions*, Vol. 28, pp. 821-827.

[56] Y. Huang and L. Wang, (2004), "Realizing high accuracy machining by applying optimal clamping forces," *International Journal of Computer Application in Technology*, Vol. 19, No. 2, pp. 107-118.

[57] A.Y.C. Nee, A.S. Kumar, and Z.J. Tao, (2000), "Intelligent fixture with a dynamic clamping scheme," *Proceedings of the Institution of Mechanical Engineers, Part B: Journal of Engineering Manufacture*, Vol. 214, No. 3, pp. 183-196.

[58] J.F. Hurtado and S.N. Melkote, (2002), "A model for synthesis of the fixturing configuration in pin-array type flexible machining fixtures," *International Journal of Machine Tools and Manufacture*, Vol. 42, pp. 837-849.

[59] B. Li and S.N. Melkote, (2001), "Fixture clamping force optimization and its impact on workpiece location accuracy," *International Journal of Advanced Manufacturing Technology*, Vol. 17, pp. 104-113.

[60] M.Y. Wang, (2002), "Tolerance analysis for fixture layout design," *Assembly Automation*, Vol. 22, No. 2, pp. 153-162.

[61] B. Li and S.N. Melkote, (1999), "Improved workpiece location accuracy through fixture layout optimization," *International Journal of Machine Tools and Manufacture*, Vol. 39, pp. 871-883.

[62] Y. Huang and T. Hoshi, (2000), "Optimization of fixture design with consideration of thermal deformation in face milling," Journal of Manufacturing Systems, Vol. 19, No. 5, pp. 332-340.

[63] K. Kulankara, S. Satyanarayana, and S.N. Melkote, (2002), "Iterative fixture layout and clamping force optimization using the Genetic Algorithm," *Journal of Manufacturing Science and Engineering*, *Transactions of the ASME*, Vol. 124, pp. 119-125.

[64] Y.G. Liao, (2003), "A generic algorithm-based fixture locating positions and clamping schemes optimization," *Proceedings of the Institution of Mechanical Engineers, Part B: Journal of Engineering Manufacture*, Vol. 217, No. 8, pp. 1075-1083.

[65] S. Vallapuzha, E.C. DeMeter, S. Choudhuri, and R.P. Khetan, (2002) "An investigation into the use of spatial coordinates for the generic algorithm based solution of the fixture layout optimization problem," *International Journal of Machine Tools & Manufacture*, Vol. 42, pp. 265-275.

[66] S. Vallapuzha, E.C. DeMeter, S. Choudhuri, and R.P. Khetan, (2002) "An investigation of the effectiveness of fixture layout optimization methods," *International Journal of Machine Tools & Manufacture*, Vol. 42, pp. 251-263.

[67] E.C. DeMeter, (1998), "Fast support layout optimization," *International Journal of Machine Tools & Manufacture*, Vol. 38, pp. 1221-1239.

[68] Q.A. Sayeed and E.C. DeMeter, (1999), "Mixed-integer programming model for fixture layout optimization," *ASME Journal of Manufacturing Science and Engineering*, Vol. 121, pp. 701-708.

[69] C. Cogun, (1992), "The importance of the application of sequence of clamping forces on workpiece accuracy," *ASME Journal of Engineering for Industry*, Vol. 114, pp. 539-543.

[70] A. Raghu and S.N. Melkote, (2004), "Analysis of the effects of fixture clamping sequence on part Location errors," *International Journal of Machine Tools and Manufacture*, Vol. 44, pp. 373-382.

[71] J.H. Ginsberg, (1998), *Advanced Engineering Dynamics*, 2nd Edition, Cambridge University Press, U.K.

[72] O.A. Bauchau, (2004), *Aerospace Structural Analysis*, Chapter 7 Variational and Energy Principles, Georgia Institute of Technology, Atlanta, Georgia, U.S.A.

[73] K.L. Johnson, (1985), *Contact Mechanics*, Cambridge University Press, U.K.

[74] J.M. Gere and S.P. Timoshenko, (1997), *Mechanics of Materials*, PWS Publishing Company, U.S.A.

[75] Y. Altintas, (2000), *Manufacturing Automation*, Cambridge University Press, U.K.

[76] R.J. Allemang and D.L. Brown, (1993), Chapter 16 Experimental Modal Analysis, *Handbook on Experimental Mechanics*, edited by A.S. Kobayashi, 2nd revised edition, Wiley, U.S.A.

[77] D.J Ewins, (2000), *Modal Testing: Theory, Practice, and Application*, 2nd Edition, Research Studies Press, U.K.

[78] J. Kenny and R.C. Eberhart, (2001), *Swarm Intelligence*, Morgan Kaufmann Publishers, U.S.A.

VITA

Haiyan Deng, the youngest daughter of Yuxiang Wang and Guowen Deng, was born and raised in Hunan, China. Haiyan received her Bachelor of Science in Mechanical Engineering with honors from Southwest Petroleum Institute in Sichuan, China in 1995. She then joined China National Petroleum Corporation and worked as an engineer till 2001.

In August 2001, Haiyan was awarded a university fellowship by Indiana University-Purdue University Indianapolis (IUPUI) and moved to the United States for graduate studies. After two years, she obtained her Master of Science in Mechanical Engineering from Purdue University with honors. In her MS thesis directed by Dr. Hazim El-Mounayri, Haiyan developed a generic approach for modeling and optimization of end milling process using solid modeling and artificial intelligence techniques.

Haiyan started her Ph.D. program of study in the George W. Woodruff School of Mechanical Engineering at Georgia Institute of Technology in Atlanta, Georgia in the Fall of 2003. Under the guidance of Dr. Shreyes N. Melkote, Haiyan performed a systematic, in-depth investigation on the dynamic performance of an arbitrarily configured fixture-workpiece system in machining with consideration of material removal effect.

Upon completion of her Ph.D. program in the Fall of 2006, Haiyan joined Caterpillar Inc. in Peoria, Illinois.